FACULDADE DE ENGENHARIA DA UNIVERSIDADE DO PORTO



In vivo measurement of forces exerted on the trapeziometacarpal joint

Inês Pereira de Fontes

Mestrado Integrado em Bioengenharia

Supervisor: Prof. Miguel Velhote Correia

Proponent: Dr. Carlos Pina

Proponent: Dra. Joana Contente

June 21, 2021

© Inês Pereira de Fontes, 2020

In vivo measurement of forces exerted on the trapeziometacarpal joint

Inês Pereira de Fontes

Mestrado Integrado em Bioengenharia

June 21, 2021

Resumo

Ao longo dos últimos anos, a esperança média de vida tem aumentado exponencialmente o que leva a um envelhecimento da população. Este envelhecimento reflete-se num aumento das doenças degenerativas, nomeadamente ao nível das articulações, tal como a osteoartrose. Esta doença afeta 500 milhões de pessoas em todo o mundo.

Uma das articulações mais afetadas por esta patologia é a trapeziometacarpiana. Esta articulação pertence ao polegar que é um elemento crucial da mão para tarefas tais como pegar em objetos, fechar zippers e escrever. Atualmente, o diagnóstico da osteoartrose nesta articulação é efetuada recorrendo a técnicas de imagiologia e testes de destreza. Contudo, estas técnicas nem sempre são suficientes a escolha do tratamento adequado sendo esta decisão tomada pelo clínico não existindo consenso na comunidade médica contrariamente ao que acontece noutras articulações com a mesma patologia.

Nas outras articulações existe um forte estudo prático e in vivo com o auxílio de sensores intra-articulares algo que ainda não aconteceu como a articulação trapeziometacarpal tornando-se, assim, necessário o desenvolvimento de um sensor intra-articular para que se possa comprovar in vivo o conhecimento adquirido ao nível laboratorial de modo a adaptar as técnicas cirúrgicas a cada estágio da doença.

O desenvolvimento de um destes sensores apresenta alguns desafios devido às dimensões reduzidas e às superfícies articulares irregulares. Assim sendo, esta dissertação apresenta um protótipo de um sistema de aquisição do valor das forças e da área de contacto. Este sistema é constituído por uma matriz de sensores piezoresistivos com as dimensões das superfícies articulares, o circuito que permite a aquisição dos sinais e um software desenvolvido em Android Studio para visualização dos sinais.

Abstract

Over the last few years, average life expectancy has increased exponentially, leading to an ageing population. This ageing is reflected in an increase in degenerative diseases, namely at the level of the joints, such as osteoarthritis. This disease affects 500 million people worldwide.

One of the most affected joint by this disease is the trapeziometacarpal. This joint belongs to the thumb, which is a crucial element of the hand for tasks such as picking up objects, zipping zippers and writing. Currently, the diagnosis of osteoarthrosis in this joint is made using imaging techniques and dexterity tests, but these are not always sufficient to choose the appropriate treatment. This decision is made by the clinician, and there is no consensus in the medical community, contrary to what happens in other joints with the same pathology.

In other joints, there is a strong practical, in vivo study with the help of intra-articular sensors, something that has not yet happened with the trapeziometacarpal joint, thus making the development of an intra-articular sensor necessary, so that the knowledge acquired at laboratory level can be proven in vivo, in order to adapt surgical techniques to each stage of the disease.

The development of such a sensor presents some challenges due to its small dimensions and irregular articular surfaces. Therefore, this dissertation presents a prototype of a system for the acquisition of force values and contact areas. This system consists of a piezoresistive sensor array with the dimensions of the joint surfaces, the circuit that allows the acquisition of the signals and a software developed in Android Studio for visualization of the signals.

Agradecimentos

A presente dissertação representa o culminar de uma jornada inesperada, intensa e, acima de tudo, de crescimento. Ao longo deste percurso foram inúmeras as pessoas que me inspiraram e apoiaram e às quais tenho de expressar a minha gratidão.

Primeiro, gostaria de agradecer ao professor Miguel Correia por me ter orientado neste projeto e cujos inputs foram fundamentais para o resultado final. Não poderia deixar de incluir o Dr. Carlos Pina e a Dra. Joana Contente pela amabilidade e disponibilidade que sempre demonstraram. Esta tese também não teria sido possível sem o auxílio do Departamento de Engenharia Textil da Universidade do Minho: ao professor Hélder, à Ana e à Isabel um muito obrigada.

Para além das pessoas que me ajudaram de uma forma direta a levar esta tese a bom porto não poderia deixar de deixar a minha palavra de apreço àqueles que se cruzaram no meu caminho ao longo destes anos. Ao Miguel e à Fátima por terem sido os melhores colegas de curso que podia ter encontrado. À Raquel, à minha companheira desde o primeiro dia, que mesmo longe esteve sempre perto. À Elsa, à Susana e à Mariana por todos os momentos de descontração. Um muito obrigada a todos os outros que se cruzaram comigo ao longo desta aventura.

Para além da faculdade, estes anos foram uma descoberta do meu lado mais humano e de uma terapia inesperada. N'O Meu Lugar no Mundo encontrei um local onde me sinto em paz. Ao Isus, ao Mateus, ao Aly, à Gaby, à Íris, ao Ricardo e a todos os outros, obrigada por, mesmosem sem saberem, me terem ajudado ao longo dos últimos anos. Para além das crianças que preencheram os meus dias tenho também de agradecer às voluntárias deste projeto. À Carina e à Carolina pelas palavras de apoio e incentivo que nunca faltaram, à Cátia, à Renata, à Teresa e à Inês por terem confiado em mim.

A minha família não podia ser deixada para traz, em particular a minha avó que sempre foi a minha maior fã e a minha madrinha, que apesar da distância, nunca se esqueceu de nenhuma data importante. À Cláudia, ao Filipe e à Marianinha a família que eu escolhi e que sempre esteveram lá a torcer por mim. Aos meus primos: Rodrigo, Tomás e Diogo que souberam sempre quando dar o abraço no momento certo. A todos eles mil obrigadas!

Finalmente, não poderia deixar de agradecer a quem tornou tudo isto possível e me ensinou a sonhar: os meus pais. São sem dúvida os meus grandes pilares e os maiores apoios não só desta jornada como da vida. À minha irmã Francisca, o meu terceiro pilar, obrigada por ter tido a paciência, as palavras de encorajamento, as panquecas e as fotos de bebés fofos nos momentos certos.

Não podia deixar de acrescentar a esta lista o meu avô António. Desde pequena, tanto ele como os meus pais, sempre me incutiram o gosto por aprender e o respeito e a ambição de alcançar o ensino superior. Não posso, por isso, deixar de lhes agradecer por isso.O meu avô partiu antes de conseguir presenciar grande parte do meu percurso escolar, mas tenho a certeza que foi a "estrelinha" que sempre me acompanhou e nunca me deixou desistir. Resta-me, por isso, dedicar-lhe o meu esforço e empenho durante estes cinco anos.

Inês Fontes

"Sê todo em cada coisa. Põe quanto és
No mínimo que fazes."

Ricardo Reis

Contents

Abstract iii

1 Introduction 1
- 1.1 Context . . . 1
- 1.2 Motivation . . . 1
- 1.3 Goals . . . 2
- 1.4 Outline . . . 2

2 Anatomical Background 3
- 2.1 Joints . . . 3
- 2.2 Trapeziometacarpal Joint . . . 5
  - 2.2.1 Anatomical Description . . . 5
  - 2.2.2 Dimensions of bones . . . 8
- 2.3 Osteoarthritis . . . 10
  - 2.3.1 Osteoarthritis Characterisation . . . 10
  - 2.3.2 Trapeziometacarpal Osteoarthiritis Classification . . . 12
- 2.4 Local anesthesia . . . 13
- 2.5 Conclusion . . . 14

3 Technological Background 15
- 3.1 Sensors . . . 15
  - 3.1.1 Capacitive . . . 16
  - 3.1.2 Resistive . . . 17
  - 3.1.3 Piezoelectric . . . 20
- 3.2 Signal transmission and processing . . . 22
- 3.3 Sensor Characterisation . . . 23
- 3.4 Sterilisation Techniques . . . 24
  - 3.4.1 Steam Sterilisation . . . 24
  - 3.4.2 Sterilisation via Hydrogen Peroxidase . . . 24
- 3.5 Regulatory Issues . . . 25
- 3.6 Conclusion . . . 26

4 State of the Art 27
- 4.1 Sensor Development . . . 27
  - 4.1.1 Piezorestistive . . . 27
  - 4.1.2 Capacitive . . . 30
  - 4.1.3 Piezoelectric . . . 31
  - 4.1.4 Fibre optic . . . 31

4.2 Medical Applications . . . 32
4.2.1 Trapeziometacarpal and Osteoarthiritis studies . . . 32
4.2.2 Other Joints studies . . . 34
4.3 Patents . . . 38
4.4 Conclusions . . . 38

5 Sensor Design **39**
5.1 Variables Definition . . . 39
5.1.1 Medical Factors . . . 40
5.1.2 Environmental Factors . . . 40
5.1.3 Signal Factors . . . 41
5.1.4 Economical Factors . . . 41
5.2 Sensor Design . . . 42
5.3 Prototype with Velostat . . . 44
5.3.1 Sensor Manufacturing . . . 44
5.3.2 Sensor Evaluation . . . 44
5.4 Prototype Screen Printing . . . 47
5.4.1 Screen Printing Definition . . . 47
5.4.2 Sensor Manufacturing . . . 47
5.4.3 Sensor Evaluation . . . 51
5.5 Conclusions . . . 52

6 Data Acquisition and Visualization **53**
6.1 Acquisition Electronic Circuit . . . 53
6.2 Data Acquisition (*Arduino*) . . . 56
6.3 Data Visualization (Android) . . . 58
6.3.1 Device connection . . . 58
6.3.2 Database . . . 59
6.3.3 Patient Data Form . . . 59
6.3.4 Data Visualisation and Events Recording . . . 59
6.3.5 Events Visualisation . . . 60
6.3.6 Export Data . . . 60

7 Conclusions and Future work **61**
7.1 General Conclusions . . . 61
7.2 Future Work . . . 62

A Final Sensors **63**
A.1 Face to face configuration . . . 63
A.2 Two layers configuration . . . 63

B Acquisition Circuit and PCB Schematics **65**
B.1 Acquisition Circuit Representation . . . 65
B.2 PCB Schematics . . . 66

C Arduino Code **67**

D Android Diagrams **71**
D.1 Android Activity Diagram 71
D.2 Android APP Screens 73
D.3 Database Structure 75

E Diagrams of complete system **77**
E.1 Component Diagram 77
E.2 Deployment Diagram 78

References **79**

List of Figures

2.1 Synarthrosis Joints . . . 3
2.2 Human body synovial Joint's representation . . . 4
2.3 Synovial Joint's representation . . . 5
2.5 Thumb configurations and movements . . . 7
2.6 Topography of the distal trapezial joint surface and motion arcs . . . 8
2.7 Osteoarthritis progression . . . 11
2.8 Kapandji Test . . . 13
2.9 Pictures taken during a prosthetic placement at CHLeiria . . . 13

3.1 Elements of a measuring instrument . . . 15
3.2 Capacitance sensor schematic representation . . . 16
3.3 Diaphragm-type sensor . . . 17
3.4 Potentiometer Interface Circuit . . . 18
3.5 FSR characteristic curves . . . 19
3.6 FSR circuit representation . . . 19
3.7 Equivalent piezoelectric sensor circuit . . . 21
3.8 PVDF sensor . . . 22
3.9 PVDF sensor circuits . . . 23
3.10 Medical Device Classification Scale . . . 25

4.1 Optic fibre pulse transmission in rest and with pressure applied . . . 32

5.1 Sensor Design Scheme . . . 39
5.2 Sensor Design Scheme . . . 40
5.3 Design Factors . . . 41
5.4 Superposition of sensors on the articular surface of the trapezium map . . . 42
5.5 Face to face sensor array circuit . . . 42
5.6 Two-layer sensor design . . . 43
5.7 Face to face unitary sensor . . . 44
5.8 Structure . . . 45
5.9 Graphical Representation of the sensor returning to the initial state after load removal 45
5.10 Pressure vs Resistance chart for Prototype with Velostat . . . 46
5.11 Graphical Representation Hysteresis Experiment for Prototype with Velostat . . . 46
5.12 Photosensibilization Results . . . 48
5.13 Proof print Results . . . 48
5.14 Face to face sensor array circuit . . . 48
5.15 Results from conductive printing . . . 49
5.16 Results from first layer of piezoresistive printing . . . 50
5.17 Results from second layer of piezoresistive printing . . . 50

5.18 Pressure vs Resistance chart for Screen Printing Prototype 51
5.19 Graphical Representation Hysteresis Experiment for Screen-printed Prototype . . 52

6.1 Acquisition Circuit Representation 53
6.2 Amplifier with a voltage divider 54
6.3 Inverting Amplifier 55
6.4 Face to face sensor array circuit 55
6.5 Arduino Activity Diagram 56
6.6 Android Activity Diagram 58
6.7 Patient Data Form 60
6.8 Aquisition Screen 60

A.1 Face to face sensor array circuit 63
A.2 Two layer sensor array circuit 64

B.1 Acquisition Circuit Representation with all the components 65
B.2 PCB circuit without ground plane 66
B.3 PCB circuit 66

D.1 Android Activity Diagram 71
D.2 Main screen 73
D.3 Menu 73
D.4 About 73
D.5 Patient Information 73
D.6 Device connection 74
D.7 Data Visualisation and Events Recording 74
D.8 Results Visualisation 74
D.9 Export Data 74
D.10 Database Structure 75

E.1 Component Diagram 77
E.2 Component Diagram 78

List of Tables

2.1 Differences between average surface areas between men and women 9
2.2 Average surface areas differences between health and OA hands 9
2.3 Proximity areas for healthy and OA trapezium and MC1 9
2.4 Average curvatures calculated along the dorsal-volar and radial-ulnar axes of the MC1 and trapezium in OA and healthy groups. Positive sign convex curvature and negative sign concave curvature 10
2.5 Kapandji Test Movements Description 13

4.1 Lapin Studies 35
4.2 Lower Limb studies using sensors 36
4.3 Upper Limb studies using sensors 37
4.4 Patents Labels 38

5.1 Correspondence between lines and columns for both prototypes 43
5.2 Pressure vs Resistance values for Prototype with Velostat 46
5.3 Values for Hysteresis Determination Experiment on Prototype with Velostat . . . 46
5.4 Parameters used during screen printing 49
5.5 Sensor resistance values without charges applied and with the maximum charge applied 51
5.6 Pressure vs Resistance chart for Screen Printing Prototype 51
5.7 Values for Hysteresis Determination Experiment on Screen Printing Prototype . 52

Acronyms and Symbols

Bluetooth Low Energy	BLE
Carbon nanotubes	CNT
Cylindrical oxide	GO
Ethylene Vinyl Acetate	EVA
First metacarpal bone	MC1
Force sensing resistor	FSR
Indium gallium zinc oxide	IGZO
Laser-induced graphene	LIG
Linear disciminant analysis	LDA
Operating Room	OR
Osteoarthiritis	OA
Peracetic acid	PAA
Plastic optical fiber	POF
Poly(3,4-ethylenedioxythiophene)	PEDOT
Polyacrylamide	PAM
Polydimethylsiloxane	PDMS
Polyethylene terephthalate	PET
Polypropylene	PP
Polystyrene sulfonate	PEDOT:PSS
Polyvinyldifluoride -trifluoroethylene	P(VDF-TrFE)
Polyvinylidenefluoride	PVDF
Principal Components	PC
Printed Circuit Board	PCB
Statistical shape model	SSM
Thin-film transistors	TFT
Titania nanolayers	TNL
Trapeziometacarpal	TMC
Wide Awake Local Anaesthesia No Tourniquet	WALANT
World Health Organization	WHO

Chapter 1

Introduction

1.1 Context

Since 2000, life expectancy has increased six years worldwide, which is a clear indicator that people live longer [1]. However, our organism is not adapting at the same velocity as molecular and cellular damage continue to occur at the same velocity as before, leading to a growing risk of degenerative diseases.

During the biological evolution, the human being has been specialising and perfecting the fine motricity of the hand. This specialisation resulted in the ability to perform the handgrip, different hand clamps and increased the range of their movements such as pronation and supination. These movements and characteristics are biomechanically complex. The trapeziometacarpal joint is the key to this process. Due to its continuous use for most daily life activities, the trapeziometacarpal joint is subject to mechanical degeneration processes such as the trapeziometacarpal (TMC) osteoarthritis (OA) that has a very significant prevalence in women under 60 years old.

There are several approaches to treat and prevent trapeziometacarpal osteoarthritis in its different stages and evolution. However, there is no medical consensus regarding the distinct therapeutic approaches contrary to what happens for the other joints. This gap occurs due to the difficulty of carrying out a practical and in vivo translation of the biomechanical knowledge acquired at the laboratory level.

1.2 Motivation

Due to the lack of medical consensus regarding the different therapeutic approaches, there is a need to deepen the biomechanical knowledge of the intrinsic changes of the trapeziometacarpal joint in vivo during the performance of several movements. Besides, there is also a need to understand the different circumstantial, temporal and functional biomechanical changes during the degenerative joint evolution.

[1] https://www.who.int/data/gho/data/indicators/indicator-details/GHO/life-expectancy-at-birth-(years)

This knowledge may allow the adaptation and personalisation of the different surgical techniques recommended in the literature, adjusted to the stages of degenerative joint evolution. Besides that, it can enable the improvement and maximisation of the functional results obtained during surgical interventions.

There are no devices on the shelf with the desired characteristics approved by regulatory bodies such as INFARMED and FDA for use in patients in a surgical setting and intra-articularly. In addition, the sensor arrays and unitary sensors on the market are either very expensive or inadequate for this dissertation. Therefore, it became necessary to develop a sensor array that fits the needs of the proposed challenge.

1.3 Goals

The main goals of this project are: identify, modify and or develop sensors and their associated software indicated for pressure and the contact area measurement between the joint surfaces of the trapeziometacarpal joint, per-operatorily.

1.4 Outline

In addition to the Introduction 1, this dissertation contains seven more chapters. Chapter 2 describes the anatomical background necessary to understand some of the options taken during the development of the project

Chapter chapter 3 presents a technological overview and summarises the acquisition conditions under which the system operates such as how the sensor can be sterilised and its classification as a medical device.

Furthermore, chapter 4 describes the state of the art of technologies used for developing flexible pressure sensors and sensors used for joints studies.

Chapter 5 refers to the sensor variable definitions that determine sensor's configuration and characteristics. Beyond that, it also presents the sensor design, the materials to be used and the manufacturing techniques. The evaluation of the sensors is also presented in this chapter.

Besides the sensor development, it is necessary to develop the electronic circuit to acquire and visualise the sensor data. This system is explained at chapter 6.

Chapter 7 presents a brief conclusion on the work carried out during this project.

Finally, there are four appendices (Chapters A-E) that contain additional information that can be useful for a better understanding of the developed work such as the final sensor design, the acquisition circuit and the printed circuit board (PCB) at a larger scale and more information about the Android APP and the relations between all components in the system.

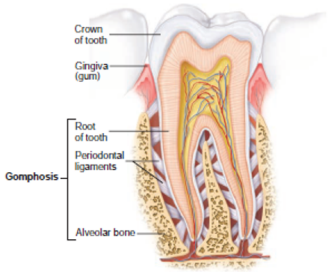
Chapter 2

Anatomical Background

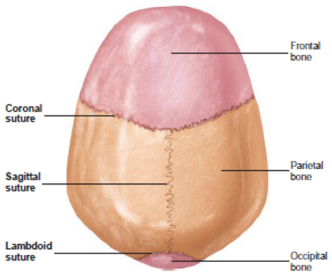
2.1 Joints

Joints are body regions where two or more bones convey. Their main functions are allowing growth and movement between bones. They are classified regarding their mobility or the nature of the intervening soft tissues (synovial). Due to the joint's complexity, it is necessary to use both classifications [99].

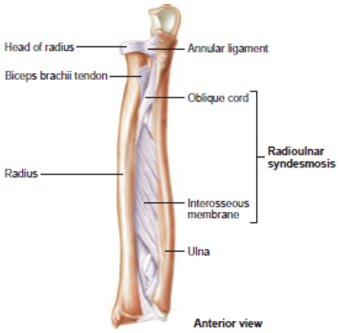
A synarthrosis joint occurs when the movement is restricted. These joints can be divided into fibrous and cartilaginous. Fibrous joints have connective tissues joining the bones. They can be of two subtypes: gomphosis (Figure 2.1a), sutures (Figure 2.1b) and syndesmoses (Figure 2.1c). Cartilaginous joints can be synchondrosis (Figure 2.1d) or symphysis (Figure 2.1e). When bones fuse, synostosis occurs [96].



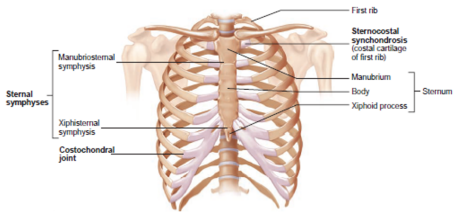
(a) Gomphosis Joint



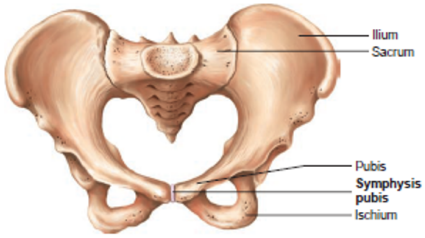
(b) Suture Joint



(c) Syndesmose Joint



(d) Synchondrosis Joint



(e) Symphysis Joint

Figure 2.1: Synarthrosis Joints retrieved from [96].

The most common type of joints in the human body have synovial in their constitution and have free movement, for this reason, they are named synovial or diarthrosis joints. Their articular surfaces are covered with smooth (hyaline) articular cartilage and synovial fluid. They vary in terms of the number of axes, articular planes, and articular surfaces' geometry [96, 99].

The classification of the joints is determined by the shape of the articular surfaces. They are pivot, hinge, saddle, plane, condyloid, and ball-and-socket joints. An example of each joint, and associated articular planes, shown at Figure 2.2 [99].

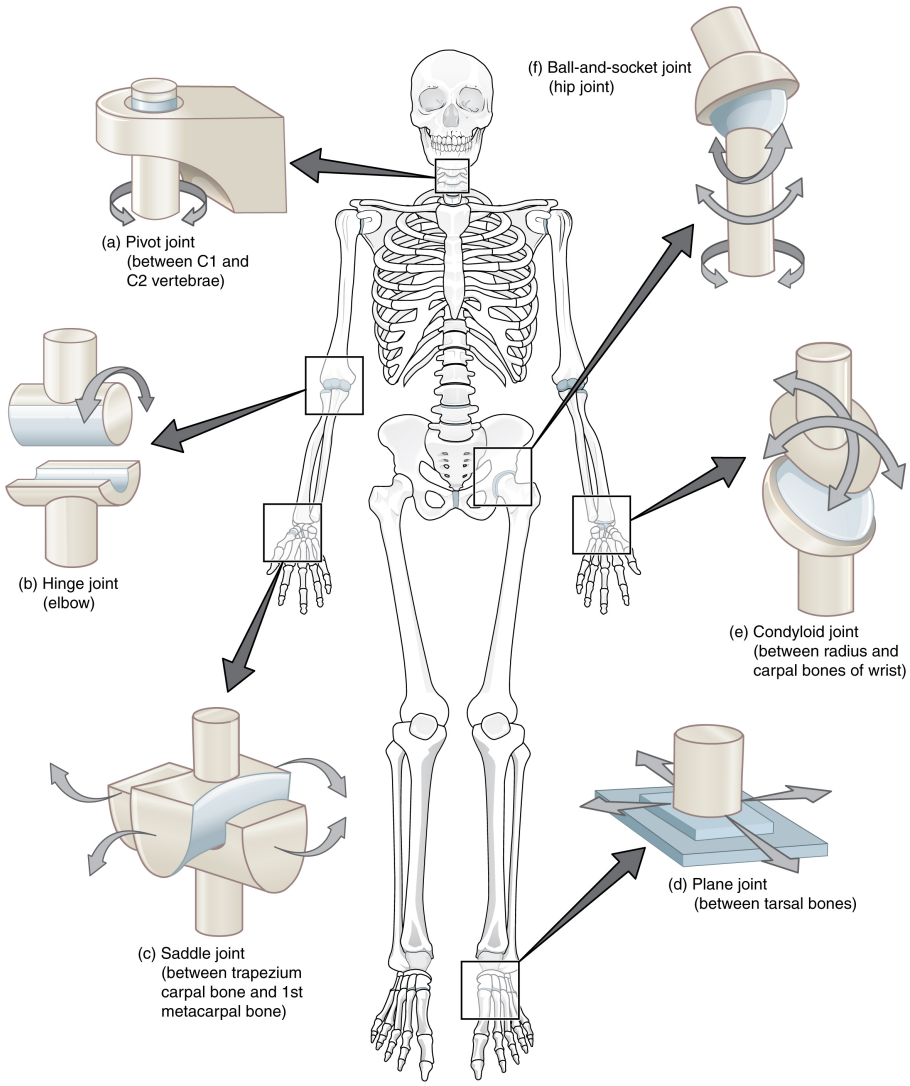


Figure 2.2: Human body synovial Joint's representation retrieved from [10]

Joints, depending on their articular planes, can perform several movements: flexion/ extension, adduction/ abduction, pronation (internal rotation)/ supination (external rotation) and circumduction. Movements are described regarding the axes number where the movement occurs: uniaxial, biaxial and multiaxial.

Synovial joints are characterised by a smooth (hyaline) cartilage, which covers the articulating bone surfaces and a viscous synovial fluid that serves as a lubricant and reduces the friction

between bones. Besides that, they also have a fibrous capsule composed of intrinsic ligamentous thickenings. The synovial membrane and the fibrous capsule form the joint capsule.

Despite those components, the joint can also include others, such as internal or external accessory ligaments responsible for the diarthrosis' stability. The joint cavity can be extended beyond the joint cavity recurring to bursas [99]. A schematic representation of the joint can be observed in Figure 2.3.

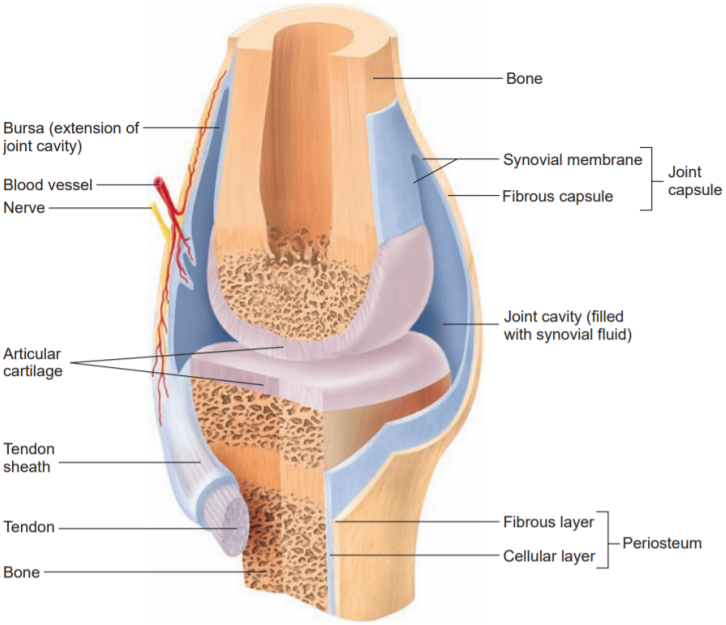


Figure 2.3: Synovial Joint's representation retrieved from [96].

Synovial joints are systematically described with the following aspects: name, bones involved, classification, articular surfaces, and their geometry, types of capsules, ligaments and movements [96].

2.2 Trapeziometacarpal Joint

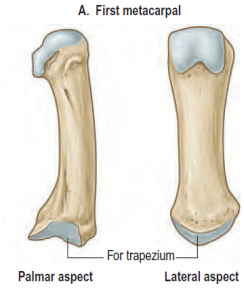
The trapeziometacarpal joint is fundamental for thumb flexibility and mobility and $40-50\,\%$ of the hand usefulness [69, 101]. Therefore, the thumb is a crucial element of the hand, representing a disability level of up to $26\,\%$ in case of thumb loss according to Committee on Legal Affairs and the Internal Market of the European Parliament [81]. Then, it is necessary to understand the joint biomechanics and the influence of OA.

2.2.1 Anatomical Description

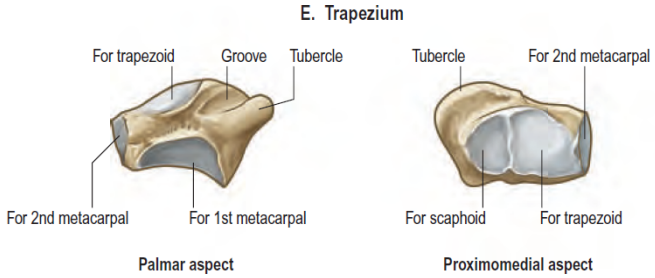
The trapeziometacarpal joint can be classified as a biconcave saddle joint between the distal surface of trapezium and the proximal surface of the first metacarpal.

The first metacarpal (MC1) (Figure 2.4a) is a long bone, independent from the other metacarpal bones and it is composed by head, body and base. The base is concavo-convex, and the articular surface with the trapezium.

The trapezium (Figure 2.4b) is one of the bones from the distal carpal row and is an irregular bone. This bone is a parallelepipedic bone with six sides [99, 91]. The palmar/volar side is laterally limited by a tubercle. There is also a dug with a groove where the tendon of flexor carpi radialis (FCR) is inserted. The dorsal side is elongated and rough and is characterised by the presence of tubercules for dorsal ligaments insertion. The trapezium has a small, proximal articular surface with a slightly concave facet with the scaphoid. The distal face has large sellar articular surface along the radioulnar axes with the first metacarpal in the concave face (mediolaterally). Besides, it also has a convex face along the dorsal-volar axes (anteroposteriorly). The lateral side is a rough large surface for radial collateral ligament and capsular ligament of the thumb carpometacarpal joint. The medial side has two articular surfaces: a concave articular surface for the trapezoid and other for the second metacarpal distally.



(a) First metacarpal bone representation



(b) Trapezium bone representation

Figure 2.4: Bones involved in TMC joint retrieved from [20]

The articular surface incongruence allows thumb mobility and flexibility. However, the articular surfaces are very unstable allowing joint to sublux during pinch and grasp [48].

This joint has lateral ligaments that converge from the lateral surface of the trapezium to the radial side of the metacarpal base. Besides, there are also palmar and dorsal ligaments that are oblique bands and converge to the ulnar side of the metacarpal base from the palmar and dorsal surfaces of the trapezium, respectively [99].

There are sixteen different ligaments stated in the literature as belonging to the TMC joint however, only five are primary stabilisers of TMC joint that form the ligamentous complex [59].

The dorsal radial ligament is the strongest and thickest ligament that allows thumb resistance to the dorsal dislocation. There is an insertion of the ligament on the radial base of the thumb first metacarpal and dorsal trapezium. The posterior oblique ligament is a capsular ligament that originates on the dorsal side of the trapezium and inserts in the dorsoulnar aspect of the first metacarpal. The volar anterior oblique ligament resists to the opposing force to abduction, extension and pronation and it is inserted on the distal trapezial tubercule and the ulnar base of the

thumb metacarpal. The ulnar collateral ligament is extracapsular, originated from the distal and ulnar margin of the flexor retinaculum insertion onto the trapezial ridge. Finally the intermetacarpal ligament is extracapsular, it arises from the dorsal radial aspect of the second metacarpal and runs towards the volar-ulnar until insertion into the first metacarpal base [59, 77].

The loss of the strong structure of accessory ligaments and connective tissue or the alteration of the properties are intrinsically related to the OA degeneration process that is described at Section 2.3 contributing to the stability loss.

Stability is also influenced by some other factors such as gender, age, population, hormonal factors. Therefore, it is important to understand TMC joint morphology variations with those factors and to OA.

Trapeziometacarpal joint is involved in the performance of several movements that are crucial for the daily living such as abduction, adduction, extension, flexion, opposition and circumduction (Subfigures 2.5a, 2.5b, 2.5c, 2.5d). These movements allow the execution of some daily activities such as jar twist, power grasp and key pinch (Subfigures 2.5e, 2.5f, 2.5g) [53].



(a) Abduction



(b) Adduction



(c) Extension



(d) Flexion



(e) Jar Twist



(f) Jar grasp



(g) Key pinch

Figure 2.5: Thumb configurations and movements

Flexion and medial rotation are linked due to to the shape of the articular surfaces and to the obliquity of the dorsal ligament. Despite ligaments and bones, muscles are crucial during movement execution. During flexion, flexor pollicis brevis and opponens pollicis, aided by flexor pollicis longus are activated. The extension is achieved by abductor pollicis longus and extensors pollicis brevis and longus. Abduction is produced by abductors pollicis brevis and longus

and adduction is produced by adductor pollicis. During opposition, opponens pollicis and flexor brevis pollicis simultaneously flex and medially rotate the abducted thumb. Interpulpal pressure, or that generated by digital grasping, is increased by adductor pollicis and flexor pollicis longus. Circumduction is produced by extensors, abductors, flexors and adductors acting consecutively in this, or reverse, order [99].

During this type of movements, articular area change, therefore, the pressure is exerted in different regions creating proximity patterns. During abduction and adduction and neutral posture and lateral key pinch, MC1 proximity area changes from radial to volar-ulnar, but the trapezium pattern remains constant. From extension to flexion, the proximity area of the trapezium is shifted from dorsal-radial to volar-ulnar, with the MC1 articular surface remain the same. In adduction, flexion and lateral key pinch, proximity areas of both bones as misaligned [20]. The distal trapezial joint surface and motion arcs are represented at Figure 2.6.

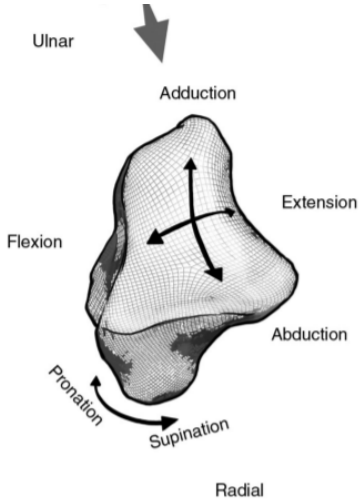


Figure 2.6: Topography of the distal trapezial joint surface and motion arcs retrieved from [59]

2.2.2 Dimensions of bones

Several three-dimensional (3D) computer models studies have determined the areas of articular surface and proximity, joint curvatures and total translations. Kovler et al.[58] performed studies in male and female cadaveric hands. Specimens with middle degeneration were considered healthy and those with moderate and severe degenerated hands.

D'Agostino [20] performed in vivo studies to understand OA degeneration patterns in the articular surfaces comparing healthy and OA surfaces in female volunteers older than 50 years. Two groups were selected: one without signals of OA and the other with patients diagnosed with a higher disease stage (Eaton-Litt Stage III-IV). This study is crucial as it is one of the first studies that compare contact biomechanics of the TMC joint in healthy and late-stage OA participants.

2.2.2.1 Articular Surface Area

In the first study, Klover et all. [58] concluded that degenerated male trapezial articular facets ($197.30\,mm^2$) are larger than females in the same conditions ($160.50\,mm^2$). The same occurs for the first metacarpal joint, and trapezial radial, ulnar recesses and metacarpal volar recess. This information is summarized at Table 2.1.

	Areas of Trapezial facet and recesses (mm^2) **(mean $\pm$ SD)**			**Areas of First Metacarpal facet and recesses** (mm^2) **(mean $\pm$ SD)**	
	Main Facet	**Radial Recess**	**Ulnar Recess**	**Main Facet**	**VolarRecess**
Male	197.30 ± 14.56	24.76 ± 7.16	23.77 ± 9.11	239.66 ± 26.03	32.12 ± 10.43
Female	160.50 ± 13.36	20.84 ± 3.72	13.68 ± 2.76	184.51 ± 19.28	21.52 ± 12.10

Table 2.1: Differences between average surface areas between men and women

In d'Agostino study [20], articular areas for the trapezium and first metacarpal for the healthy group are smaller than the OA group. In the healthy group, the articular area of MC1 was larger than trapezium, while in the OA the difference was not significant (Table 2.2). Generally, standard deviation values are higher in the OA group due to differences in OA progression. These values are congruent with the OA degeneration process described in Section 2.3. These values are important in order to define the sensor measuring area.

	Articular areas of Trapezium (mm^2)	**Articular areas of MC1** (mm^2)
Healthy	128	135
OA	267	283

Table 2.2: Average surface areas differences between health and OA hands

Other studies, such as Cheema et al. [15], corroborate these values. The minimal joint space is the minimum distance between the two closest vertices between the proximal articular facet of MC1 and the distal facet of the trapezium [20].

For healthy cartilage, the physiological space of the joint is the thickness of the MC1 and trapezium cartilage layer (1.5 mm). The set of MC1-trapezium points with a Euclidean distance below this value belongs to the proximity area [20].

Proximity areas are smaller in the OA group than in the healthy group. In the OA group, due to the space narrowing characteristic from the disease, the minimal joint space is close to zero in almost all configurations. The proximity areas for healthy and OA joints are represented at Table 2.3. In the healthy group, neutral, adduction, extension and lateral pinch configurations are smaller than during the abduction, flexion, power grasp and jar twist configurations.

	Trapezium (mm^2)	**MC1** (mm^2)
Healthy group	190.3	188.3
OA group	58.5	58.6

Table 2.3: Proximity areas for healthy and OA trapezium and MC1

2.2.2.2 Proximity patterns and joint curvature

Joints can perform several tasks as described in Section 2.2.1, that is achieved due to a change of bone configurations. Therefore, it is possible to determine proximity patterns during the seven configurations: abduction, adduction, extension, flexion, key pinch, jar grasp and neutral. As space narrowing occurs due to OA, there is no significant difference in the proximity patterns between configurations. In the healthy group, task-dependent proximity is observed.

Curvatures were also analysed to understand the OA influence. As it is possible to observe through Table 2.4, in the dorsal-volar axes, the convexity of the trapezium is flatter for the OA group. The MC1 curvature changes from concave to convex. In radial-ulnar axes curvatures are distinct which does not allow comparisons. Female bones are usually smaller than males and have

		Curvature OA (mm^{-1})	**Curvature Healthy** (mm^{-1})
Dorsal-volar	MC1	-0.03±0.03	0.02±0.05
	Trapezium	0.16±0.03	0.06±0.05
Radial-Ulnar	MC1	0.11±0.05	0.14±0.04
	Trapezium	-0.01±0.07	-0.07±0.07

Table 2.4: Average curvatures calculated along the dorsal-volar and radial-ulnar axes of the MC1 and trapezium in OA and healthy groups. Positive sign convex curvature and negative sign concave curvature

a lower congruence which results in a smaller area of contact pressure [54, 95]. The smaller the bones, the lower the moment of the associated muscles and a greater force is required for the same activity (opening a jar for example) when compared to a joint with a higher aspect ratio (length to width) [95]. This may lead to excessive joint laxity and the development of premature joint degenerative changes when repetitive activities occur [52, 27].

2.2.2.3 Forces at TMC joint

Regarding forces, biomechanical studies verified that forces increase exponentially from the tip of the thumb to the TMC joint with grasp and forceful pinch. The joint reactive force at the base of the thumb is twelve times greater than that generated at the tip of the thumb with a lateral pinch, and compressive forces of as much as 120 Kg may occur at the trapeziometacarpal joint with forceful grasp [59]. The pressures observed at this joint are generally in the range $60 - 700$ KPa [15].

2.3 Osteoarthritis

2.3.1 Osteoarthritis Characterisation

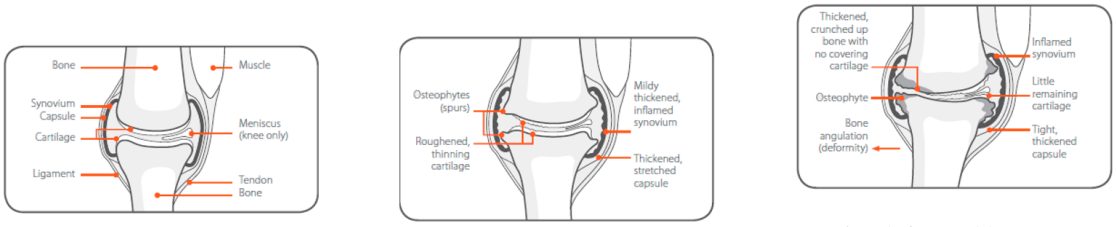
According to the World Health Organisation (WHO), osteoarthritis (OA) is the most frequent pathology that affects the articular cartilage[1]. This pathology affects 500 million people world-

[1] https://www.who.int/chp/topics/rheumatic/en/

wide[2]. This number tends to increase in the next few years due to the increase in life expectancy and other factors such as obesity, genetics, among others. This disease has a higher prevalence in middle age and older people. WHO estimates that 80 % of those with osteoarthritis will have limitations in movement, and 25 % will lose their ability to perform daily activities[3]. Hip, knee, foot, ankle and wrist joints are the most affect joints.

This pathology is characterised by a progressive loss of the articular cartilage and subchondral bone sclerosis. Joint changes through time are represented in Figure 2.7.

During disease evolution, cartilage roughens and becomes thinner. A cartilage surface is fragmented, clone chondrocytes, vertical clefts in the cartilage. Bone articular faces thicken and grow with the formation of spurs osteophytes and a gap between bones narrow. The inner layer joint capsule (synovium) thickens and produces excess fluid, leading to joint swelling with the contraction and thickening of the capsule and ligaments. In the later stages of the disease, the loss of cartilage causes the bones to rub against each other and wear them out. This swelling inhibits complete muscle activation associated with the joint (arthrogenous inhibition) which, combined with lack of use, leads to muscle weakness and atrophy.



(a) Normal Joint

(b) Joint with mild osteoarthritis

(c) Joint deformed by severe osteoarthritis

Figure 2.7: Osteoarthritis progression

OA has several symptoms: joint pain, stiffness, and movement limitation and several degrees of local inflammation. Depending on the severity of disease and joint's type, OA has a strong impact in daily life. The lack of mobility, fatigue and sleep deprivation are strong consequences which leads to a decline in quality of life.

According to the European League Against Rheumatism, these symptoms associated with established methods, such as radiographic changes are used to diagnose OA depending on the joint type. TMC OA is the second most common type of OA in the hand and when prevalent strongly impairs hand function. In Portugal, according to EpiReuma, there is a higher prevalence of OA in women (13.8 %) than men (3.2 %).

In a recent study from Johnston County Osteoarthritis Project and used by the American Arthritis Foundation in 2020, the risk of developing symptomatic hand OA is higher than the Portuguese study, with a risk percentage of 47 % for women and (25 %) for men [7, 86].

Risk factors depend on the joint type and disease stage, nevertheless, some common factors increase the disease development. OA can be caused by damage to the joint due to repeated and

[2] https://www.oafifoundation.com/en/what-is-osteoarthritis/
[3] https://www.who.int/chp/topics/rheumatic/en/

excessive load in the joint over time (repetitive and physically demanding work) or an injury. Besides, there are several risk factors including joint abnormalities, genetic factors, ageing, obesity, bone density and gender. According to NHS[4] the major symptoms regarding thumb osteoarthritis, include stiffness, painful and swollen finger and, sometimes, a bump at the base of your thumb might occur. Opening jars, turning keys or writing are tasks that may become harder with this disease.

2.3.2 Trapeziometacarpal Osteoarthiritis Classification

The Eaton-Litter classification system is the most common method for OA classification and is based on lateral radiograph analysis of synovitis, joint space and capsular laxity. In fact, this is a four stages classifier being the Stage 1 the healthiest stage and stage 4 the most severe stage.

In Stage I, the joint articular contours are normal, there is no evident joint space narrowing, cyst formation and subchondral changes. The subluxation of the joint is smaller than 1/3. Stage II presents a significant capsular laxity and osteophytes with a diameter smaller than 2 mm adjacent to the dorsal and volar facets of the trapezium. The subluxation of the joint is visible (1/3).

Stage III and IV are the most severe stages of the disease.In Stage III, subluxation, and osteophytes ($> 2\,\text{mm}$) increases, a joint space narrowing occurs.Stage 4, the most severe, presents a very narrow joint space, changes in the cystic and sclerotic subchondral bone and a major subluxation of the joint.

Besides the Eaton-Stage method, patient history of pain and dysfunction is essential to understand the pathological impact on patient life. Grind test, metacarpal flexion, metacarpal extension and pressure-shear tests, and total opposition test (Kapandji score) are also used access hand functionality and determine the most suitable treatment. The Kapandji score is a 10-degree scale, based on the ability of the patient to touch with the tip of the thumb in several locations of the hand [53]. These locations and the score are represented in Figure 2.8 and systematised in Table 2.5.

In the more advanced stages of the disease, the only solutions for life quality improvement are surgical options. The most common options are osteotomy, the placement of a total TMC prosthesis and trapeziectomy with or without ligament reconstruction [77, 84].

Patients who will be selected for the trial will mostly be subjected to the first surgical technique, however, if the trial criteria are extended there may be patients whose pathological evolution requires one of the other surgical techniques.

[4] https://www.nhs.uk/conditions/osteoarthritis/symptoms/

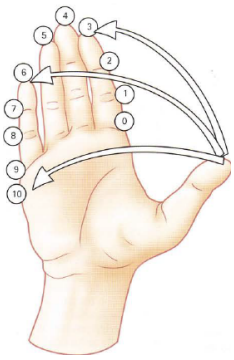


Figure 2.8: Kapandji Test retrieved from [53]

Score	Location
1	Radial side of the proximal metacarpal of the index finger
2	Radial side of the middle metacarpal of the index finger
3	Tip of the index finger
4	Tip of the middle finger
5	Tip of the ring finger
6	Tip of the little finger
7	Distal interphalangeal joint crease of the little finger
8	Proximal interphalangeal joint crease of the little finger
9	Metacarpophalangeal joint crease of the little finger
10	Distal palmar creased

Table 2.5: Kapandji Test Movements Description

2.4 Local anesthesia

At Centro Hospitalar de Leiria (CHLeiria), hand OA related surgeries are performed under a novel anaesthesic technique named as WALANT (Wide Awake Local Anaesthesia No Tourniquet). This anaesthesic technique gives patient a full control of his/her hand without feeling the inherent pain.

In this technique, two drugs common drugs are administered: lidocaine and epinephrine. The former blocks the pain and is used as an anaesthetic, while latter is a vasoconstrictor controlling the bleeding. Theses medications are used during dental procedures and do not require preoperative test or monitorization. Furthermore, as the patient is awake during the surgery, he/she can perform movements which allow the surgeon to adjust tendons and bones or even the prosthesis after observing the executed movements as it is possible to observe in Figures 2.9 that were taken during a prosthetic placement at CHLeiria. Additionally, post-operatory precautions can be explained during the procedure [60].



(a) First movement example (b) Second movement example (c) Third movement example

Figure 2.9: Pictures taken during a prosthetic placement at CHLeiria

During pre-operatory preparation, the patient is injected with 7 mg of 1 % lignocaine with 1:200000 adrenaline per Kg and 2 mg of 0.5 % bupivacaine per Kg at the regions where the surgery will be performed [11]. The surgical procedure can start 15-20 minutes later. If necessary, during the procedure more anaesthesic solution can be administered.

Sedation is only necessary for the patient to tolerate the discomfort caused by the tourniquet and anaesthesia. Besides, sedation is the most expensive part of the surgery and might be critical for patients with associated pathologies such as diabetes or pulmonary diseases [60]. Furthermore, this surgical technique allows freeing up the opeating room (OR) for more complex procedures.

2.5 Conclusion

This chapter focused on the main anatomical concepts regarding joints and the description of the TMC joint, in particular its anatomical description, its dimensions and particular characteristics. In addition, OA was also analysed as it affects the articular cartilage and prevents the normal functioning of the joints. There is also presented a a brief list of the most common surgeries and a explanation of the new anaesthetic technique allows the patient to execute the movements, which allows them to understand, still in the operating room, the results of the surgery.

This chapter is important to understand the purpose of which the sensor will be developed and the definition of some sensors' characteristics such as dimensions, range of forces that will be measured.

Chapter 3

Technological Background

The main goal of this dissertation is the development of a device to measure forces/pressure and contact area per-operatively and in-vivo in the TMC. Therefore, it is necessary to select not only the sensor but also the signal processing, transmission and output display and recording [78]. A schematic representation of the elements of a measuring instrument is available in Figure 3.1. Therefore, this chapter will present the available solutions.

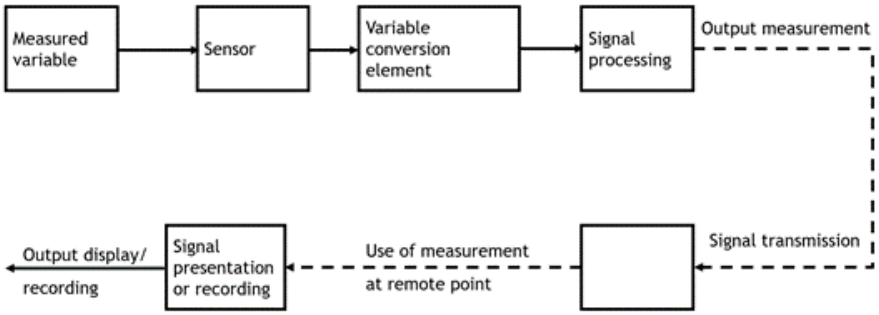


Figure 3.1: Elements of a measuring instrument adapted from [78]

3.1 Sensors

A sensor converts the mechanical measurand (force/pressure) to an electrical property when placed in an interface with the living tissue. For pressure sensors, there are three types of outputs available: resistance, capacitance and charge.

Regarding the operating mode, sensors can be signal modulators (passive) or signal generators (active). The first type of sensors needs an energy source in addition to the measurand such as resistive, inductive and capacitive. The second type of sensors, otherwise, outputs the electrical signal without another type of energy sources, some examples are thermoelectric, piezoelectric, photoelectric, among others.

For pressure measurement, three types of sensors are suitable: capacitive, resistive, and piezoelectric.

3.1.1 Capacitive

A capacitive sensor consists of two parallel conductive plates separated with air or another medium between them (Figure 3.2). When an external load is applied, the dielectric thickness decreases, which results in a change of capacitance. Assuming ε_0 is the relative dielectric constant in the free space, ε is the dielectric constant of the insulator, A the plate area and d the plate distance, Equation 3.1 represents this event [112].

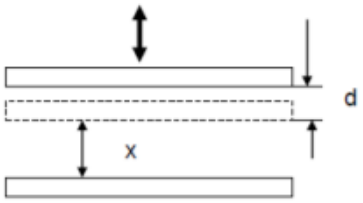


Figure 3.2: Capacitance sensor schematic representation retrieved from [112]

$$C = \varepsilon_r \varepsilon_0 \frac{A}{d} \tag{3.1}$$

This type of sensor can be used with magnitudes capable of causing variations in any of the parameters A, d and ε. Distance between plates is used for pressure and force measurements.

3.1.1.1 Distance variation between plates

In this particular case the capacity after displacement is given by:

$$C_{initial} = \varepsilon \varepsilon_0 \frac{A}{d} \tag{3.2}$$

$$C_{\Delta} = \varepsilon \varepsilon_0 \frac{A}{d+x} \tag{3.3}$$

$$C_{initial} - C_{\Delta} = \varepsilon \varepsilon_0 A \left(\frac{1}{x} - \frac{1}{x+d}\right) = \frac{\varepsilon \varepsilon_0 A}{x} \frac{d}{(x+d)} \tag{3.4}$$

The sensitivity K of the capacity sensor to the variations in the distance between plates is given by Equation 3.5:

$$K = \frac{\Delta C}{\Delta x} = -\varepsilon_0 \varepsilon \frac{A}{x^2} \tag{3.5}$$

Generally, capacitive sensors for pressure or force measurements are a diaphragm-type device (Figure 3.3). The diaphragm displacement (z) is determined by measuring capacitance variation

between the diaphragm and the metal plate that is nearby. The diaphragm deformation decreases the capacitance and can be quantified through Equation 3.6 [78], where S is the radial stress, p the pressure applied, r diaphragma radius.

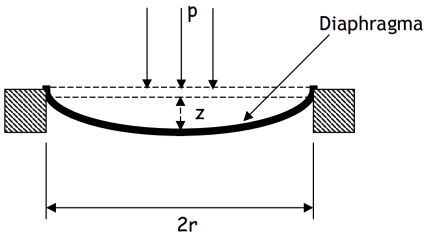


Figure 3.3: Diaphragm-type sensor retrieved from [112]

$$C = \frac{r^2 p}{4S} \tag{3.6}$$

These type of pressure sensors have a simple structure, are easily fabricated, highly sensitive and low cost. However, there are some disadvantages such as the need for a complex electronic circuit and the presence of hysteresis and non-linear output signal [3].

3.1.2 Resistive

Resistive sensors are based on the resistive principle, therefore, the measurand causes a change in the resistivity or in one or more geometric factors. In order to understand the mechanism it is important to understand the principle behind.

Considering a homogeneous electrical conductor wire, the resistance R of the wire depends on the resistivity of the material ρ and the geometric factors of the wire, length l and cross section S (Equation 3.7):

$$R = \rho \frac{l}{S} \tag{3.7}$$

In a resistive sensor, the mensurand is obtained directly and indirectly with the variation of the resistance. According to the Ohm's Law (Equation 3.8), it is possible to evaluate the resistance variation through the measurement of the voltage or the electrical current:

$$V = V_b - V_a = RI \tag{3.8}$$

There are three main groups of resistive sensors for force or pressure measurements: potentiometers and extensometers and Force Sensing Resistors (FSR).

3.1.2.1 Potentiometers

Potentiometers are a piece of resistive material circular or linear, with two contacts at the end, and third sliding contact along the length. It can be made of metallic wire or film, conductive plastic, or ceramic material. It can be used as a position, displacement, or pressure sensor.

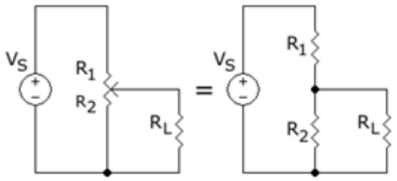


Figure 3.4: Potentiometer Interface Circuit from [112]

When a potentiometer is subjected to a constant electrical voltage in the end terminals and the voltage at the sliding contact is proportional to its position (Equation 3.9):

$$V_s = V\frac{Rb}{Ra} = V\frac{b}{a} \propto b \tag{3.9}$$

In order to read the output voltage (V_L), a load resistor (R_L) is usually introduced to the voltage divider circuit with the resistors R_1 and R_2 and the output voltage reading of the potentiometer (Equation 3.10) is obtained:

$$V_L = \frac{R_2||R_L}{R_1+R_2||R_L}V_S = \frac{R_2R_L}{R_1R_L+R_2R_L+R_1R_2}V_S \tag{3.10}$$

If R_L»R_2, then

$$V_L = \frac{R_2}{R_1+R_2}V_S \tag{3.11}$$

The resolution of this type of sensors depend on the type of construction. When the sensor is composed by resistive films, a continuous variation of the resistances is obtained, however when the resistance is obtained by coiled metal wire, the variation is discontinuous and consequently the resolution is dependent of the spacing between the turns of the winding.

3.1.2.2 Extensometers

Strain gauges are generally composed of a resistive material (metallic wire or deposited film or a semiconductor bar) bonded to a matrix connected to two terminals. When the strain gauge is compressed or pulled within the limits of elasticity its resistance varies due to variations in length, straight section and wire resistivity (Equation 3.12):

$$\frac{dR}{R} = (1+2\mu)\frac{dl}{l} + \frac{d\rho}{\rho} \tag{3.12}$$

In the Equation 3.12, the first part of the sum corresponds to the dimensional effect and the second to the piezoresistive effect. The measurement of displacements with strain gauges can only be done indirectly, associating them with a resistance bridge, with an external supply.

The piezoresistive pressure sensors are easily manufactured, have a high sensitivity, good sensitivity, long time stability, low noise, short response times and easy circuit interface and low cost. However, they are stiff and frail, present a nonlinear response, hysteresis and signal drift.

When the temperature piezoresistivity coefficient is high, the sensors performance is limited and temperature compensation methods must be used [3, 8].

3.1.2.3 Force sensing resistor

A Force Sensing Resistors (FSR) is a polymer thick film device, that exhibits a decrease in resistance with an increase in the applied force to the active surface. They can be used in dynamic measurement and only qualitative results are obtained [49]. The typical sensor characteristic curves are available in Figure 3.5.

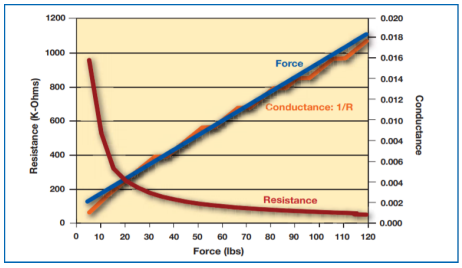


Figure 3.5: FSR characteristic curves retrieved from [76]

FSR is a piezoresistive sensing technology therefore, they are passive elements that functions as a variable resistor in an electrical circuit (R_{FSR}) (Figure 3.6). In a simple force-to-voltage conversion, the output can be described by the Equation [28], where V_{out} is the output voltage, V_+ is the input voltage, R_M is the fixed resistance.

$$V_{out} = \frac{R_M V_+}{R_M + R_{FSR}} \tag{3.13}$$

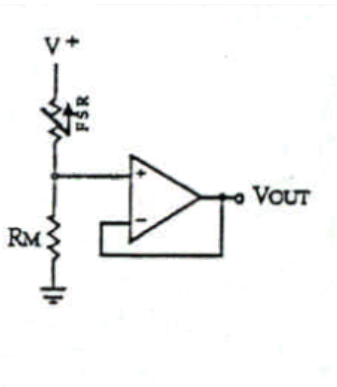


Figure 3.6: FSR circuit representation retrieved from [28]

Output voltage increases with the increasing force. These type of sensors are low-cost, of-the-shelf with a wide resistance range, high linearity, low drift and low power consumption [76].

3.1.3 Piezoelectric

A piezoelectric sensor is constituted by a disc of piezoelectric material placed between two plates of conductive material. The assembly is tightened rigidly and subjected to a pre-stressing. This pre-stressing is very important to ensure that the system functions both in compression and tension and a close contact between the plates and the piezocristal [112]. Piezoelectric materials generate an electric potential when mechanically strained, and conversely, an electric potential can cause physical deformation of the material.

When the crystal is distorted, a charge reorientation occurs, causing a displacement of negative and positive charges. These displaced charges induce surface charges of opposite polarity on opposite sides of the crystal. The surface charge is determined by the difference voltage between electrodes attached to the surfaces. Assuming an initial infinite leakage resistance, the total induced charge q is directly proportional to the applied force f. The proportionality constant k is the piezoelectric constant (Equation 3.14) [78]:

$$q = kf \tag{3.14}$$

If we assume that the system acts like a parallel-plate capacitor where the voltage v across the capacitor is charge q divided by capacitance C, the change in voltage is obtained with Equation 3.15.

$$\frac{kf}{C} = \frac{kfx}{\varepsilon_0 \varepsilon_r A} \tag{3.15}$$

Piezoelectric materials have high and finite resistance, due to that, when a static deflection is applied, the charge leaks through the leakage resistor. Therefore, the input impedance of the external voltage-measuring device must have a resistance value higher than that of the piezoelectric sensor [78].

The piezoelectric sensor can be described by the equivalent circuit represented at Figure 3.7 is helpful to understand and quantify dynamic-response characteristics of the sensor.

This circuit can be simplified by converting the charge generator to a current generator, i_s:

$$i_s = \frac{dq}{dt} \tag{3.16}$$

In the modified circuit and assuming that the amplifier does not draw any current:

$$i_S = i_C + i_R \tag{3.17}$$

$$v_o = v_C = \frac{1}{C}\int i_c dt \tag{3.18}$$

$$i_S - i_R = C\frac{dv_0}{dt} = K\frac{dx}{dt} - \frac{v_o}{R} \tag{3.19}$$

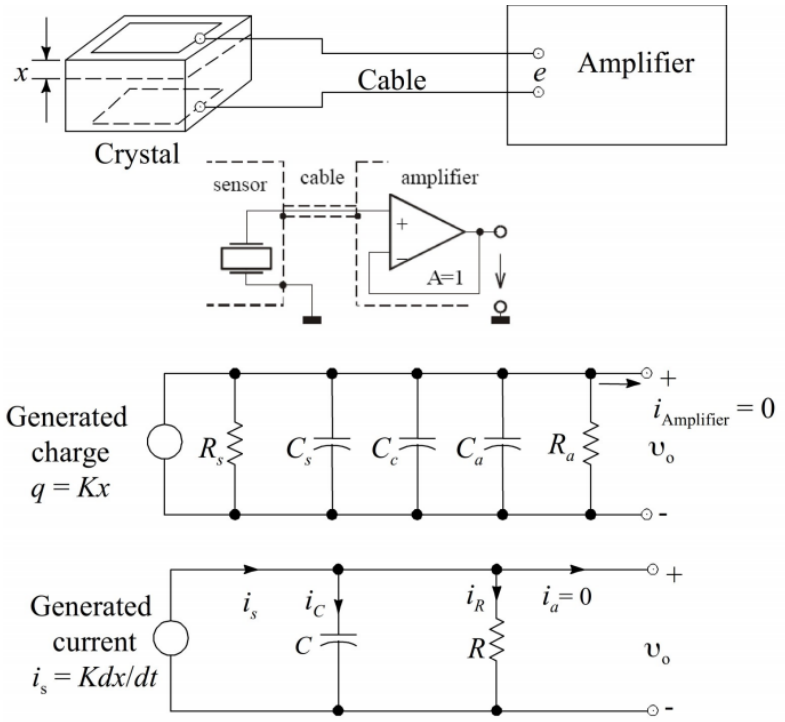


Figure 3.7: Equivalent piezoelectric sensor circuit retrieved from [112]

$$\frac{V_o(jw)}{X(jw)} = K_s \frac{jw\tau}{jw\tau + 1} \tag{3.20}$$

Where $K_s = K/C$ (sensitivity, V/m) and $\tau = RC$ (time constant) [78].

Miniaturized piezoelectric sensors are suitable for dynamic pressure sensor applications due to their impulsive output signals [46]. These sensores present a dynamic response with high bandwidth, but has some demerits such as temperature sensitivity and electronic connections not so robust [3].

3.1.3.1 Polyvinylidenefluoride sensor

Polyvinylidenefluoride (PVDF) is an inert chemical polymer that becomes piezoelectric when polarized in an electric field. A design for this type of sensors is available in Figure 3.8. This sensor cannot measure static pressures, because the load generated on the electrodes through the sheet voltage is slowly discharging.

When a pressure change is applied to the sensor, the PVDF film is deformed and, due to its piezoelectric properties, an electrical load and voltage is generated on the electrodes. The output signals can be measured by three types of circuits that are represented at Figure 3.9 [97].

In the first circuit (Figure 3.9a), there is a voltage divider that reduces the voltage, followed by a voltage follower with an input impedance of about 10 G . In this particular case, the output voltages are calculated as:

$$U_{out} = \frac{Q}{C_{PVDF}} \frac{R_2}{R_1 + R_2} \tag{3.21}$$

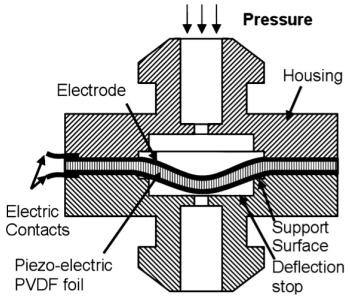


Figure 3.8: PVDF sensor retrieved from [97]

In the second circuit (Figure 3.9b), the capacitor C_0 is connected in parallel to the PVDF film and intends to reduce the output voltage followed by the voltage follower with an input impedance of about 10 G. The output voltages are calculated by:

$$U_{out} = \frac{Q}{C_0 + C_{PVDF}} \tag{3.22}$$

In the third circuit (Figure 3.9c), there is a charge amplifier (Figure 3.9c) and the output voltage is calculated as:

$$U_{out} = \frac{Q}{C_0} \tag{3.23}$$

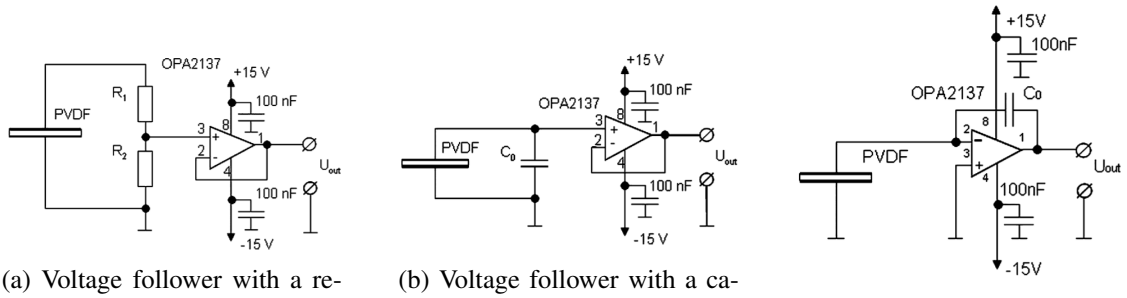
In the previous equations, C_{PVDF} is the capacitance of the PVDF film, Q the load generated by the PVDF film, C_0 the capacitance in the corresponding electronic circuit and R_1, R_2 are the resistances in the voltage divider. Experiments have shown that the second and third electronic circuits are more suitable for the pressure sensor than the first due to the leakage currents [97].

3.2 Signal transmission and processing

The measuring system is composed not only by the sensor, but also by an electronic device responsible to acquire and perform the initial processing. Therefore, the measured signal data will be transmitted to a microcomputer. A microcomputer can be used for calibration and signal processing, enhancing the reliability of the instrument. Besides, it is also possible to insert data necessary to the data processing as sometimes there are factors that influence the data interpretation such as age, gender, height and weight or even sensor characteristics. Some sensors are already sold with the microcontroller and the necessary signal processing. Therefore, in those cases, it is not necessary to build the circuit or understand the data acquisition process and it is only necessary to analyse the data.

Arduino boards have a microcomputers integrated. Arduino allows signal acquisition and signal output via input/ output pins. It is easily programmable and communicates with sensors following the I2C protocol through two signals the SDA-Serial Data and the SCL-Serial Clock.[1]

[1] https://store.arduino.cc/arduino-uno-rev3



(a) Voltage follower with a resistive voltage divider

(b) Voltage follower with a capacitor parallel to a PVDF film

(c) Charge amplifier

Figure 3.9: PVDF sensor circuits retrieved from [97]

The connection between the microcomputer and the device that performs data treatment and visualisation can be achieved in two different ways: through a direct connection or through a Bluetooth connection.

Bluetooth is a wireless technology that enables the connection and exchange of information between devices via a short-range radiofrequency. Depending on the objective two different types are available: the classic Bluetooth and the Bluetooth Low Energy.

The Classic version is designed for low power operation, can transmit data over 79 channels, supports data rates from 1 Mb/s to 3 Mb/s, and supports multiple power levels, from 1 mW to 100 mW, multiple security options, and point-to-point network topology.

The Bluetooth Low Energy (BLE) radio is designed for very low power operation, transmits data over 40 channels in the 2.4 GHz frequency band. Besides it supports data rates from 125 Kb/s to 2 Mb/s, multiple power levels, from 1 mW to 100 mW, as well as multiple security options up to government grade. This technology supports multiple network typologies, including point-to-point, broadcast and mesh networking. [2]

3.3 Sensor Characterisation

When designing a sensor it is important to understand the sensor behaviour and characteristics, therefore there are some parameters that must be analysed.

In order to describe the variation in the observations, measures of data dispersion such as standard deviation and coefficient of variation (CV) must be calculated. The range or span defines the minimum and maximum values of a quantity that the instrument is designed to measure.

Dead space is defined as the range of different input values over which there is no change in the output value.

Sometimes, the output reading of an instrument is not linearly proportional to the quantity being measured, therefore, it is important to establish the equation that relates the typical output reading of an instrument when a sequence of input quantities are applied. The non-linearity is usually expressed as a percentage of full-scale reading.

[2] https://www.bluetooth.com/learn-about-bluetooth/radio-versions/

Hysteresis is another characteristic that may occur in piezoresistive sensors and can be defined as a non-coincidence between loading and unloading curves. Other factors can be calculated, however, they will depend on the population characteristics and desired comparisons.

3.4 Sterilisation Techniques

During surgery there are some rules that must be followed in order to ensure that the environment is sterile. Therefore it is important to sterilise sensors before their use. As the main objective is to reuse sensors during surgeries, it is important to select a sterilisation method that is available at CHLeiria: Steam Sterilisation and Sterilisation via Hydrogen Peroxidase.

3.4.1 Steam Sterilisation

Pressure Saturated Steam Sterilisation, commonly known as "autoclave", is very used in healthcare facilities. This type of sterilisation uses saturated steam at 121-132 ° C that destroys structural and metabolic components of microorganisms [62]. Commonly, the standard steam sterilisation is achieved after 15-30 minutes under a pressure of 106 KPa (1 atm) [62]

This technique combines a shorter exposition time and lower temperatures compared to others. Steam sterilisation is simple, effective, safe, environment-friendly, and low-cost. Physical parameters such as moisture, temperature, time are monitored to assure sterilisation efficiency. It is used to sterilise liquids, reusable metallic devices and instruments and hospital linen [62].

However, some materials are damaged during this process, including most polymers. The damage depends on polymer composition and properties. While polypropylene (PP), PTFE, aromatic polyurethanes, nylons, polycarbonate can be sterilised without losing properties, others such as some polyurethanes may result in a toxic hydrolytic product: dimethyl aniline [62]. Some high carbon steel devices used for surgical and dental instruments are corroded and lose the cutting edges' protection. Besides that, electronics are also affected. To avoid this degradation, the instruments should be cleaned and dried before sterilisation. The corrosion of carbon steel instruments can be reduced by immersing them in an anti-corrosive solution before autoclaving [62].

3.4.2 Sterilisation via Hydrogen Peroxidase

Hydrogen peroxide gas plasma is a low-temperature (55 °C) sterilisation alternative with short cycle times and material compatibility and is time, temperature, and concentration-dependent. Besides that, this process does not require aeration [34].

During this sterilisation process, an electric or magnetic field is created for the conversion of an aqueous solution of hydrogen peroxide into gas plasma through radio-waves. [34] The aqueous solution of H_2O_2 produces destructive hydroxyl free radicals that attack membrane lipids, DNA and other essential cell components. H_2O_2/ peracetic acid (PAA) can also be used. PAA is an oxidising agent that denatures protein, disrupts cell wall permeability and oxidises sulphur bonds in proteins, enzymes, and other metabolites [34].

Gas plasma sterilisation is the best technique for metals, natural rubber, silicone and various polymers such as polyvinyl chloride, polyethylene and polyurethane [98]. Heat and moisture-sensitive instruments and microsurgical instruments are often sterilised recurring to this method. Some examples are: objective lenses for microscopes, nonfabric tourniquets, medication vials, insulated electrosurgery and cautery instruments, and metal instruments [34].

However, oxidative chemical sterilising agents can induce surface oxidation in some materials such as biomedical elastomers, liquids, oils, powders, gloves and biological tissues derived from plant fibres such as paper, cotton, and linen, gauze sponges [98].

3.5 Regulatory Issues

Medical devices used for clinical investigation according to Infarmed are "any device intended for use by an investigator in a research centre for investigations (...) in an appropriate clinical and human environment and may only be used in the context of the clinical investigation for which they were set up and under the responsibility of the personnel authorised in that investigation"[3]. There are laws to be followed, but CE labelled and unlabelled devices can be used as long as they comply with the conditions set out in Law n.º 21/2014 or Annexes I, VIII, XV and XVI part I of Decree-Law No. 145/2009 respectively [19].

Besides, medical devices are classified according to the potential inherent risks regarding the type of involved device and its purpose [4]. In Portugal (and Europe), according to Decree of Law nº 145/2009, of 17th of June [19], medical devices are divided into the four risk classes represented in Figure 3.10.

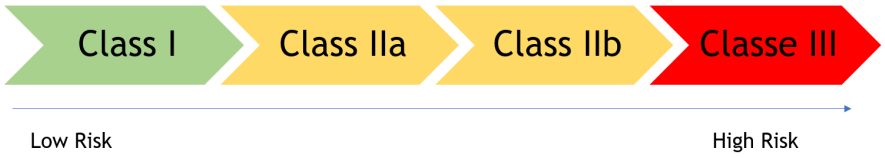


Figure 3.10: Medical Device Classification Scale

This classification will depend on four major segments:

- Duration of the contact with the human body: temporary, short or long
- Invasiveness of the human body
- Anatomical structure affected by the use
- Potential risks from the manufacture and technical design

[3] https://www.infarmed.pt/web/infarmed/perguntas-frequentes-area-transversal/dm/div

[4] https://www.infarmed.pt/web/infarmed/entidades/dispositivos-medicos/classificacao-e-fronteiras

When a device can be used in different parts of the body, it is classified based on the most critical interaction. Besides, when the sensor requires an electrical source to actuate it is considered an active medical device, regardless of the origin.

Class I devices are noninvasive, therefore present low risk to patients and can be self-certified by the manufacturer, except for sterile products or measuring devices. Wheelchairs and Stethoscopes belong to this class.

Class IIa devices present medium risk to patients and are invasive to human body via natural body orifices. They include therapeutic diagnostics and devices for wound management such as surgical clamps and tracheotomy tubes. Class IIb are also medium risk devices, but are partially or totally implantable. They can also modify the biological or chemical composition of fluids such as the bone fixation plate and lung ventilators.

Class III present a high risk to patients and affect the functioning of vital organs. Pacemakers, heart valves and implanted cerebral simulators belong to this category [5].

Taking into consideration all the segments and the ANNEX IX of the present Decree of Law, the device in development can be classified as Class IIa. The device will be used pre-operatively at the beginning of each surgery, with contact with the human body lower than 30 minutes. Therefore it can be considered a short term invasive device of the surgical type.

3.6 Conclusion

There are several types of sensors available and it is necessary to select the device that meets the sensor design requirements. It is also important to select a transmission method suitable for the environment in which it will be used and to know the characteristics of the sensor.

In addition, it is important that the sensor complies with Infarmed standards and that it can be sterilised by the sterilisation methods available in the hospital for practical use.

[5] https://www.phgfoundation.org/documents/briefing-what-is-the-ivdr.pdf

Chapter 4

State of the Art

The evaluation of force and pressure variations is carried out in various fields from touch screens to medical devices. This chapter presents more recent studies regarding the development of sensors and the application of sensors in human joints.

4.1 Sensor Development

Depending on the context the sensors will have different characteristics in order to be optimised for the application. Generally there is a demand for thin, flexible, accurate, fast and sensitive sensors with low production costs. Therefore, in the last years there has been a strong research in this area, namely in materials and manufacturing processes for all types of sensors.

4.1.1 Piezorestistive

In 2015, Gerlach et al. presented a low cost and flexible plantar sensor based on multi-walled carbon nanotube (MWCNT)- polydimethylsiloxane (PDMS)-composite. The layer system is composed of two polymer foil substrates: the first substrate carries a screen-printed MWCNT-polymer-film and the second substrate carries the electrodes (screen printed silver ink).This matrix can be used to produce small single electrodes to map pressure [37].

Fatema et al. and Suprapto et al. developed low-cost piezoresistive sensors. This sensor was composed by a three layers sandwich structure: two layers with copper electrodes in a vertical and horizontal alignment respectively to improve conductivity. The middle layer was composed by a Velostat sheet. It has good physical and chemical properties in terms of flexibility, foldability, and printability. In this case, the response for a given load is uniform and repeatable [32, 100].

Carvalho et al. developed an polymerbased piezoresistive sensors for e-textiles integration. The main goal of this investigation was to determine the influence of different sensor constructions, varying film thicknesses, electrode materials and encapsulations on sensor performance. The sensor was developed with a transducing piezoresitive film and two electrodes on each side of the piezoresistive film allowing electrical connection. These electrodes were prepared with copper

tape, conductive fabric, and conductive knitted stretch fabric. The sensor was protected by a foam that introduces some instability [13].

Manapongpun et al. also used Velostat a sensing element due to its piezoresistive properties. In this matrix an acrylic board was used for stiffness and an ethylene Vinyl Acetate (EVA) as a foam cushion. This sensor consists in 15 rows and 15 columns of electrodes with a sensing element between them [72].

Baldoli et al. characterized a textile sensor assembled by a piezoresistive fabrics sheet between two fabric composed by rows of columns of conductive material. The piezoresistive sheet composed of 91 % of nylon and 9 % of elastane, while the other two fabric were composed by a nonconductive textile with sewed parallel conductive stripes to create a pattern of alternate conductive and insulating bands. This is a low cost, easy to use and robust solution [8].

The location of the applied force can be identified by detecting the position where the change of resistances occurs between the external conductive paths. This solution presents a good response for both low and high pressure measurements with the tuning of circuit parameters. However the latest presented a limited sensitivity. During the analysis of static characteristics (e.g. drift, repeatability, temperature dependence and SNR) the sensor is stable under shear, stretch and on curved surfaces [8].

Poly(3,4-ethylenedioxythiophene) (PEDOT) is often used as a sensing element in several studies. Lim et al., for example, developed a system based on a conductive polymer thin film-coated textile fabricated using a microfibre fabric (Welcron, nylon/polyester splitting yarn) by VPP for application in textile-based pressure sensors [68].

Hoang et al. created a highly flexible, stretchable and ultrathin piezoresistive tactile sensor array. The sensor is composed with a precise conductive polymer - Poly(3,4-ethylenedioxythiophene): polystyrene sulfonate (PEDOT:PSS) with Polyacrylamide (PAM) hydrogel [44].

The sensing materials are dropped by micropipette to fill 12x8 pre-cut holes on isolating layer before half-drying and stack three layers together. The top and bottom electrodes are two Sylgard 184 (PDMS) top substrate films with 200µm thickness casted the 12x8 electrode patterns, which are assembled together with an isolating layer 400µm thickness sandwiched in the middle [44].

Other researchers studied the possibility of using Polydimethylsiloxane (PDMS) as substrate for piezoresistive sensor. The PDMS is a biocompatible elastomer, which can be easily integrated, as well as flexible and stretchable sensor device; therefore, the PDMS substrate is widely used in mechanical piezo-resistive sensor.

Electronic skin is one of the most common solutions that use this type of elastomer and has been researched by several investigation groups.

Yu et al. produced a high performance resistive pressure sensor based on carbon nanotube/ polydimethylsiloxane arrays (PDMS) that was fabricated using an ultra-violet/ozone (UV/O3) microengineering technique. PDMS microstructure is coated with Cu electrodes. This type of sensor has a broad pressure sensing range between 7 Pa and 50 KPa and can be used to measure radial artery pressure, epidermis/muscle movements during speaking and breathing patterns [116].

Luo et al. created an external tactile force sensing electronic skin in a PDMS substrate with a better repeatability and cycling stability when compared with most reported flexible medium-pressure sensor. The sensing element is a GNPs/MWCNT/ polymer composite that allows line detect-writing on a PDMS substrate. The substrate presents a laminated and irregular surface structure that improves the pressure sensing capability and response performance allowing the wrist pulse monitorization (small pressures) [71].

Gong et al. developed a flexible resistive pressure sensor by sandwiching ultrathin gold nanowire-impregnated tissue paper between two thin PDMS sheets. Gold presents a low electrical resistivity therefore is a good material for conducting electricity. This sensor presents low energy consumption, fast response time and high sensitivity and stability [38].

Wakabayashi et al. developed a flexible sensor sheets but with different sensing elements. In this case, the sensor is composed by PDMS films with laser-induced graphene (LIG) layers and the tactile pressure device laminated by PDMS onto polyethylene terephthalate (PET) films [110].

Zhang and Tao produced a stitched fabric composed by a piezoresistive array of two orthogonally contacted electrical conductive yarns and coated with elastic polymer. This sensor is flexible, robust, lightweight, and breathable. The magnitude of the pressure is given by the resistance change between the two contacted sewn yarns system. [118].

Yuanzheng Luo et al. also developed a pressure sensitive array PDMS using a sugar template method. This sensor is fabricated in three steps. First, cylindrical oxide (GO)/foam graphene was mounted into the holes of the sugar mould and copper lines attached to its surface. The liquid polymer was poured into the sugar mould consisting of PDMS and a two-part polymer, elastomer base. Once solid, the sugar is removed by dissolving in hot water. The hierarchical structure of the pressure sensitive matrix consists of the upper electrodes, the pressure sensitive GCF, the porous substrate insulator, and the lower electrodes [117].

Liang et al. developed a integratable piezoresistive pressure sensor based on carbon nanotubes (CNTs) layed over a PDMS layer and a photoresist porous insulation layer. The two CNT electrodes that are initially separated by photoresist layer, can easily contact with each other under a tiny pressure. Although there are many ways to create a porous insulation layer on a CNTs electrode, photolithography, that is the most common and suitable method for mass production [67].

Choi et al. developed a novel sensor based on the guided formation of straight mechanical cracks. The patterned holes on the surface of the device concentrate the stress near patterned holes connected by uniform cracks. These cracks increase the resistance of the metal layer, and the sensor becomes highly sensitive to pressure and strain. This sensor allows the detection of the physiological signal of the wrist pulse and presents an ultrahigh sensitivity to external forces as pressure. [16].

Several companies developed FSR sensors.Teckscan developed the FlexiForce sensors. These type of sensors are suitable to measure both static and dynamic forces, thin and non-intrusive [3]. These type of sensors are often used for medical research in cadaveric joints. These will be explained at Section 4.2.1.

4.1.2 Capacitive

Most capacitive sensors are arranged in a matrix of a parallel plate capacitor with a layer between them.

The sensing matrix can be composed by two copper electrodes layers with a dielectric layer composed by a polymeric foam layer [90] or a silicone layer [73]. The top electrodes are connected to the readout circuit and the bottom electrodes are connected to the voltage source by means of a shielded wire. The sensor must be elastic enough to allow deformations without breaking.

A different low-cost flexible pressure sensor based on an porous elastomer film PDMS with uniformly distributed micro-pores as a dielectric layer was manufactured by Lee et al.. The phase separation between a prepolymer material of the PDMS and an insoluble solvent of water in solution and an evaporation of the solvent within the polymer matrix after polymerization created a uniform dispersion of micropore in the elastomer matrix as a dielectric layer. Despite PDMS layer, this sensor is also composed by line patterns of indium-tin-oxide electrodes prepared on two PET substrates in perpendicular directions 3mm spaced [61].

Another transparent and flexible pressure sensitive sensor alternative was developed by An et al. and consists of an array of pressure-sensitive field-effect transistors (FET) with local air gaps as a dielectric layer between the amorphous layer of indium gallium zinc oxide (IGZO) and the top-gate electrode. This sensor has good electrical properties and high reliability under ambient conditions, due to the clean interface between IGZO and air. Here, an elastomeric dielectric layer (Ecoflex 0030) was located on the 4-μm-thick air gap (below a 100-μm-thick, transparent cover layer of the CNF+AgNF hybrid), and its thickness can decrease by applying pressure with increasing the capacitance of IGZO FET [5].

Li et al. developed a capacitive highly sensitive and flexible pressure sensor in a honeycomb weave architecture. Carbon fibres were used as electrodes due to its flexibility and conductivity, lower density, higher axial strength, and modulus when compared with silver -plated nylon wire and conductive copper yarn as electrodes [66].

Capacitive sensors can be used in the development of electronic pressure-sensitive skin.

Nela et al. developed a carbon nanotube thin-film transistors matrix (CNT TFTs). CNT TFTs are made of highly purified solution tubes. The active matrix exhibits superior flexible TFT performance with high mobility and large current density [79].

Yang et al. developed an electronic skin based on nanofibre membranes through screen printing and ultrasonic bonding techniques. This sensor is constituted by three different materials: a layer-by-layer poly(vinylidene fluoride) structure as substrate, silver nanowires electrodes and a thermoplastic polyurethane dielectric layer[115].

There are several capacitive sensors available at the market such as the XSENSOR. This device is a matrix of capacitive sensing elements that can be used in several fields with an high sensitivity, dynamic range and conformability. The sensors are constructed by enclosing the conductive lines and dielectric material in a thin, pliable, and durable cover layer to protect the active layers. The cover layer is printed with a grid to indicate the active area of the system [18].

4.1.3 Piezoelectric

Piezoelectric sensors can be manufactured using a piezoelectric polymer film of polyvinylidene fluoride (PVDF) and different types of treatments and electrodes.

In 2017, Parida et al. created a triboelectric sensor composed by a self- polarized polyvinyldifluoride -trifluoroethylene (P(VDF-TrFE)) sponge able to detect a large range of pressure (0.05-600 KPa) with high pressure and high sensitivity. The sponge was fabricated using the modified breath-figure technique: the P(VDF-TrFE) was dissolved in N,N-dimethylformamide and drop-cast onto cleaned glass. This solution was placed in a humidity chamber with precise conditions ($T = -20$C and 50 %HR) for an hour and latter air-dried at room temperature. With this process the water was removed and a porous, free-standing, flexible, self-poled P(VDF-TrFE) was produced and removed from the glass. The P(VDF-TrFE) was embedded between one gold plate and PDMS plate forming a sensing element [83].

Al-Saygh et al. studied the reinforcement of PVDF with nanolayers of titanium dioxide (titania nanolayers, TNL) synthesized by hydrothermal method. A hybrid composite is prepared by incorporating the TNL (2.5 wt%) with reduced graphene oxide (rGO) (2.5 wt%) synthesized by improved graphene oxide synthesis to form a PVDF/rGO-TNL composite. Theses additives increased the sensitivity by 333.46 % at 5 KPa,200.7 % at 10.7 KPa and 246.7 % at 17.6 KPa compared to the individual PVDF composite of TNL. The material is flexible with high response in short time [2].

Rajala et al. designed an in-sole plantar pressure sensor. The sensor is made of a piezoelectric polymer film (PVDF) with evaporated 200 nm thick film of copper electrodes. In these type of sensors, the pressure values varies from 58 KPa to 486 KPa. These sensors measure the dynamic stress and respond to pyroelectric signal and for this reason, they can be challenging to use in conditions where the ambient temperature may vary. These type of sensors sensitivities are affected by temperature changes, therefore it is necessary to know the sensitivities for each temperatures [88].

4.1.4 Fibre optic

Fibre optic sensors are an alternative for pressure sensor arrays development. The integration of these sensors into textiles can occur through several processes that allow the customization of the matrix structure.

Quandt et al. integrated a flexible photonic sensor on textiles to prevent pressure ulcers. Fibres were introduced into a thin, black, breathable polyester membrane, laser welded to form the optical fibre-crossing. The selected polymers contained 90 % siloxane but with different chain length, that confers high elasticity to the sensor during cyclic loadings. Despite complex applications, there is an investment in the development of low-cost plastic optical fibre (POF) pressure sensor matrix [87].

Sartiano and Sales created a low cost pressure sensor mattress. The fibres have a core of polymethyl-methacrylate of 980 µm and a cladding of fluorinated polymer with a diameter of

1000 µm. The POFs have been sensitized to pressure, cutting part of the jacket, the cladding, and the core. The fibres were then arranged in a matrix with the cuts positioned in the crossing points and embedded in a mattress cover sample as it is possible to understand at Figure 4.1. The computer acquires the data from the board, that controls the current (light intensity) in the LEDs and converts the voltage values that are serially outputted from the photodetectors array [93].

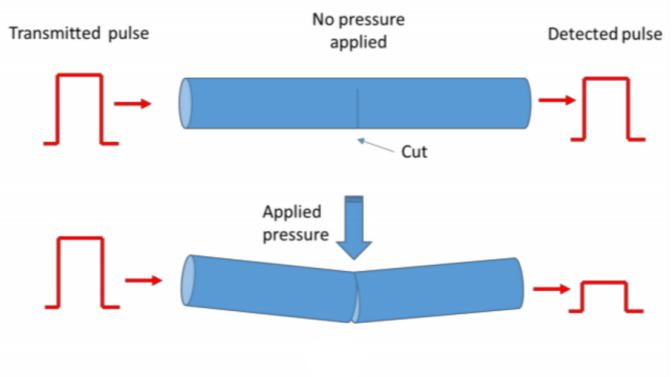


Figure 4.1: Optic fibre pulse transmission in rest and with pressure applied retrieved from [93]

4.2 Medical Applications

Research in the medical field, particularly in biomechanics, often makes use of pressure and force sensors to evaluate joints. This section provides an overview of the use of sensors in joints.

4.2.1 Trapeziometacarpal and Osteoarthiritis studies

Over the last few years, some attempts have been carried out to understand TMC as well as its associated pathologies. Some studies regarding the movements performed by the thumb in which the TMC is strongly involved were also developed.

Eaton and Glickel were responsible for the creation of the diagnostic scale of OA through X-rays which is explained in the Section 2.3.1. When the method is determined, the means of treatment is considerably simplified and the multiple procedures that have been proposed for "basal joint arthritis" can be applied more accurately[26]. Dela Rosa et al. tried to optimise this classification by selecting the best radiographic plans to analyse trapezium as its shape and orientation do not allow the visualisation of this bone [21].

In 2007, Batra and Kanvinde tried to gather all treatment options for each OA stage, from the conservative to surgical options to treat joint pain and restore joint stability. Ligament reconstruction or osteotomy are a common option for early painful laxity, while trapezioctomy, arthrodesis and arthroplasty are used in more severe osteoarthritis. However, more studies are necessary to create a precise decision tree for OA treatment [9].

Domalain et al. tried to understand the changes in degrees of freedom (DoF) that occurs during surgical procedures. An intact joint has 2 DoF, while during arthrodesis condition, the DoF

decreases to 0DoF and muscle forces also decreases. However, during an arthroplasty condition, the DoF increases to 3 DoF and the joint forces become 13 timess larger than the 2-DoF joint. This study contributes to the knowledge of the biomechanical consequences of changing a joint's DoF by surgery and the importance of understanding joint behaviour during decision making [23].

D'Agostino conducted a large cadaveric study to validate the use of dynamic CT for direct quantification of the thumb motion in using a protocol which is feasible in a clinical context. Besides, another study in patients with specific thumb joint pathologies was performed. This study highlights and quantifies the trapezium and scaphoid kinematics together with the first metacarpal during thumb motion, while the wrist is fixed. This study confirms and quantifies the existence of a screw-home mechanism at the TMC joint during thumb flexion and the complexity of thumb kinematics with coupled rotations and translations of the entire thumb chain. This study protocol will be the base for our own study [20].

Dourthe et al. used a combination of indentation testing and contrast-enhanced computed tomography to assess the morphological and mechanical properties of trapeziometacarpal cartilage in fresh frozen ones. Some of the assessed mechanical properties included load-displacement behaviour, the normal force and Young's modulus. During this study, no significant difference was found in cartilage thickness between the trapezium and first metacarpal, but the cartilage around the volar aspect of both the first metacarpal and the trapezium was thinner. Besides, the first metacarpal cartilage was stiffer than the trapezial cartilage [25].

Schneider characterised the morphological differences between healthy and early osteoarthritic (EOA) trapeziometacarpal (TMC) with statistical shape model (SSM). A linear discriminant analysis (LDA) classifier was trained on the principal component (PC) weights to characterise features of each group. TMC bones from early OA subjects exhibited a lower aspect ratio and the articular surface is enlarged, deepened and there is bulging bone growth along the concave margin. Multivariable statistical analysis was performed on the PC to investigate morphological differences. The leave-one-out classification was performed to evaluate the performance of the classifiers. This classifier can detect these features automatically and can be used as a clinical tool [95].

Garcia-Elias and Orsolini tried to understand the relationship between thumb laxity (passive mobility), the shape of the trapezium and trapezial mobility relative to the second metacarpal. The shortest distance of the thumbnail to the radius when the thumb was forcefully approximated to the forearm with the wrist in flexion was measured and the inclination of the distal surface of the trapezium (angle b) and the mobility of the trapezium relative to the second metacarpal was assessed using dynamic X-rays in maximal radial and ulnar deviation [36].

Halilaj et al. performed a study that aims to determine differences in TMC joint space with sex, age and early OA in the thumb carpometacarpal joint space through CT scans. In this case, the joint space was used to assess joint space (the articular surface that is less than 1.5 mm). In this study, joint space areas are significantly different between healthy young men and women. Trends indicated that patients with early-stage OA have larger TMC joint space areas than healthy subjects of the same age group and that older healthy women have larger joint space areas than younger healthy women. This study suggests that ageing in women may lead to joint space narrowing

patterns that precede early OA, which is a compelling new insight into the pathological processes that make TMC OA endemic to women [40].

Cheema et al. tried to understand the benefits of opening wedge trapezial osteotomy in cadaveric specimens for altering the contact mechanics of the trapeziometacarpal joint as a possible deterrent to the initiation or progression of osteoarthritis explained by other investigators. Therefore, a study with cadaveric specimens to determine whether opening wedge osteotomy of the trapezium was successful in reducing radial subluxation of the metacarpal base and to quantify the contact area and pressure on the trapezial surface during a simulated lateral pinch. The flexor pollicis longus, abductor pollicis longus, adductor pollicis, abductor pollicis brevis, and flexor pollicis brevis/opponens pollicis tendons were each loaded to simulate the thumb in lateral pinch position. The radial subluxation from anteroposterior radiographs was measured before and after placement of a 15° wedge. Besides, two real-time sensors (Model 6900; Tekscan, Inc., South Boston, MA) were used to analyse contact pressure and contact area distribution on the trapezium. These pressure sensors can measure the range typically observed by the joint (60˜700 KPa), have 121 individual sensing elements and a 196 mm^2 area. Sensor 1 was placed between the thumb and a fixed plate to monitor continuous lateral pinch, while sensor 2 was placed in the TMC joint space by an orthopaedic surgeon. The soft tissue and joint capsule superficial to the TMC joint were incised longitudinally to allow access to the joint space. The incision size was only slightly larger than the width of the sensor to allow for insertion with minimal disruption of the joint and disturbance of the surrounding stabilising ligaments. This study is extremely important to the selection of the type and dimension sensor that will be used. To understand joint behaviour, it is important to understand the movements in which they are involved [15].

Vergara et al. [108] surveyed human grasps. The results show that the most commonly used grasps are: pinch, non-prehensile, cylindrical, lateral pinch and lumbrical. The presence of these grasps in the areas of activities of daily living is, however, very different (e.g., the pinch is widely used in food preparation and very little in driving). Some grasps were used more frequently with one hand or when both hands were used simultaneously (e.g., the special pinch was hardly used by the left hand).

It is important to highlight that no studies were found available concerning the use of intra-articular sensors in TMC.

4.2.2 Other Joints studies

There are studies of various joints' type using sensors including the knee, wrist, ankle and other. Some of these studies are available in the comparative tables (tables 4.2 and 4.3). After the tables' analysis, it is possible to understand that the TekScan pressure-sensitive sensors are the most used. It has also been observed that, as for the TMC joint, most of the studies were conducted in cadavers. However, some joint studies were performed during surgery which validates the possibility that the joint can be studied during surgery. Pressure sensors were used to study pressure in sutures for acromioclavicular stabilisation and different suture anchor fixation techniques evaluation in bone fractures [69]. Pressure, Temperature, and Humidity parameters in casts can be evaluated

Ref.	Region of interest	Types of Sensor/ Technology	Monitored Joint Parameters	Monitoring conditions
[63]	Quadriceps	custom-made cuff-type electrode	Contact areas and peak pressures Force	Animal under anestesia
[64]	Tibiofemoral	Low and medium-grade pressure-sensitive films (Fuji prescale film) Low range pressure sensitive film (1-10MPa)	Contact areas Peak pressures Torque Force transmission across knee compartments	Animal under anestesia

Table 4.1: Lapin Studies

by thermocouples and small forces sensing resistors sensor [106, 113]. Some studies have been carried out on lapins using sensors to measure pressures, forces and contact areas as shown in the Table 4.1.

Ref.	Region of Interest	Types of Sensor/Technology	Monitored Joint Parameters	Monitoring conditions
[104]	ankle	pedobarography system (MatScan, Tekscan) ACUSON S3000 Ultrasound System 9L4 probe (4–9 MHz) (Siemens Medical Solution)	Peak pressure, mean pressure, maximum force, contact area, pressure-time integral, force-time integral thickness, cross-sectional area and stiffness of the intrinsic foot muscles	in vivo
[42]	knee	polyimide-based MEMS strain-sensing	Strain-sensing	mechanical knee simulator
[102]	knee	pressure-sensitive conductive sensor sheet	Pressure	sensor test
[22]	knee	prosthesis instrumented with force transducers Finite Element Model	Knee Kinematics and Forces	patient with tibial prosthesis
[94]	knee	radiofrequency-based electronic load sensor (VERASENSE Knee System)	Medial and lateral compartment loads	patients undergoing 60 posterior stabilized TKA
[109]	knee joint	Piezoresistors of type AP120-2-12/Au/BP in a polymer contact layer	Measured pressure values in dependency on the walking cycle in knee arthroplasty	sensor test
[6]	medial compartment of the knee joint	electronic pressure sensor (Iscan 6900, Tekscan)	Peak pressure distribution total force	patients during routine arthroscopic surgery
[4]	menisc	K-Scan 4011 I-Scan sensor (Tekscan)	Direct intra-articular loads and the contact area	fresh-frozen human cadaveric knees
[92]	patellofemoral	Pressure sensor device (K-SCAN2, 4010N)	Force vs Distraction	amputated human knees
[24]	patellofemoral ligament	calibrated pressure-measurement system six-degree-of freedom knee-joint simulator	Contact pressure	human cadaver knee
[51]	tibial plate	Biodex Multi Joint Isokinetic testing system (Biodex Corp., Shirley, NY, U.S.A.)	Quadriceps torque production and knee intraarticular pressure during active knee extensions	participants
[33]	tibio talar joint	FEM analysis and (Tekscan) pressure sensor	Stress shielding	in vivo
[70]	Tibiofemoral	Pressure mapping device (Model 4000, Teckscan)	Mean and peak contact forces pressure Contact area	fresh-frozen cadaveric knee

Table 4.2: Lower Limb studies using sensors

Ref.	Region of interest	Types of Sensor/Technology	Monitored Joint Parameters	Monitoring conditions
[74]	Metacarpohalangeal joint	MRI	Area of the flexor digitorum profundus tendons at the carpal tunnel level at flexion, neutral and extension	hands and forearms of subjects
[75]	Carpal Tunnel	DeltranTM DPT-100, Utah Medical products connected to catheters	Pressure	in vivo
[114]	Coracoclavicular joint	piezoresistive sensor Tekscan Sensor Model/Map 6900	Intra-articular pressure	cadaver
[17]	Distal radius joint	high-resolution peripheral quantitative computed tomography	Joint forces and moments	human cadaveric forearms
[80]	Hand	pressure sensor (Tekscan Sensor Model 5101)	Contact area and force distribution during push/pull	in vivo
[14]	Humeroradial joint	TekScan Flexiforce B201 force-sensitive sensor	Intra-articular pressure measurements	cadaver
[43]	Raciocapitellar joint	pressure transducer Tekscan at the elbow strain gauge between bones K-Scan system model 6900 (flexible thin-film sensor)	Small joint pressure	cadaver
[41]	Radioulnocarpal joint	Pressure-sensitive conductive rubber	pressure	fresh frozen human upper extremities
[89]	Radioulnocarpal joint	Capacitive pressure sensor	Pressure before, during after load	fresh frozen human upper extremities
[107]	Scaphoid	CT-images	contact area and pressures	cadaver
[29]	Scaphoid	sensor position in CT: eight attached strain-gauges (4 x LY11 0.6/120 and 2 x XY21 0.6/120) (HBM1)	torque and force	cadaver
[82]	Shoulder	F-Socket 9811 force sensor (Tekscan)	peak impact forces	shoulder pad
[35]	Upper Limb	textile piezoresistive sensor (Dragon Skin 10, Smooth-On) IMU MPU 9250	load distribution of a prosthetic socket during real time operation	Amputees patients
[30]	Wirst	Medical Sensor 4201 (Tekscan)	Intra-articular measurements	fresh frozen human upper extremities
[31]	Wrist	Multi-body simulation software AnyBody	Contact area, muscles length, force transmition	patients

Table 4.3: Upper Limb studies using sensors

4.3 Patents

A patent search was performed in the Espacenet [1] database to find any sensor for intra-articular pressure measurement. The following keywords were used: intra-articular, pressure sensor, joint and trapeziometacarpal, in vivo, no patents were found.

However, one patent was found with a very interesting sensor: "Smart Joint Implant Sensors" from Zimmer INC for hip and knee. The operating sensor for sensing pressure and is composed of an array of sensors. Three capacitive sensors that measure the pressure on the X and Z axis. Besides, it also measures several joint properties: viscosity, pH, cell count, hyaluronic acid, leukocytes among others in the synovial fluid. These indicators allow the evaluation of some kind of infection [57].

However, when the search was extended to "pressure sensor array" several sensor arrays were found. Some of these sensors are schematised in the 4.4.

Author	Year	Sensor Type
Izaki et al.	2002	Piezoresistive
Taylor	2003	Piezoresistive
Horie et al.	2003	Capacitive
Guerrieri et al.	2004	Capacitive
Ken Kawahata	2005	Capacitive
Hughes and Knowles	2006	Capacitive
Komistek et al.	2008	Capacitive
Li et al.	2009	Piezoresistive
Camprubi et al.	2009	Piezoresistive
Abele	2014	Capacitive

Table 4.4: Patents Labels

4.4 Conclusions

Over the last few years several researchers have developed new pressure sensors from the less to the most complex manufacturing techniques and for all price application ranges.

Besides, several authors, from the medical field, have developed studies on TMC and the influence of pathologies on its behaviour. However, none of them analysed the joint per-operatorily. The only studies with with in-vivo joints were developed through imaging or cadaveric models. In addition, the use of pressure sensors in other joints allows the conclusion that it is possible to develop an intra-articular sensor for TMC.

[1] https://worldwide.espacenet.com/patent/my-espacenet

Chapter 5

Sensor Design

5.1 Variables Definition

The main focus of this master thesis is to develop a sensor to study the forces acting inside the TMC joint as well as the contact area during surgery. These will be considered the measurand and allow the beginning of problem formulation according to the design process taken from [111] which is represented in the scheme of Figure 5.1.

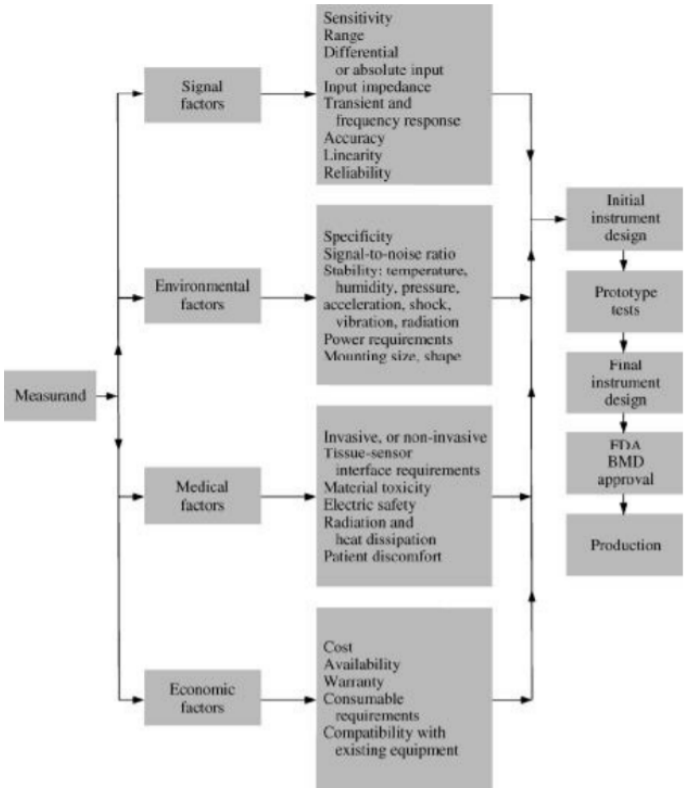


Figure 5.1: Sensor Design scheme retrieved from [111]

Despite measurand relations, it is necessary to take in account other factors in order to select the ideal sensor such as medical, signal, environmental and economic factors.

5.1.1 Medical Factors

As mentioned in the previous sections, this will be an intra-articular and therefore invasive device. As it will be used in the operating theatre it should be electrically safe with all its electronic devices, with the exception of the sensor area in contact with the joint, electrically isolated. The patient will be under anaesthesia so the discomfort will be minimal. Regarding the toxicity of the material, as it will be in the human body less than 30 minutes there is no risk, however, this device will have to be sterilised before each surgery using one of 2 techniques in the Section 3.4: Steam Sterilization and via Hydrogen Peroxidase.

5.1.2 Environmental Factors

This sensor will be used in a surgical environment and therefore no significant environmental changes will occur.

In Portuguese operating theatres, the temperature varies between 17-27ºC and the relative humidity will be between $30-60\,\%$[85]. Since the sensor will be used intra-articularly, it will have to work at human body temperature (around 37ºC). Although anaesthetic promotes the vasoconstriction of the region (Section2.4), the joint area is still very moist and can be irrigated with saline solution. Therefore, the device must be prepared for wet environments.

The movements that are performed during surgery, are relatively slow since the patient does not have much sensitivity in the hand due to the anaesthesia, the accelerations are relatively low. As the joint surfaces are quite irregulars, some shocks may occur between the two surfaces. Regarding vibration and radiation they will not be significant.

The device will present the size of a female TMC joint with OA as the surgeries will be performed on women over 60 years with this type of pathology. Therefore, it will have an area between $190\,mm^2$ and $283\,mm^2$ and a shape that fits the joint surfaces mapped by D'Agostino (Figure 5.2).

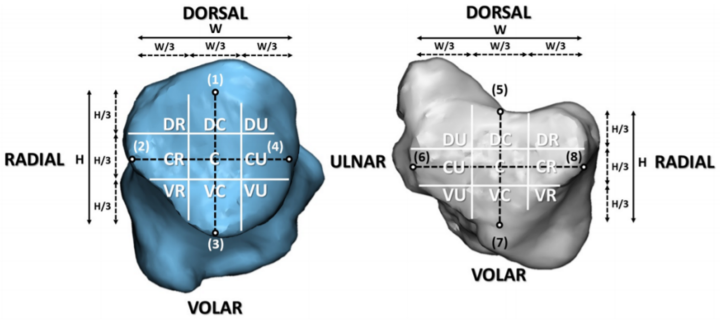


Figure 5.2: Articular Surfaces mapping retrieved from [20]

Since it will be performed in a surgical environment it will be important to avoid wired connections and prioritise signal processing and data storage units with Bluetooth connections. Due to that reason, it will be necessary to add a small battery.

5.1.3 Signal Factors

Regarding signal factors, knowing that the pressures exerted on the joint are in the range 60 – 700 KPa it is necessary that the measurements have a high reproducibility and sensitivity at this range since the final objective of the sensor is to be used on several patients in order to detect patterns and anomalies.

Furthermore, it is important that the sensor has a high accuracy and reliability in order to be able to compare the different measurements. When designing the circuit it is important to try to make the response as linear as possible.

5.1.4 Economical Factors

As this project is an independent investigation without financing, the cost of the equipment should be reduced. Apart from the sensor itself, the rest of the circuit can be used at all experiments. The software must be compatible to android devices and the electronic devices available to the end-users inside the operating room (OR).

During clinical trials at least two sensor matrices for each surgery must be available. In this way, there is a sensor available in case there is any contamination or problem with the sensor in the OR.

All the variables are summarised in the diagram in Figure 5.3.

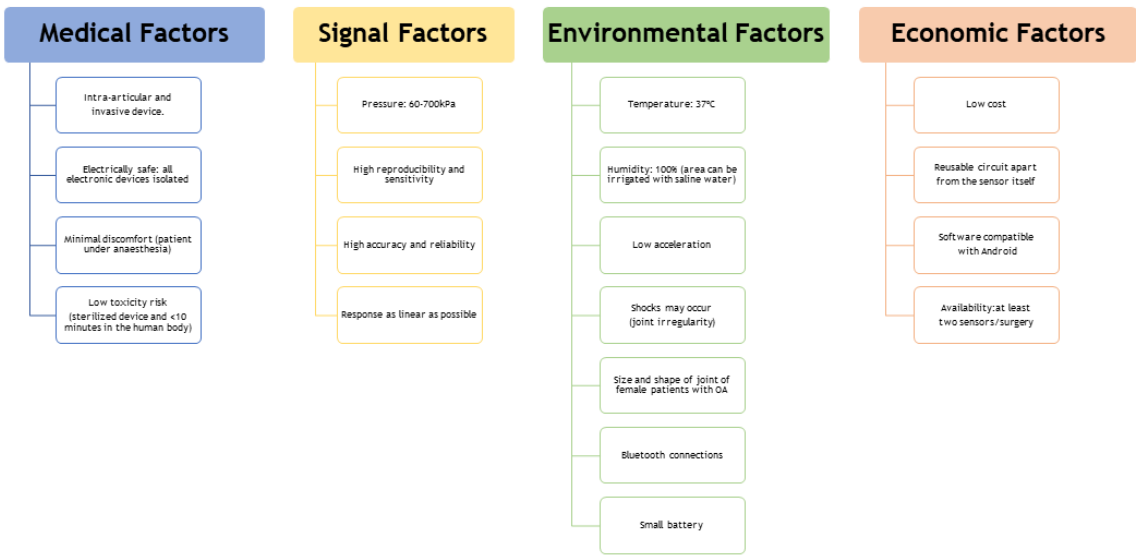


Figure 5.3: Design Factors

5.2 Sensor Design

Considering all the above conditions it was necessary to create a low cost, flexible pressure sensor matrix sensor. After some market research it was possible to conclude that the sensors available were over the estimated budget of this project. Therefore, it was necessary to develop sensors that meet the needs of the problem.

The main challenge of this dissertation consists in the creation of a sensor with dimensions and the articulation shape. Thus, starting from the mapping of the joint by d'Agostino [20] a sensor array that maps the nine divisions of the joint was designed. The superposition of sensors on the articular surface of the trapezium is represented in Figure 5.4.

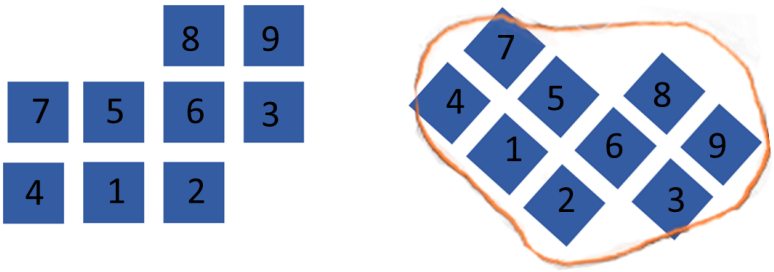
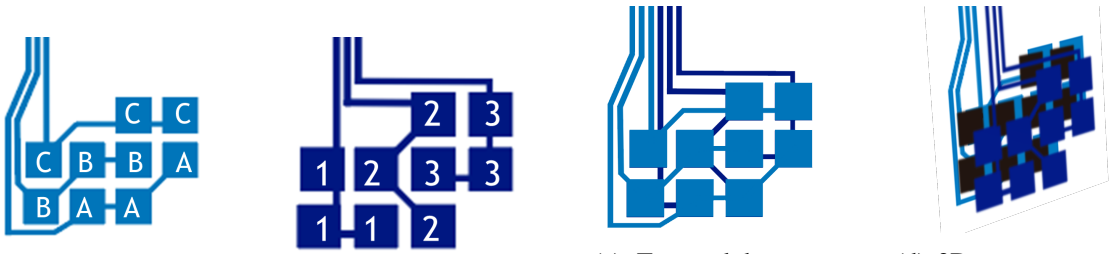


Figure 5.4: Superposition of sensors on the articular surface of the trapezium map from [20]

As it was possible to conclude at State of the Art (Chapter 4), the most common solutions for sensors pressure matrix are piezoresistive sensors as they suffer a resistance variance as a result of a mechanical effort. Piezoresistive sensors can have two different configurations, the face-to-face or two layers that were tested in the experimental work and drawn with Adobe Ilustrator.

The face-to-face configuration is composed by two faces with a layer of conductive paint and another layer of piezoresistive paint on each of the faces. The electrodes are square with 4 mm sides and are located at a distance of 1 mm from each other. In order to be able to tell which unit sensor is active it is important that upper and lower circuits are independent. The Figure 5.5 represent the connections between the top and bottom face.

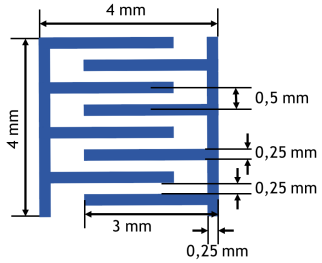


(a) Bottom Layer (b) Top Layer (c) Top and bottom layers overlaped (d) 3D sensor representation

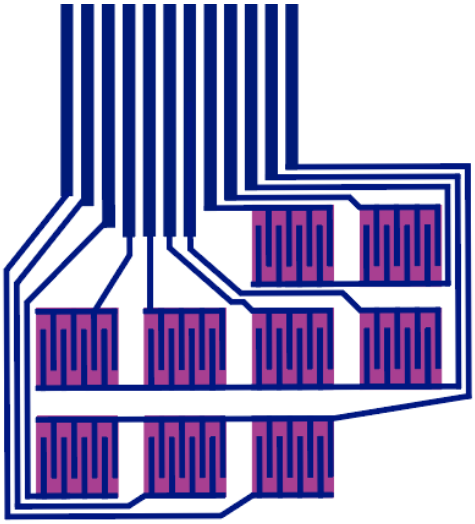
Figure 5.5: Face to face sensor array circuit

In the two-layer configuration, a layer of piezoresistive electrodes is made up the same as above, but the conductive layer is present on one face only. The conductive layer is in a square with 0.25 mm lines spaced 0.5 mm apart and alternating sides as shown in Figure 5.6a. In this case

the electrodes are connected in three diferent groups (3-4-2) and have independent connections to the output circuit (Figure 5.6).



(a) Two-layer unitary electrode



(b) Two-layer unitary sensor array

Figure 5.6: Two-layer sensor design

The correspondence between lines and columns of the circuit array for both prototypes are available at Tables 5.1a and 5.1b.

Sensor	Bottom Layer	Top Layer
1	A	1
2	A	2
3	A	3
4	B	1
5	B	2
6	B	3
7	C	1
8	C	2
9	C	3

(a) Prototype 1

Sensor	Line	Column
1	12	1
2	12	2
3	11	7
4	12	3
5	11	5
6	11	6
7	11	4
8	10	8
9	10	9

(b) Prototype 2

Table 5.1: Correspondence between lines and columns for both prototypes

Once the possible designs for the sensor were defined, it was necessary to find the ideal materials to manufacture it. For that, two alternatives were studied: the first with Velostat and the second with screen printing of sensors with conductive and piezoresistive ink using the screen printing technique. These two options will be presented in the next sections.

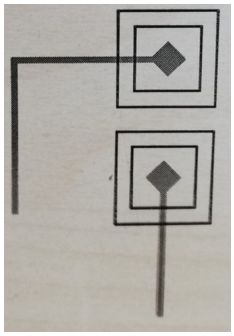
5.3 Prototype with Velostat

5.3.1 Sensor Manufacturing

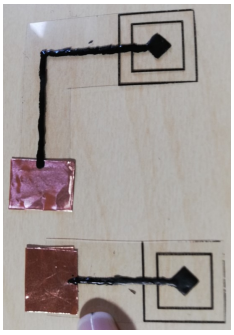
In this prototype, the sensor consists of two layers of transparent vinyl paper painted with conductive paint [1] and a sheet of Velostat. This is a piezoresistive material that, when pressed, shows a decrease in its resistance.

During the development of the sensor, an unitary sensor was developed inn order to understand the response of the unitary sensor to the application of force. This sensor was drawn in Adobe Illustrator and printed on acetate paper to facilitate the placement of the conductive ink in the correct size. This conductive part of the sensor is square shaped with 4 mm side and the piezoresistive part is a square with 10 mm side in order to mimic the mesh of the final sensor. A copper tape was glued and bonded to the conductive paint.

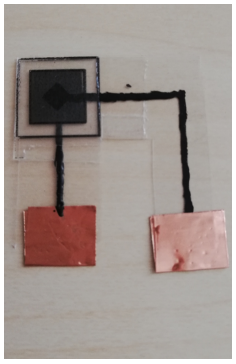
The two-layer model was not developed for this material as it is not possible to accurately design the sensor manually and the Velostat response proved unpromising with the face-to-face model.



(a) Unitary sensor design



(b) Conductive layers of unitary sensor



(c) Complete sensor

Figure 5.7: Face to face unitary sensor

5.3.2 Sensor Evaluation

After sensor manufacturing, it is important to understand its behaviour to understand if it is optimized for our purpose. Therefore, static, and dynamic trials are performed.

In this way, it was possible to determine the relationship between the analogue reading intervals, the sensor resistance and the applied pressure. After the development of the sensor in Velostat, three different tests were performed.

The evaluation of the sensors is usually performed in an automated way, however, during the development of this sensor, these systems were not available. Therefore, a structure was developed so that the forces were applied only in the active region of the sensor (Figure 5.8) with the materials available at teleworking. This structure consists of a cardboard box with a funnel whose bottom

[1] https://www.bareconductive.com/collections/electric-paint

has a lego piece that will apply the pressure on the unitary sensor. This piece has a radius of 4.8 mm and therefore has an area similar to that of the sensor and a weighs 40 g. A digital multimeter was used to measure the circuit resistance.

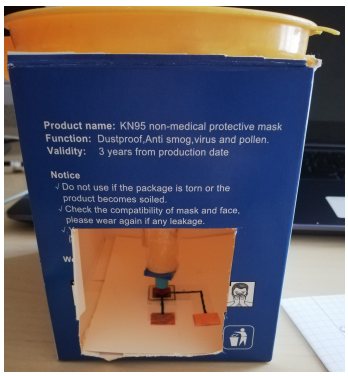


Figure 5.8: Structure

The loads that were applied to the funnel were calibrated weights whose values are 200 g, 250 g, 1000 g and 2000 g. To this calibrated weights it is necessary to add the structure weigh (40.0 g). Therefore, the applied pressures are,respectively, 141.10 kPa, 177.74 kPa, 330.97 kPa, 637.43 kPa and 1250.35 kPa, which cover the range of bibliographic values that the joint can exert.

Besides, sensor evaluation will allow us to determine the value of the fixed resistance of the readout resistor circuit. This value should be similar to the sensor resistance when the maximum weight is applied.

The first test performed consisted in analysing the sensor response to the application of a 2000 g load (1250, 35 kPa) and the sensor response to its removal. When the load was applied, the resistance was measured and the value obtained was 50.0 kΩ. These tests were performed with measurements every 30 seconds over a period of 11.5 minutes in order to understand the sensor return to the initial state. However, this sensor did not respond as expected, i.e. with the removal of the load, the resistance increases as it is possible to observe at 5.9. It therefore exhibits random behaviour and this may lead to measurement errors.

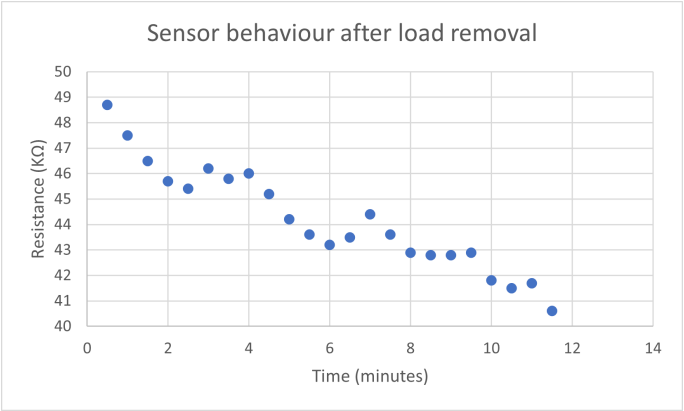


Figure 5.9: Graphical Representation of the sensor returning to the initial state after load removal

Tests were also performed for the calibration of the sensors. For that a graph of resistance variation was built, these values are presented in the Figure 5.10 and in the Table 5.2. This test was repeated three times in order to understand sensor reproducibility.

Polynomial trend lines were applied with a coefficient of correlation higher than 0.97 for trial 1 and 3 and 0,91 for the trial 2. Observing the three curves it is possible to conclude that the values follow the same trend curve, but with different intersections in the vertical axis which allows us to conclude that the sensor cannot be used for our purpose since the objective is to characterise the forces quantitatively and not qualitatively.

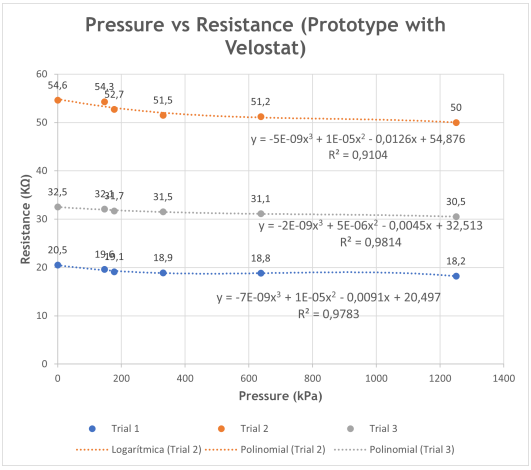


Figure 5.10: Pressure vs Resistance chart for Prototype with Velostat

Pressure (kPa)	**Trial 1** (kΩ)	**Trial 2** (kΩ)	**Trial 3** (kΩ)
0	20.5	54.6	32.5
147.10	19.6	54.3	32.1
177.74	19.1	52.7	31.7
330.97	18.9	51.5	31.5
637.43	18.8	51.2	31.1
1250.35	18.2	50	30.5

Table 5.2: Pressure vs Resistance values for Prototype with Velostat

The hysteresis study was carried out for maximum loads of 1820 g. The applied load intervals were achieved by applying the following pressures: 147,1 kPa, 300,33 kPa, 606,79 kPa. These loads will be incremented and then withdrawn at 2 minute intervals. Looking at the results (Figure 5.11 and Table 5.3), it is possible to conclude that the maximum difference between the increasing and decreasing direction is 0.05 kΩ and the minimum difference is 0.03 kΩ. The hysteresis value for this sensor 23,81 %. This value is extremely high, therefore represents a drawback for the sensor final aplication.

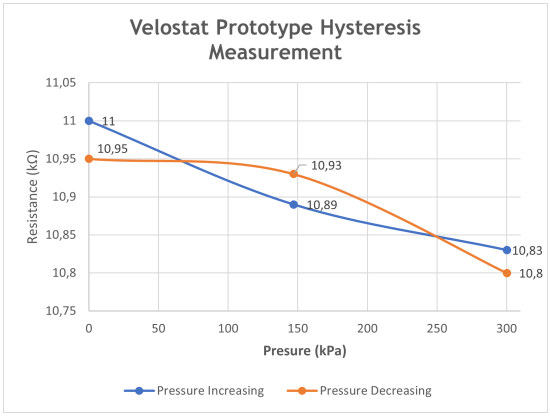


Figure 5.11: Graphical Representation Hysteresis Experiment for Prototype with Velostat

Pressure (kPa)	**Loading** (kΩ)	**Unloading** (kΩ)	**Uncertainty** (kΩ)
0	11	10.95	0.05
147.10	10.89	10.93	0.04
300.33	10.83	10.8	0.03
606.79	10.79	–	– height

Table 5.3: Values for Hysteresis Determination Experiment on Prototype with Velostat

5.4 Prototype Screen Printing

Due to the poor results of the first prototype, it became necessary to look for another solution that better suited the needs of this challenge. Therefore, the screen printing technique was used with conductive and piezoresistive inks from Nanopaint and PET substrate.

The main advantage of PET is its biocompatibility, flexibility and resistance, besides the fact that it can be sterilised using one of the sterilisation methods of the CHLeiria. One of the commercial names for this polyester is Mylar [105].

5.4.1 Screen Printing Definition

The Screen Printing is a technique widely used in the textile industry for being very simple and easy to handle that allows printing on various materials such as PET, MELINEX and textile, which are the materials indicated by the manufacturer of the inks that were used [2].

The equipment consists of a fabric screen, a squeegee and inks. The screens can have different mesh spacings depending on the design to be printed and the ink viscosity. In the case of the sensor design and due to the ink properties, screens with 81 points per centimeter and 106 points per centimeter were selected for the conductive and piezoresistive ink, respectively.

There are different types of screen printing, however the most suitable for this study is screen printing by cylinder. In this case the pattern is deposited through rotation on the tractor when connected to the screen roller. In the rotary screen, the ink and a squeegee are rotated inside the screen where the printing cylinder presses on the substrate printing the circuit design [56].

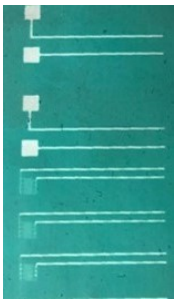
5.4.2 Sensor Manufacturing

After the selection of the screen, the photosensibilization was performed. This process consists of passing the two sensor models to the screen: face-to-face and two layers (5.5d and 5.6b). Despite the full sensors some unitary sensors were also produced as in the Velostat prototype manufacturing process.

The photosensibilization of the screen for the piezoresistive layer consists of the sensing areas was successful for all the unitary and matrix sensors. However, the same did not happen for the conductive screen. In this case, the photosensibilization of the two layers model did not go as intended. It can be seen in Figure 5.12.

A proof print was then carried out with a textile print paste to predict the print result before using the final materials. The results of this printing are present in the Figures 5.13. As can be observed, the unitary sensors presented a good result, the arrays of the same prototype presented some flaws. The two-layer model, on the other hand, presented quite a few defects both in the unitary sensors and in the matrix. Besides, during the cleaning of the screen, some of the lines of this matrix disintegrated. Due to the narrow paint width of the conductive layer, this sensor was

[2] https://nanopaint-tech.com/wp-content/uploads/nanopaint-piezoresistive-inks-2-datasheet.pdf



(a) Unitary sensors



(b) face to face matrix

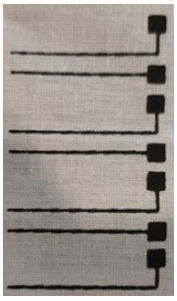


(c) Two layers matrix

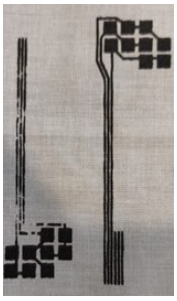
Figure 5.12: Photosensibilization Results

quite difficult to manufacture as there was no equipment with sufficient resolution. Nevertheless, the circuit design could be useful for a future iteration of the project.

Therefore, for the proof of concept, only the face-to-face sensors were printed in unit and matrix format on PET sheets.



(a) Face to face unitary sensor



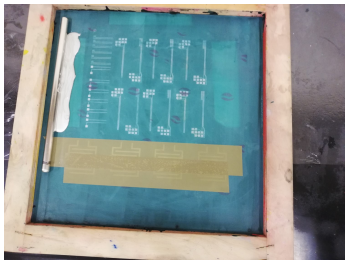
(b) Face to face matrix sensor



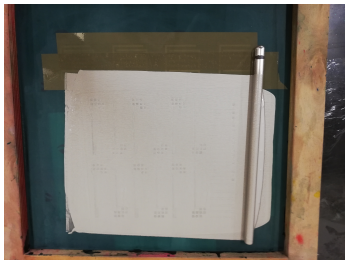
(c) Two layers matrix sensor

Figure 5.13: Proof print Results

The success of the print depends on several factors such as the mesh count of the screen, the characteristics of the rod used to spread the ink, the number of passes of the rod through the screen and the level of the magnetic field. In addition, the temperature and drying time in the oven also change the final result. Three prints with conductive ink were made in order to understand the best parameters for the sensor arrays prints.



(a) Screen printing before spilled paint



(b) Screen printing with spilled paint



(c) Screen printing for piezoresistive sensor

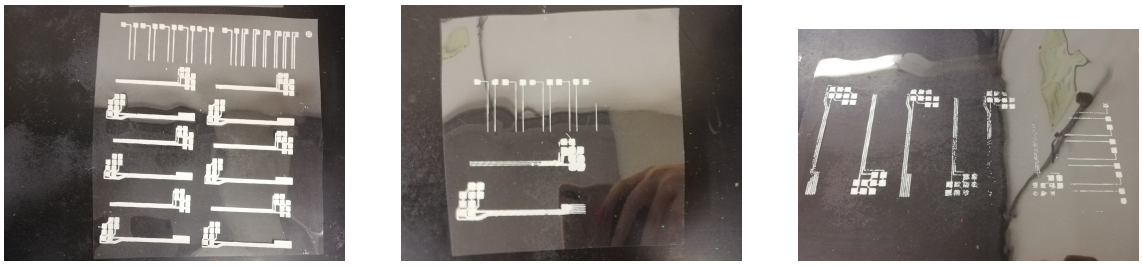
Figure 5.14: Face to face sensor array circuit

In the first print a smooth rod with a diameter of 12 mm, a magnetic field of level 4 and two passes of the rod on the screen were used. In the second print a screen with a superior mesh count, a magnetic field of level 2, a splined rod with a 6 mm diameter and only one passage of the rod on the screen was used. The third print was performed with the following parameters: the screen of the first print and the parameters of the second print. These parameters are summarized in the table 5.4. The conductive ink printed on the PET sheets were dried in an oven at 120ºC for 10

PET Sheet/ Printing	**Screen mesh**	**Magnetic level**	**Rod**	**Passage**
1	Larger	4	Plain 12 mm	2
2	Thinner	2	Splined 6 mm	1
3	Larger	2	Splined 6 mm	1

Table 5.4: Parameters used during screen printing

minutes.



(a) First printed PET (b) Second PET sheet (c) Third PET sheet

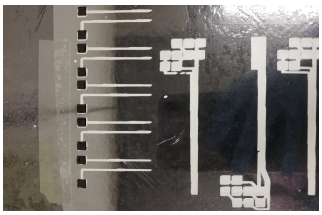
Figure 5.15: Results from conductive printing

After this step, the piezoresistive ink was printed with the screen prepared for this purpose. In this case, the previous conditions were maintained for each of the PET sheets. The sheets were placed again in the oven, but at a lower temperature: 60ºC for 10 minutes.

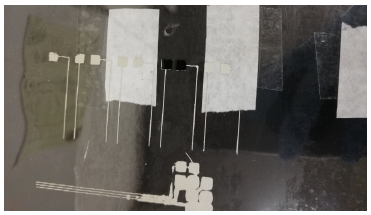
During the process, it was observed that the ink was a ink spreading on the PET sheet which led to different dimensions between conductive than the piezoresistive squares. This adimensionality could lead to a short circuit when the sensor was placed together.

To minimise this unforeseen event, a second printing of the piezoresistive layer was performed in which an attempt was made to cover the sensitive areas that were not yet covered with piezoresistive ink. In the second printing, the PET sheets were positioned in a different way and in the third printing the areas to be printed were drawn on the part of the screen that had not yet been subjected to photosensitization.

Although the manufacturer's instructions were followed, printing with the conductive ink did not go as expected. Therefore, it will be important to study the adhesion of the conductive and



(a) First PET sheet



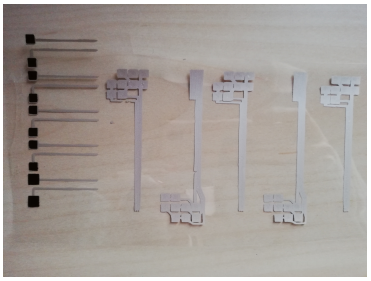
(b) Second PET sheet



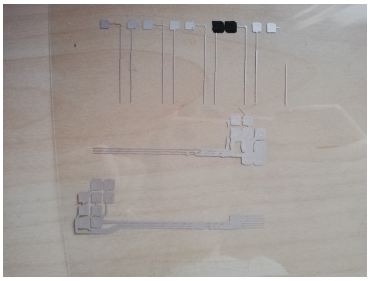
(c) Third PET sheet

Figure 5.16: Results from first layer of piezoresistive printing

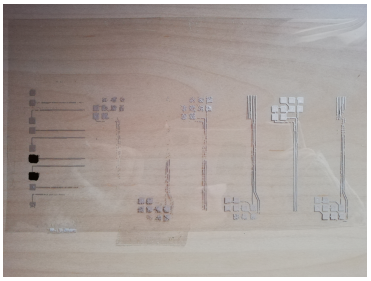
piezoresistive ink to the PET material and between them to optimise the manufacturing process and change the designs so that the two layers are overlapped during printing.



(a) First printed PET



(b) Second PET sheet



(c) Third PET sheet

Figure 5.17: Results from second layer of piezoresistive printing

The unitary sensors were successfully printed and it was possible to evaluate them in order to assess these materials can be the solution to the proposed problem. However, the matrices were not correctly printed. In the first printing, the sensing areas are not well defined and the tracks are joined. In the second print, some regions of the tracks are not well defined and others are flawed. In the third print there are some flaws in the print so the signal will not be conducted. Due to these imperfections, the piezoresistive ink was only applied to the single sensors. The unitary sensors with double layer were printed with conductive ink to try to understand the feasibility of printing this type of sensors, but the resolution was not ideal.

5.4.3 Sensor Evaluation

In order to evaluate these sensors, it was used same structure from Velostat prototype evaluation. First, it was necessary to understand if the sensor was working correctly, so resistance without pressure applied and with the 2000 g weight was calculated. However, the sensor from the first printing was the only that has presented resistance, therefore the other two sensors, were not evaluated. This can be justified by some lack of conductive ink that is not perceptible at naked eye, therefore it is necessary to improve the manufacturing process in order to solve this problem.

Regarding the first sensor the experiment was repeated twice and the results are presented at Table 5.5. This values are important to understand the resistance value that will be used in the acquisition circuit. These values are important to know the sensor output range: 511 K for the first trial and 450 K for the second trial.

Pressure applied (kPa)	**Trial 1** (K)	**Trial 1** (K)
0	620	620
1250.35	109	170

Table 5.5: Sensor resistance values without charges applied and with the maximum charge applied

A second test was carried out to understand sensor behaviour with different charges applied. As it is possible to understand from Figure and Table, as higher the pressure applied, the lowest is the resistance value. These values are important for sensor calibration (Table 5.6 and Figure 5.18).

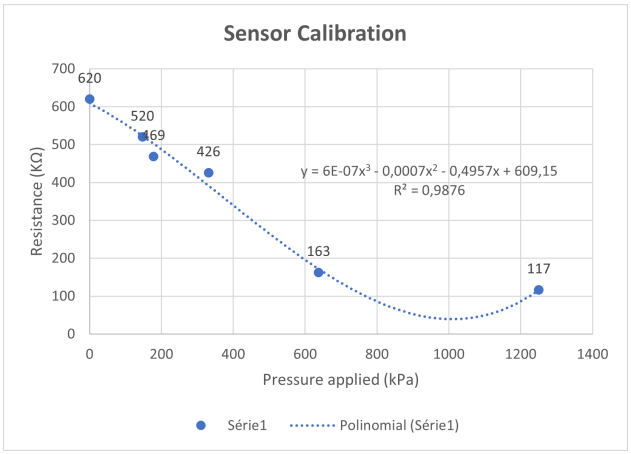


Figure 5.18: Pressure vs Resistance chart for Screen Printing Prototype

Pressure applied (kPa)	**Resistance** (KΩ)
0	620
147.10	520
177.74	469
330.97	426
637.43	163
1250.35	117

Table 5.6: Pressure vs Resistance chart for Screen Printing Prototype

The hysteresis was also evaluated by incrementing and decrementing the load applied to the sensor using the same weights from Velostat Prototype (Section 5.3.2).

As we can see from the results of the Table 5.7 and Figure 5.19, for the face to face sensor the increase and decrease of load present a second degree polynomial behaviour.

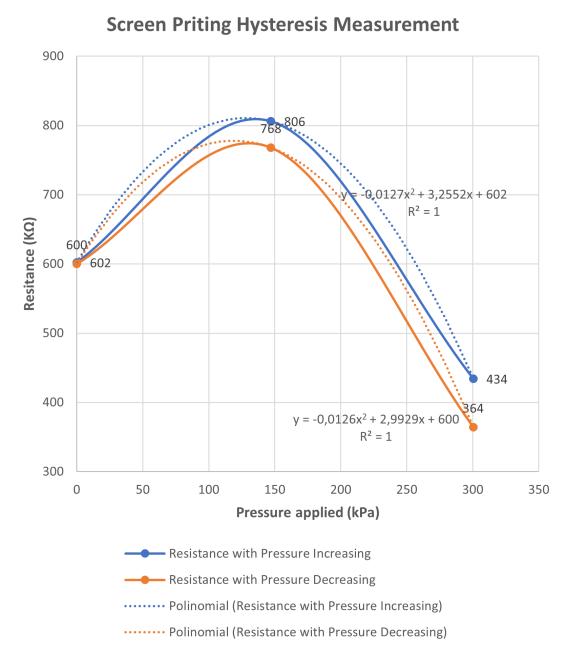


Figure 5.19: Graphical Representation Hysteresis Experiment for Screen-printed Prototype

Pressure (kPa)	**Loading** (KΩ)	**Unloading** (KΩ)	**Uncertainty** (KΩ)
0	602	600	2
147.10	806	768	38
300.33	434	364	70
606.79	206	206	0 height

Table 5.7: Values for Hysteresis Determination Experiment on Screen Printing Prototype

.

The following steps of this dissertation (Chapter 6) were developed taking into account face-to-face model being necessary some minimal changes so that the circuit and Arduino code can be used with two layers model.

5.5 Conclusions

The manufacturing process of the first sensor was manual which leads to a lower precision in the construction than the sensor built with the screen printing method which is mechanical and therefore allows a uniformity in the distribution of the inks. Furthermore, the sensor manufactured by the first process presents a rather irregular behaviour that cannot be used in our application. The sensors manufactured by screen printing present more satisfactory results and adequate to the end user needs. The unitary face to face prototype presented very satisfactory results, however it is necessary to optimise the printing variables such as the mesh count and the magnetic level or select another method with an higher resolution to manufacture the final sensor and even the two layer sensor .

In the case of the unitary face-to-face sensor configuration, this presents a better response both in terms of hysteresis and recovery from the initial resting state, something quite important in the case of dynamic tests. Besides, the maximum and minimum resistances were always kept in the same range of values, which allows us to conclude that this sensor will have a low absolute deviation, which allows us to conclude that it can be used to measure the forces in the TMC joint.

Chapter 6

Data Acquisition and Visualization

6.1 Acquisition Electronic Circuit

As already mentioned in the previous Chapter (Chapter 5), the pressure matrix is organised into groups the numbers and the letters that, when combined, allow the pressure determination in each unitary sensor. Therefore, it is be necessary to build an acquisition circuit in order to obtain those values. This circuit can be divided into three main groups: the components that are connected to the numbers, the ones that are connected to the sensor and the microcomputer. The first group are tree buffers with voltages dividers that are responsible to feed the sensor with a constant current. The second group consist on the amplification of the sensor values. The circuit is represented at Figure B.1.

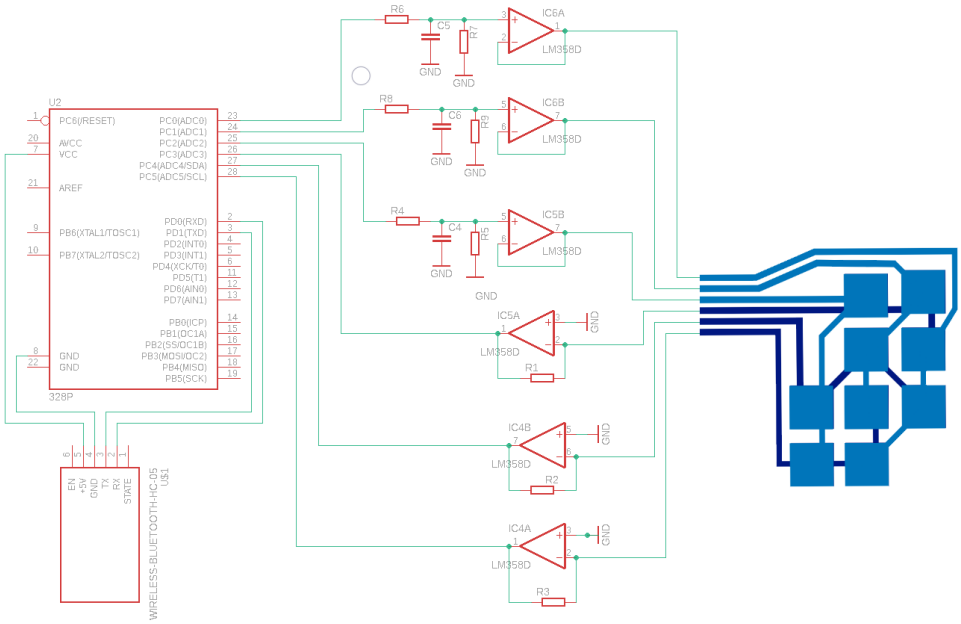


Figure 6.1: Acquisition Circuit Representation

As the main requirements of this project is maintain the development cost low and common

operation amplifiers (op-amps) can be used during circuit assembly, three LM358 op-amps were selected. The components of the circuits are powered with a voltage of 5 V.

The buffers with voltage dividers make the input voltage constant in the sensor branches. According to the FSR guide [28] the current in piezoresistive sensors should be limited to 1 mA/cm^2. Knowing that each unitary sensor has 16 mm^2 and that each line has three sensors the circuit should be fed with a maximum current of 0.48 mA. Therefore, it is necessary that the circuit voltage is approximately 2.5 V. Thus, it is necessary to use 100 KΩ resistors in the voltage dividers (Figure 6.2).

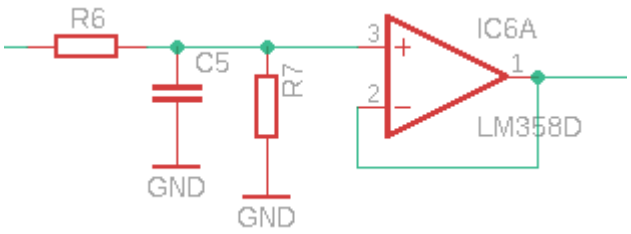


Figure 6.2: Amplifier with a voltage divider

The capacitor acts as a filter decoupling the possible noise. These values were obtained using the following Equations:

$$V_{out} = V_{in}\frac{R_2}{R_1 + R_2} \tag{6.1}$$

$$\frac{V_{out}}{R_2} = -V_{in}\frac{R_2}{R_1 + R_2} \tag{6.2}$$

$$\frac{V_{out}}{R_2} = \frac{V_{in}}{R_1 + R_2} = 0.48mA \tag{6.3}$$

Assuming that R_1=R_2 and $V_{in} = 5$ V:

$$\frac{5}{R_1 + R_2} = 0.48mA \tag{6.4}$$

$$R_2 = R_1 = 100k\Omega \tag{6.5}$$

$$V_{out} = 2,5V \tag{6.6}$$

In each of the columns will be introduced an inverting amplifier that can be described by the equation 6.7 and allows to obtain the values to which the sensor is subject. This equation will be used in the Arduino code that allows the conversion of voltage into resistance and will allow the forces and pressures exerted on each sensor to be calculated by the Arduino.

$$V_{OUT} = \frac{V_{REF} * R}{R_{Sensor}} \tag{6.7}$$

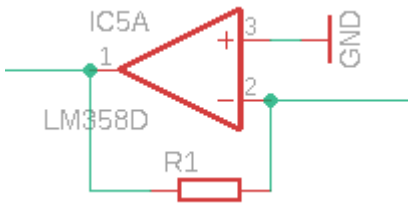
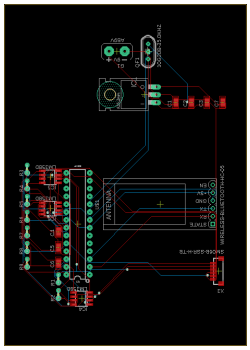


Figure 6.3: Inverting Amplifier

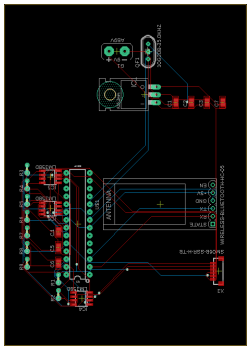
The values of resistances used in the inverting amplifier (R) are the value of the resistance when the maximum weight is applied and that was calculated during the evaluation of the sensors in the Section 5.3.2.

Since the circuit will be used in surgeries where space is limited and already has several cables (debriders, vital signs meters and bone saw) it is important to minimize the existence of power and communication cables. Therefore, it is important to power the circuit with a portable battery such as a 9V battery. The circuit was designed on a PCB board to minimise its size and avoid cables as in conventional circuits and is represented at Figure B.3. Besides, a ground polygon was design in each layer (top and bottom) to minimise electromagnetic interferences and crosstalk.

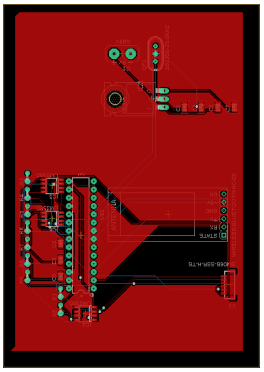
The PCB and Arduino were then placed in a box to facilitate sterilisation and handling of the device.



(a) Top Layer without ground plane



(b) Bottom Layer without ground plane



(c) Top Layer with ground plane

Figure 6.4: Face to face sensor array circuit

6.2 Data Acquisition (*Arduino*)

The Arduino with the associated Bluetooth module has as its main function to feed the acquisition circuit and to access the reading and interpretation of the information obtained for each sensor and the sending of that same information to the visualisation and data recording software (Section 6.3). The diagram of activities of the Figure 6.5 schematises this interpretation.

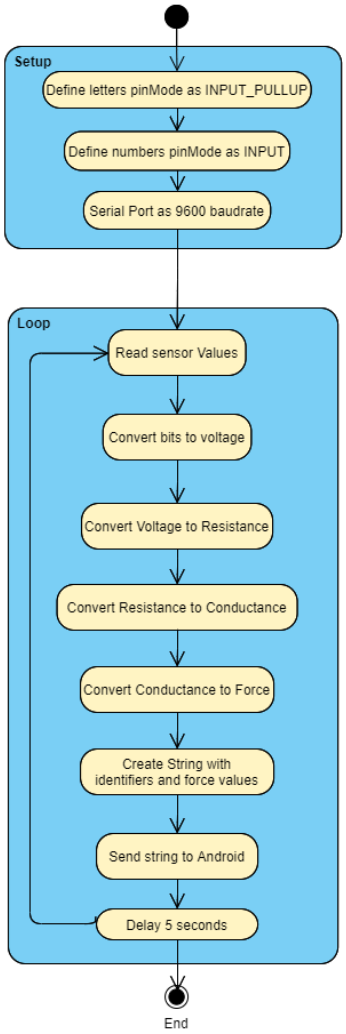


Figure 6.5: Arduino Activity Diagram

As the main goal is to determine the pressure quantitatively, the analog pins were selected. The analog pins receive values between 0 and 1023 that can be converted into a scale, allowing the determination of the pressure value and only if the pressure is being applied. In this case, the analog pins A0, A1 and A2 were chosen for the lines , and therefore as *INPUT_ PULLUP pinMode*. The analog pins A3, A4 and A5 were chosen for the sensor's output (and as pinMode *INPUT*). This code goes through the matrix and read the value of each sensor by traversing the rows and columns in a for loop.

There are three functions that allow the reading,conversion and transmission of the sensor signal.

The *readSensors()* function reads the analog value for each row and column according to the schemes explained in Figure 5.5. This function is inside void loop() and therefore is a cycle that is repeated every 5 seconds.

In the *sendAndroidValue()* function sends the values in string format to the android program. The symbols + and ˜ represent the beginning and the end of the string respectively. This way, the Android system can recognise the string containing the force values per unitary sensor area or pressure.

The *getForceValue()* function converts the values of the output voltage from the array that is acquired by the sensor and converts them into force. assuming the output voltage is given by:

$$V_{OUT} = \frac{V_{REF} * R_G}{R_{Sensor}} \tag{6.8}$$

The reading of the analogue value ranges from 0 to 1023 being mapped between 0 and 5 V (5000 mV). This conversion is obtained through the Equation 6.9.

$$VoltageValue = \frac{SensorValue * 5}{1023} \tag{6.9}$$

As the sensor voltage is

$$ResistanceValue = \frac{(5000 - VoltageValue) * R_G}{VoltageValue} \tag{6.10}$$

The value of conductance is obtained

$$Conductance = \frac{R_G}{ResistanceValue} \tag{6.11}$$

When the calibration curves for our sensor are defined, it is necessary to proceed to an approximation of the force. Therefore, assuming that it behaves as a typical FSR, if the conductance is <=1000, the force is

$$Force = \frac{Conductace}{80} \tag{6.12}$$

When the conductance is greater than 1000:

$$Force = \frac{Conductace}{30} \tag{6.13}$$

6.3 Data Visualization (Android)

In addition to developing an acquisition system, it was necessary to develop user-friendly software so that end users could easily adapt to the device. To this end, an interface was developed on the Android system that allows not only to graphically display the values that were being acquired, but also to decide which values should be recorded.

The graphic interface also allows the selection of the device to be paired, enter the data of the patient being studied, decide which values are recorded for each position determined by the surgeon and save them to the database. Moreover, there is also the option of viewing the values recorded for each of the movements since the surgeon may collect more than one value for each movement. The activity diagram of the Figure 6.6 represents the software operation in a simplified. The front-end is operated by the user, the back-end corresponds to the Android back-end and data base (SQLite) and the device corresponds to the Arduino Code.

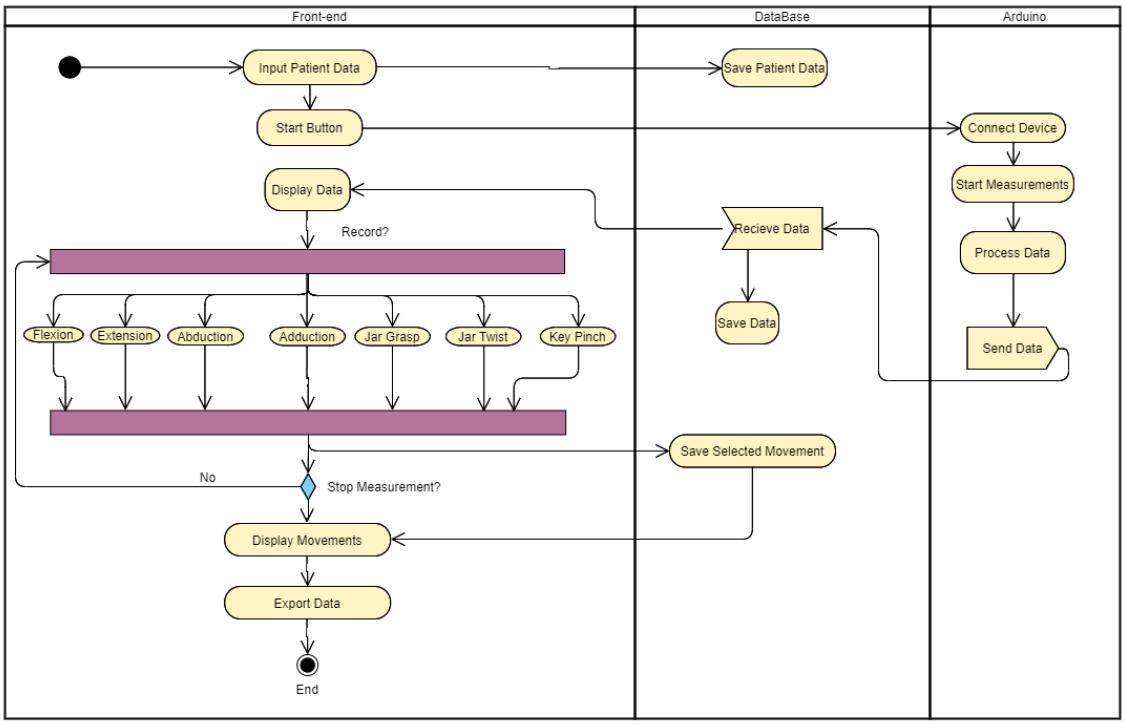


Figure 6.6: Android Activity Diagram

6.3.1 Device connection

During this project and after a visit to OR where the surgeries are performed it was clear that the connection between the sensor and the Android application should be established through Bluetooth. Therefore, there was necessary to add Bluetooth permissions to the manifest. When there are Bluetooth devices near the Android device they are displayed in a list and you need to

choose the sensor. If the sensor does not appear in the list of sensors, you need to pair it first in the device settings.

6.3.2 Database

The SQLite database was used in order to store the data in a more systemic way. In this database, nine different tables are stored:

1. Patient Information;
2. Sensor data during the entire experiment;
3. Saved Flexion data
4. Saved Extension data
5. Saved Adduction data
6. Saved Abduction data
7. Saved Key Pinch data
8. Saved Jar Twist data
9. Saved Jar Grasp data

6.3.3 Patient Data Form

There are several factors that determine the type of surgery to be performed in patients with OA in the TMC joint, such as age, gender and the stage of the disease. In addition, before the patient is anaesthetised, a hand dynamometer is used to test their strength. In this case there are three positions which are assessed and must be collected and saved on a form before surgery begins. In addition, there is a field for any additional notes that may be required. All this information must be gathered in a form for each patient that will be saved in the database.

6.3.4 Data Visualisation and Events Recording

The library *MPAndroidChart* library was used to display the sensor values in real time in a bubble chart. in this chart the sensors are arranged in a visual way to facilitate the surgeon's understanding. Thus, the sensors are arranged in the chart as in figure 6.8a.

During the evaluation of the force/pressure that the patient can exert before and after the surgical procedure, he is required to perform several movements that are represented in the Figures 2.5a to 2.5g from Anatomical Background (Chapter 2.2.1). As these movements are not performed successively, there are buttons with the above-mentioned images so that the recording of the acquired values in each of the positions can be performed in a random way.

Besides that, there are also buttons to start and finish the acquisition so that all the values of the test are recorded in a table.

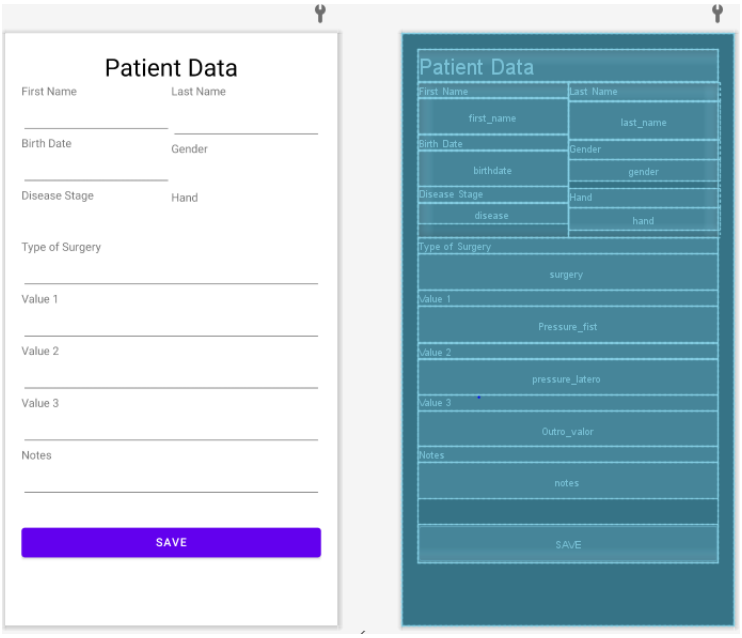


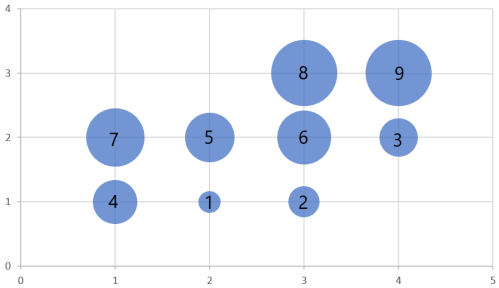
Figure 6.7: Patient Data Form

6.3.5 Events Visualisation

In order for surgeons to get an insight into the impact of surgery for the patient's hand mobility, there is the possibility to compare the recorded results for each movement through a vertical bar graph from MPAndroidChart library. The graph can be selected through a spinner that selects the movement that will be displayed. These values are stored in the myDb database.

6.3.6 Export Data

Since the main purpose of this device is to acquire pressure values from the TMC joint during surgery, it is easily understandable that the values will be processed and analysed by surgeons. Therefore, it is important that the data is stored in a format that they can use to draw conclusions. Thus, there is the possibility of exporting the tables to a ".csv" file which can then be used in data processing software such as Excel, SPSS and others.



(a) BubbleChart Organization



(b) Aquisition Buttons

Figure 6.8: Aquisition Screen

Chapter 7

Conclusions and Future work

7.1 General Conclusions

This project consisted of a work of Research and Development becoming necessary to carry out a thorough study on the characteristics and specificities of the TMC joint that is subject to surgery. Therefore, it was necessary to know the joint, its dimensions, curvatures, forces it exerts and the hand movements in which it is involved, the common pathology (OA) and its consequences on the joint to understand how to measure the TMC forces at this pioneering project.

Sensor development was one of the most challenging stages of the project due to its dimensions and lack of off-the-shelf sensors approved by health regulatory authorities, it was necessary to develop custom sensors. During this dissertation, two types of sensors were designed, and two sets of materials were selected. The first attempt consisted of a face-to-face sensor made of conductive paint and Velostat, but the reproducibility of this material was insufficient for developing this sensor.

Later, face-to-face, and two-layer sensors were manufactured by screen printing. Due to the reduced dimensions and the available material, it was not possible to print a complete array since the adhesion of the conductive ink on PET is not yet properly studied. The evaluation of the unitary face-to-face sensor revealed that these inks could be the solution for the fabrication of the sensor, but it is necessary to study the variables to optimize the printing or even to find other fabrication methods.

Besides the development of the sensor, the whole acquisition circuit was also developed, as well as the PCB board so that the device can be used during surgery. The associated Arduino code allows the conversion of the values obtained by the sensor into pressure values that surgeons can easily understand results during surgery.

Finally, an Android application was also developed, which allows not only the visualisation of the data in real-time but also the recording in a database. Additionally, it allows the user to collect the patient's data and the relevant measurement instants (movements) in a table. This data will be visualised in a bar chart allowing conclusions to be drawn while still in the per-operative period.

As all the data can be exported to the local memory of the device being used, this device gains a new utility as it can be used for further biomechanical studies and various types of clinical trials.

It is important to consider the conditions in which this dissertation was developed and the constraints inherent to it. This led to some delays in the development of this dissertation. Therefore, we can conclude that the main goal of this dissertation was achieved, since a major advance was made in the development of the system that allows for the measurement of intra-articular and per-operative forces.

7.2 Future Work

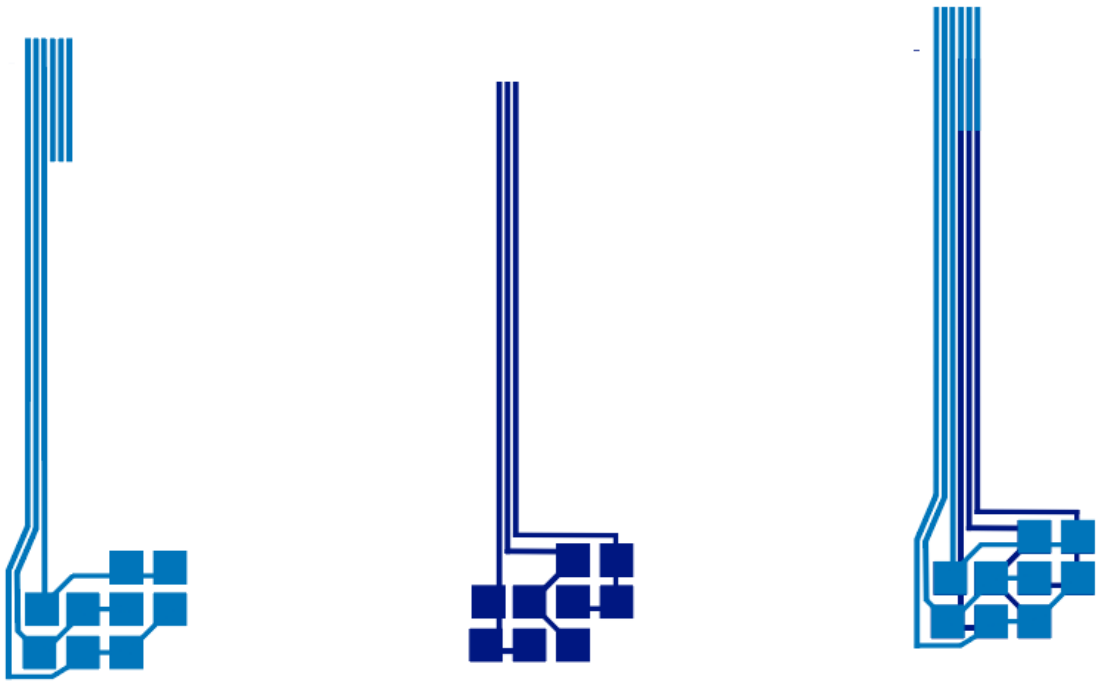
As it has been explained, only the unitary sensor was fully manufactured, therefore it is necessary to complete the sensor manufacturing process. Besides, it is also necessary to test the sensor with the PCB circuit and with the software. Therefore, this will be the next step in the continuation of this project. After the whole device has been tested and the necessary adjustments have been made (namely the resistances used), the sensor may be integrated in the clinical tests that are being carried out at the CHLeiria, in order to be tested in a real environment. As one of the solutions for the treatment of advanced OA is the implantation of a prosthesis in the TMC joint, it would be interesting to produce a second sensor that would adapt to the prosthesis head, in order to assess the success of its application and make the necessary adjustments more precisely, as patients do not always cooperate as desired.

Appendix A

Final Sensors

In this Appendix the negatives that were produced with screen printing are available.

A.1 Face to face configuration



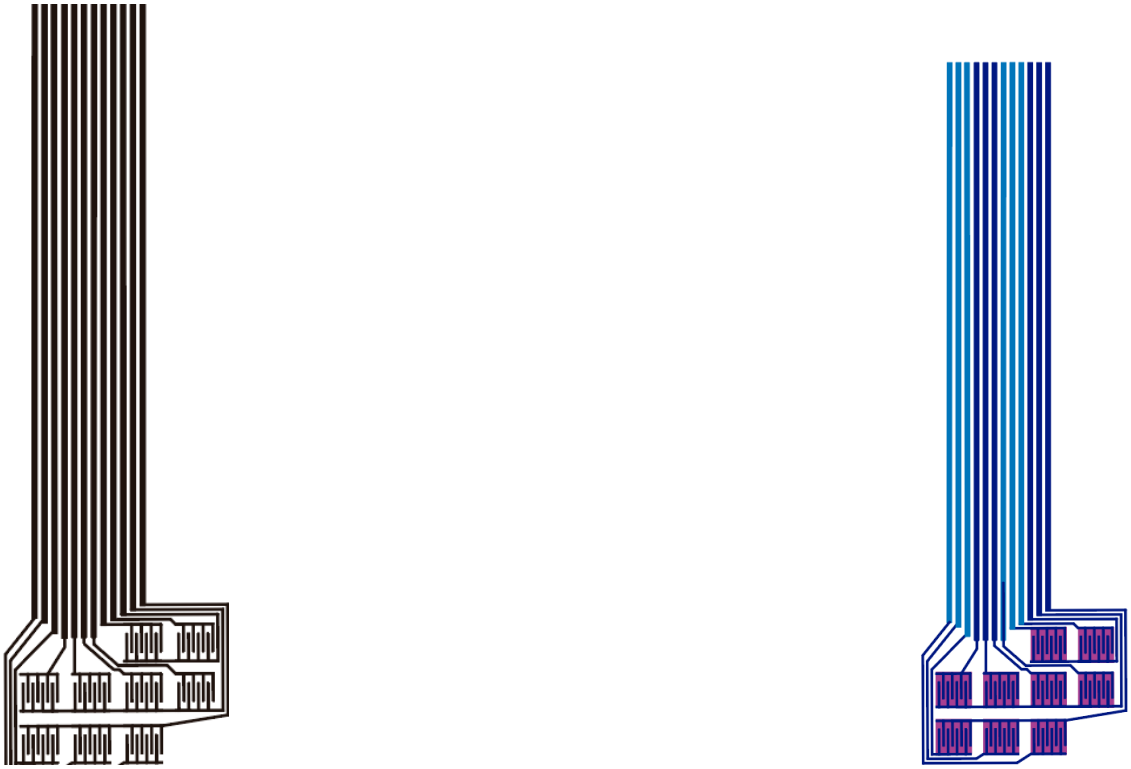
(a) Bottom Layer

(b) Top Layer

(c) Top and bottom layers overlaped

Figure A.1: Face to face sensor array circuit

A.2 Two layers configuration



(a) Conductive layer

(b) Top Layer

Figure A.2: Two layer sensor array circuit

Appendix B

Acquisition Circuit and PCB Schematics

B.1 Acquisition Circuit Representation

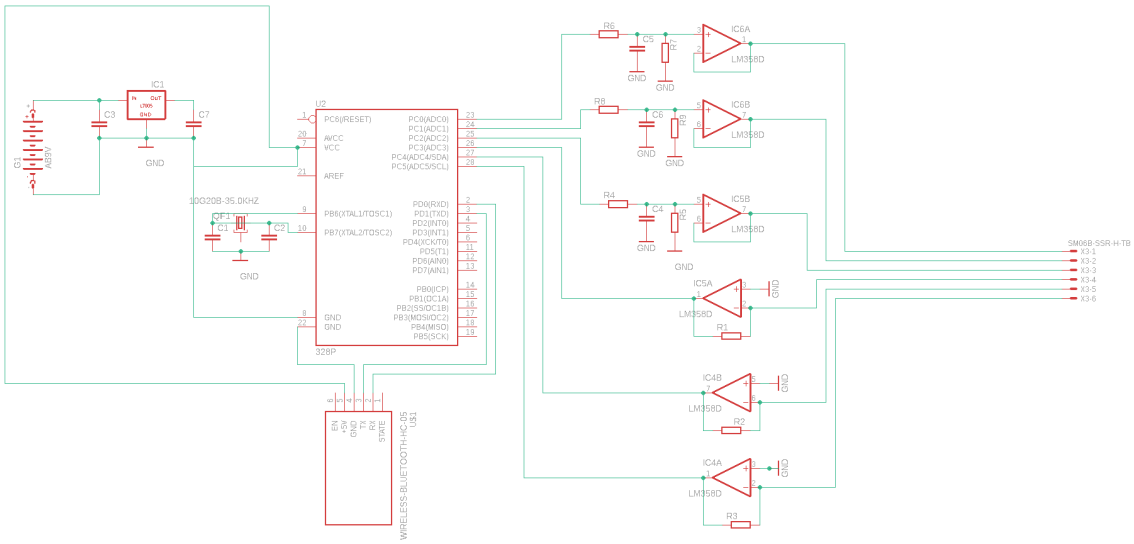
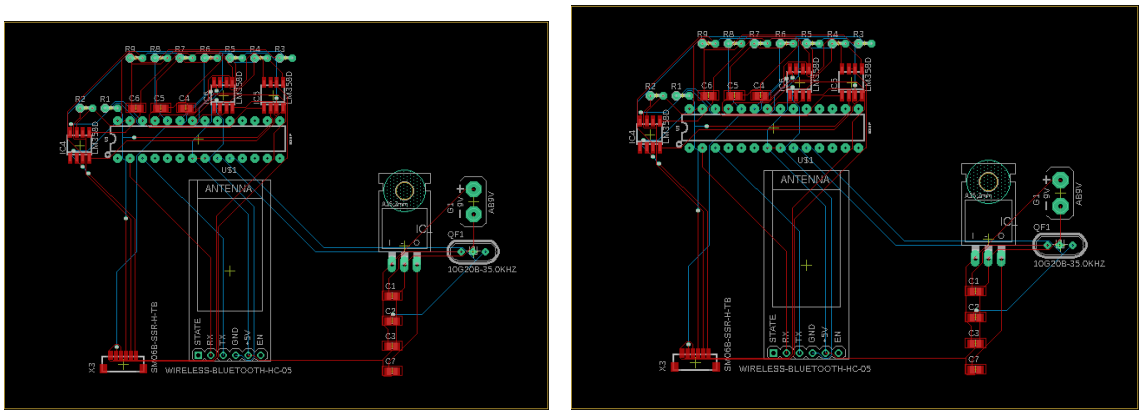


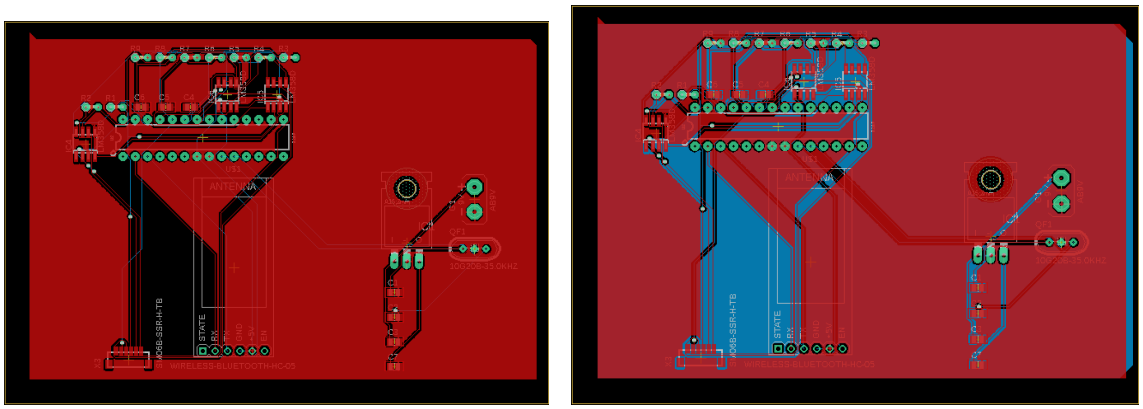
Figure B.1: Acquisition Circuit Representation with all the components

B.2 PCB Schematics



(a) Top Layer (b) Bottom Layer

Figure B.2: PCB circuit without ground plane



(a) Top Layer (b) Bottom Layer

Figure B.3: PCB circuit

Appendix C

Arduino Code

```
#define numLetters 3
#define numNumbers 3
#define numSensors 9

int numbers[3] = {11, 10, 9};
int letters[3] = {A0, A1, A2};

//Fixed value
int R_fixed = 100000; //Value that sensor dependent

//Arrays for the 4 inputs
float sensorValue[9] = {0, 0, 0, 0, 0, 0, 0, 0, 0};
float VoltageValue[9] = {0, 0, 0, 0, 0, 0, 0, 0, 0};
float ResistanceValue [9] = {0, 0, 0, 0, 0, 0, 0, 0, 0};
float CondutanceValue [9] = {0, 0, 0, 0, 0, 0, 0, 0, 0};
float ForceValue [9] = {0, 0, 0, 0, 0, 0, 0, 0, 0};
float PressureValue [9]={0, 0, 0, 0, 0, 0, 0, 0, 0};

//Char for reading in Serial characters
char inbyte = 0;

void setup() {
  // put your setup code here, to run once:
  for (int i = 0; i < numLetters; i++)
  {
    pinMode (letters[i], INPUT_PULLUP);
  }
  for (int i = 0; i < numNumbers; i++)
```

```
29   {
30     pinMode (numbers[i], INPUT);
31   }
32   Serial.begin(96000);
33 }
34
35 void loop()
36 {
37   // reads sensor values
38   void readSensors()
39   {
40     int i = 0;
41     for (int numberCount = 0; numberCount < numNumbers;
          numberCount++)
42     {
43       pinMode(numbers[numberCount], OUTPUT);
44       digitalWrite(numbers[NumberCount], LOW);
45       for (int letterCount = 0; letterCount < numLetters;
            letterCount++)
46       {
47         sensorValue[i] = analogRead(letters[letterCount]);
48         i++;
49       }
50       pinMode[numbers[numberCount], INPUT];
51     }
52   }
53
54   void sendAndroidValues()
55   {
56     Serial.print('#');
57     for (int k = 0; k < numSensors; k++)
58     {
59       Serial.print(PressureValue[k]);
60       Serial.print('+');
61     }
62     Serial.print('~');
63     Serial.println();
64     delay(5000);
65   }
66
```

```
67 void getForceValue(){
68     for (int x = 0; x < numSensors; x++)
69     {
70       // The voltage = Vcc * R / (R + Sensor)
71       // so Sensor = ((Vcc - V) * R) / V
72 
73       VoltageValue[x] = ((sensorValue[x] / 1023) * 5);
74 
75       //Voltagem sensor 5000 mV
76       ResistanceValue[x] = 5000 - VoltageValue[x];
77       //Resistance value
78       ResistanceValue[x] *= R_fixed;
79       ResistanceValue[x] /= VoltageValue[x];
80 
81       CondutanceValue [x] = 1000000;
82       CondutanceValue [x] /= ResistanceValue;
83 
84       if (ConductanceValue[x] <= 1000)
85       {
86         ForceValue[x] = ConductanceValue[x] / 80;
87         PressureValue[x] = ForceValue[x] *6.25;
88 
89       }
90       else
91         ForceValue[x] /= 30;
92         PressureValue[x] = ForceValue[x] *6.25;
93 
94     }
95   }
96 }
```

Appendix D

Android Diagrams

D.1 Android Activity Diagram

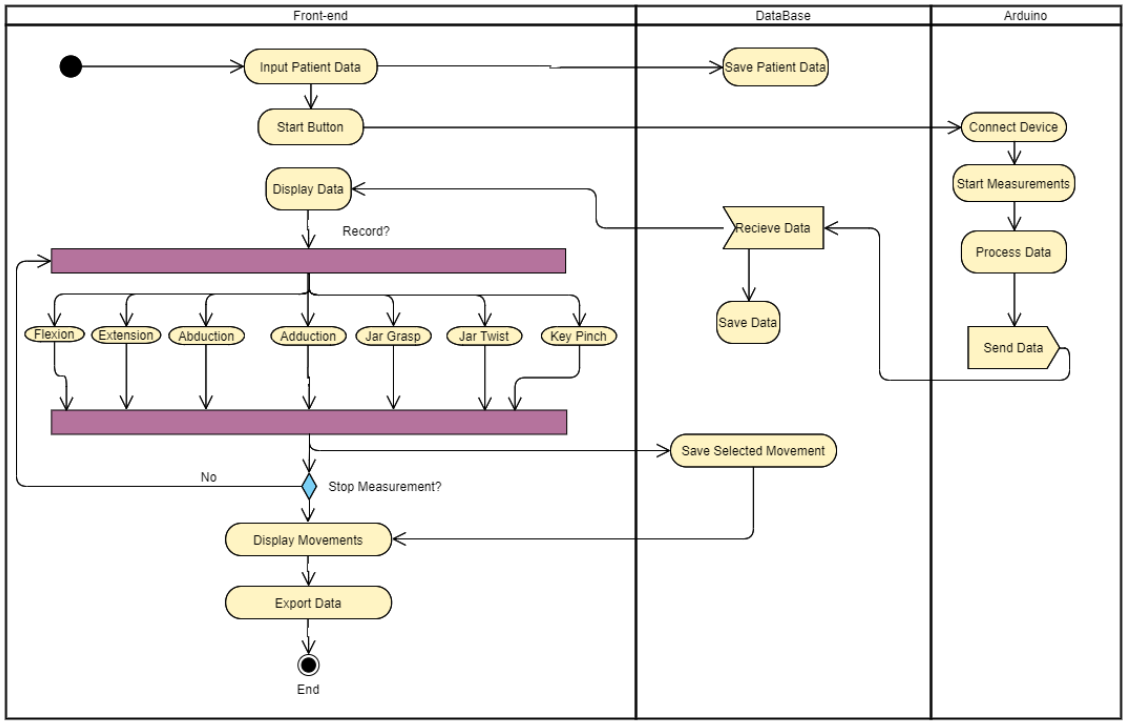


Figure D.1: Android Activity Diagram

D.2 Android APP Screens

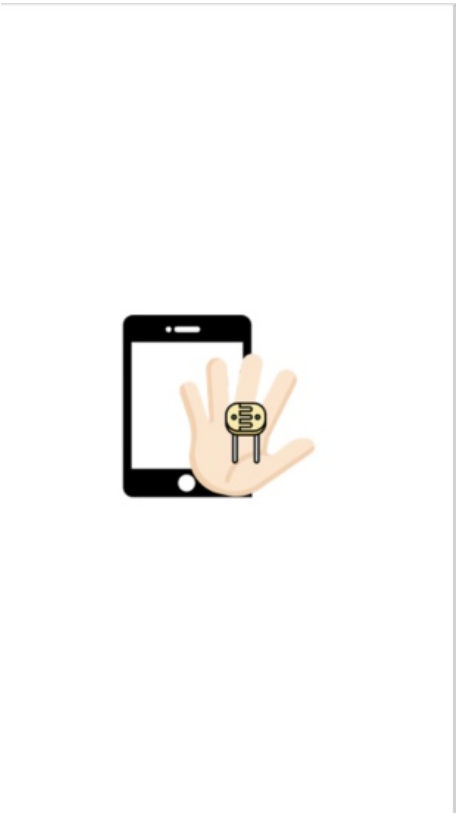


Figure D.2: Main screen

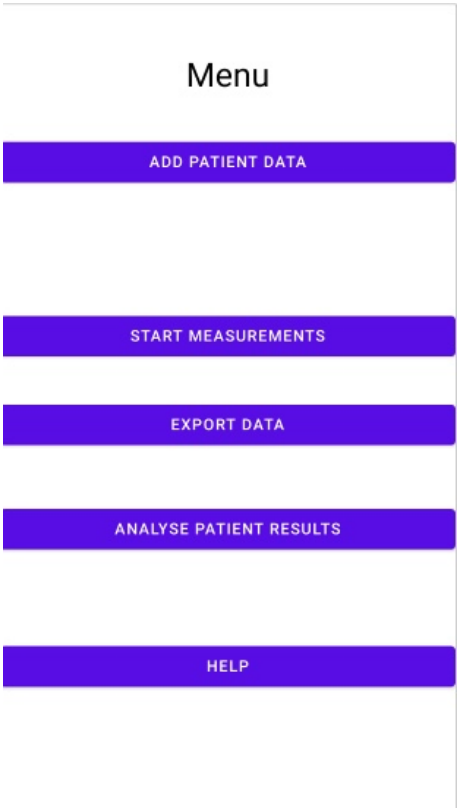


Figure D.3: Menu

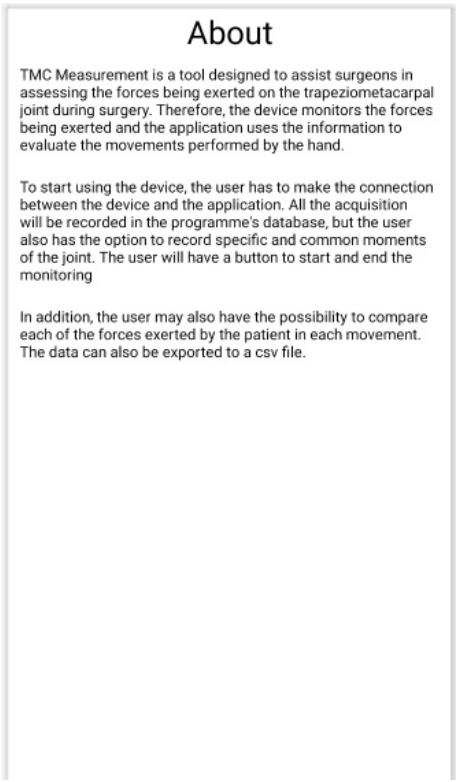


Figure D.4: About

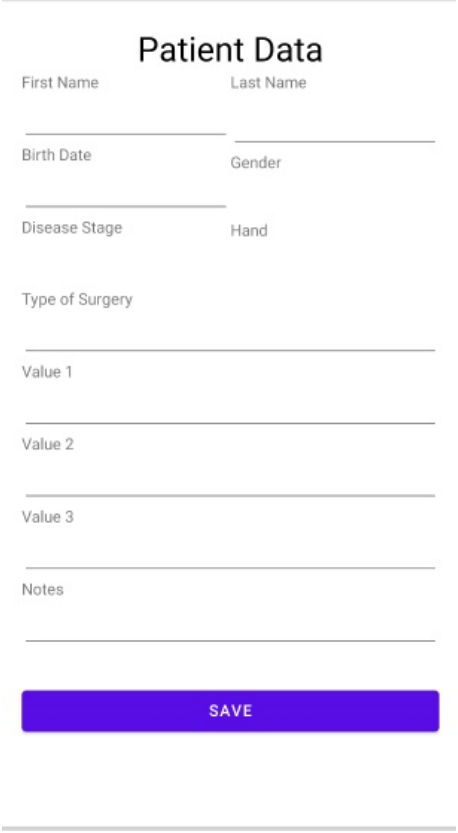


Figure D.5: Patient Information

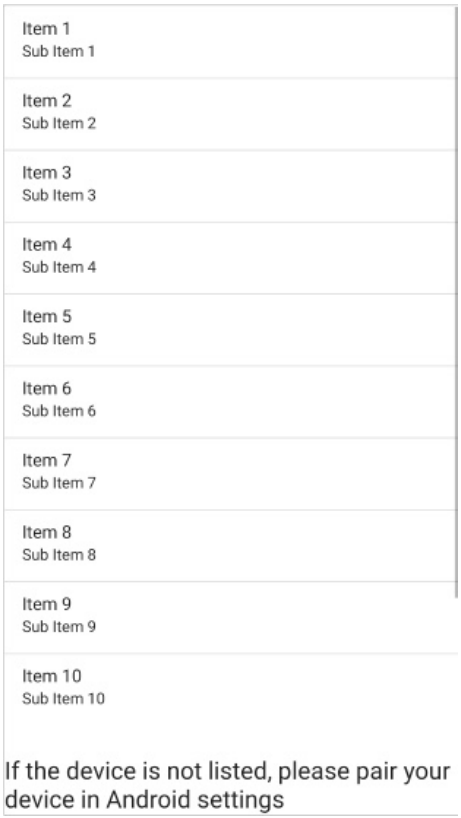


Figure D.6: Device connection

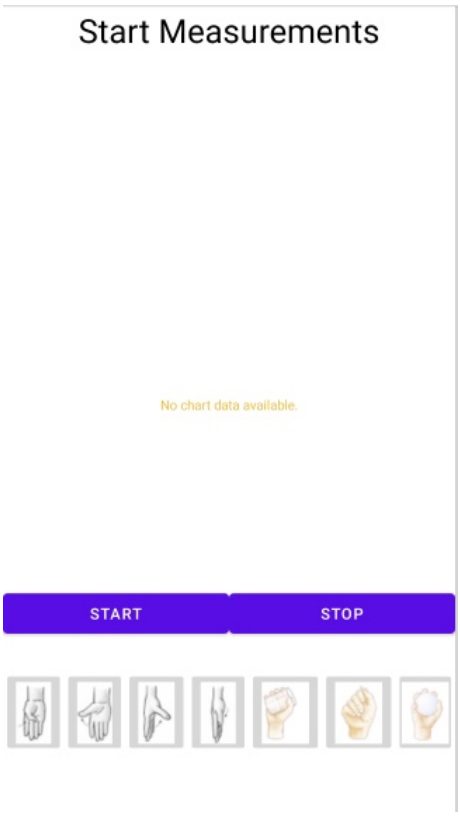


Figure D.7: Data Visualisation and Events Recording

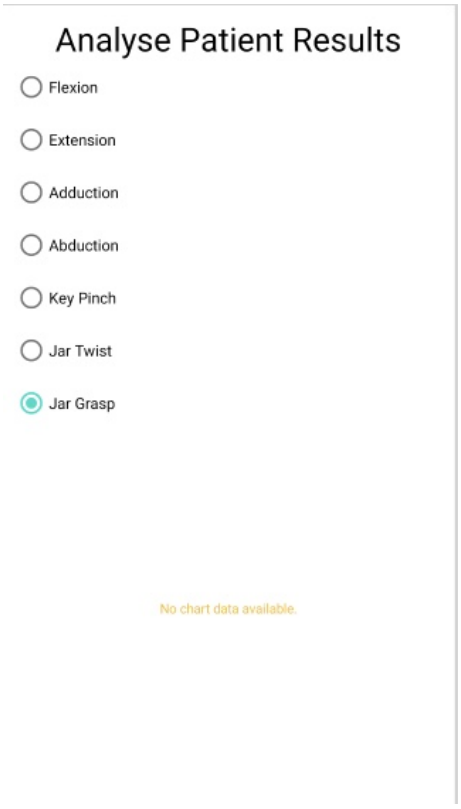


Figure D.8: Results Visualisation

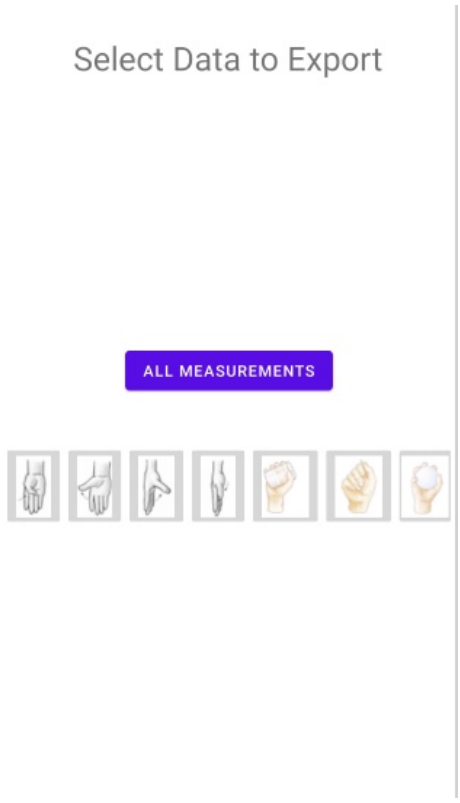


Figure D.9: Export Data

D.3 Database Structure

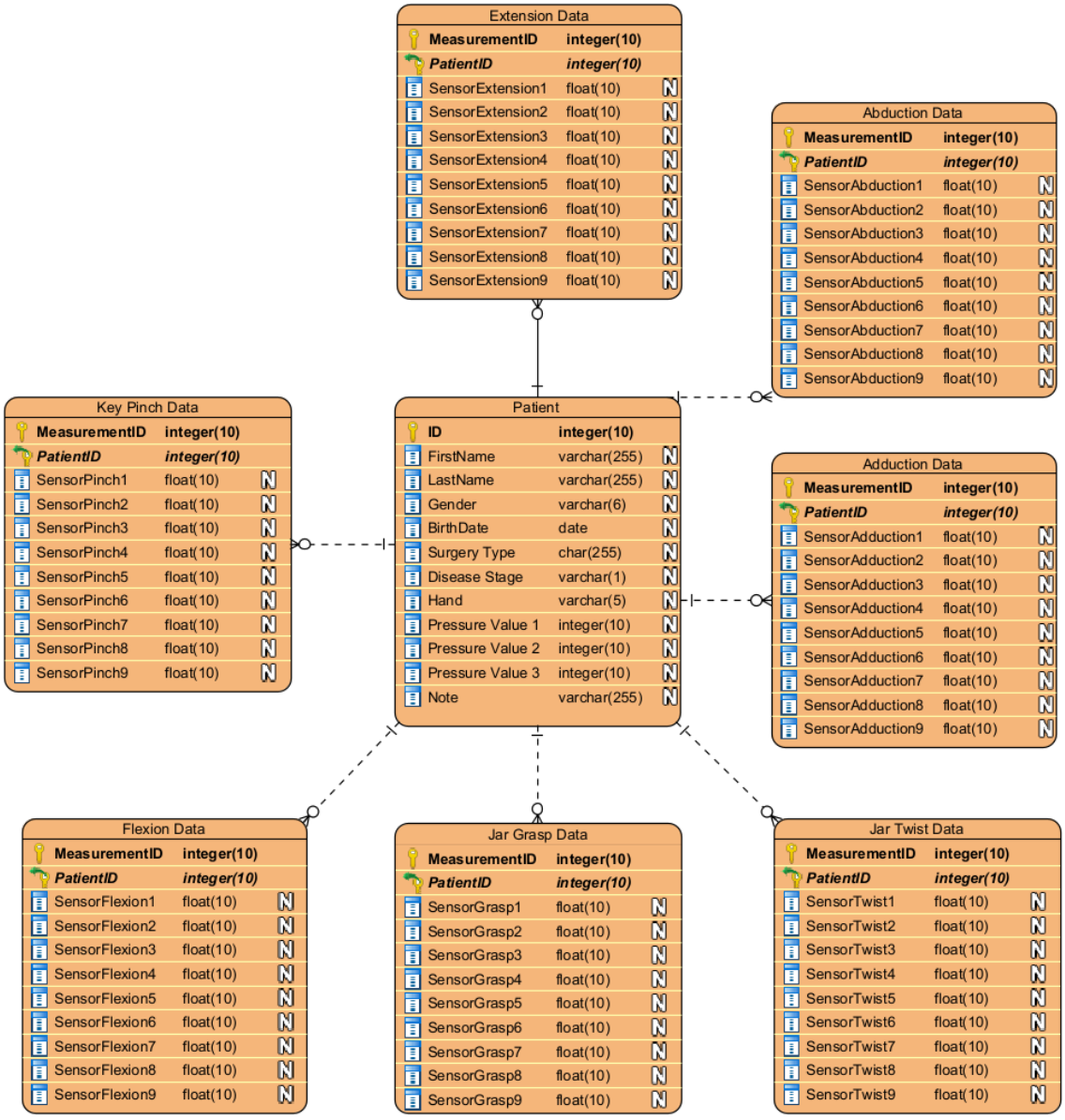


Figure D.10: Database Structure

Appendix E

Diagrams of complete system

E.1 Component Diagram

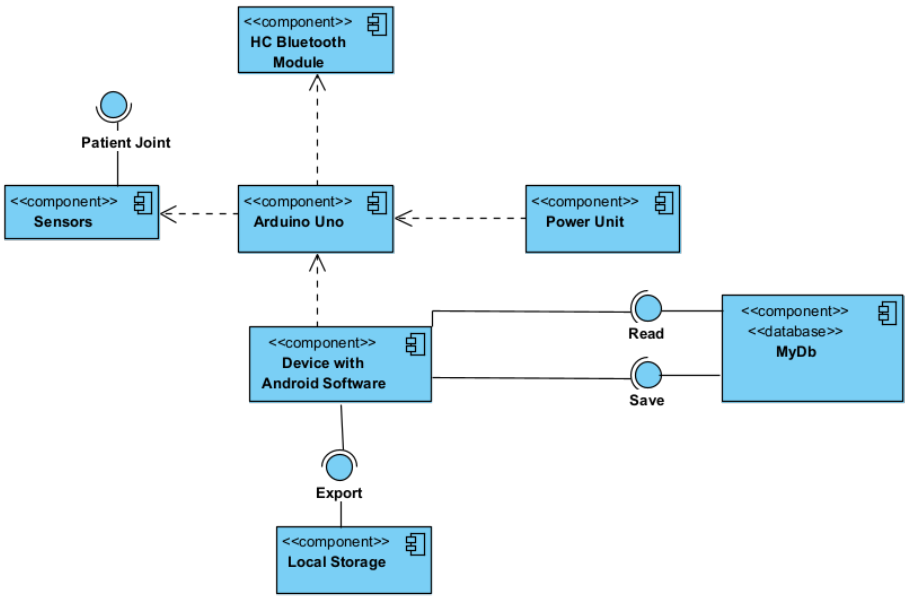


Figure E.1: Component Diagram

E.2 Deployment Diagram

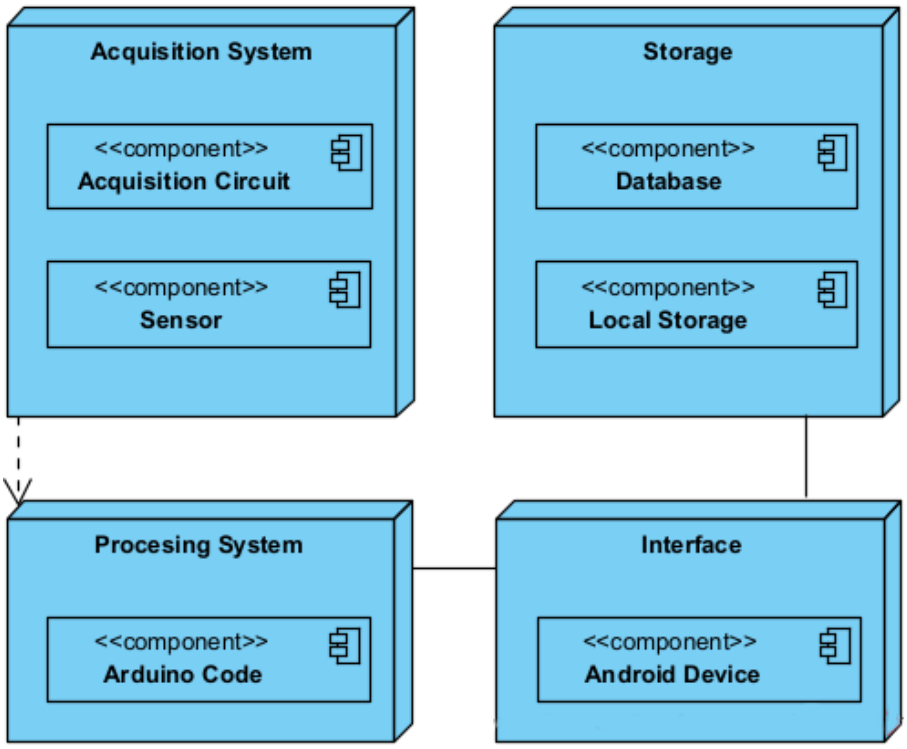


Figure E.2: Component Diagram

References

[1] Abele, N. (2014). Microelectronic pressure sensor.

[2] Al-Saygh, A., Ponnamma, D., AlMaadeed, M., Vijayan P, P., Karim, A., and Hassan, M. (2017). Flexible Pressure Sensor Based on PVDF Nanocomposites Containing Reduced Graphene Oxide-Titania Hybrid Nanolayers. *Polymers*, 9(12):33.

[3] Almassri, A. M. M., Hasan, W. Z. W., Ahmad, S. A., and Ishak, A. J. (2013). A sensitivity study of piezoresistive pressure sensor for robotic hand. In *RSM 2013 IEEE Regional Symposium on Micro and Nanoelectronics*, pages 394–397, Daerah Langkawi, Malaysia. IEEE.

[4] Ambra, L. F., Mestriner, A. B., Ackermann, J., Phan, A. T., Farr, J., and Gomoll, A. H. (2019). Bone-Plug Versus Soft Tissue Fixation of Medial Meniscal Allograft Transplants: A Biomechanical Study. *The American Journal of Sports Medicine*, 47(12):2960–2965.

[5] An, B. W., Heo, S., Ji, S., Bien, F., and Park, J.-U. (2018). Transparent and flexible fingerprint sensor array with multiplexed detection of tactile pressure and skin temperature. *Nature Communications*, 9(1):2458.

[6] Anderson, I. A., MacDiarmid, A. A., Harris, M. L., Gillies, R. M., Phelps, R., and Walsh, W. (2003). A novel method for measuring medial compartment pressures within the knee joint in-vivo. *Journal of Biomechanics*, 36(9):1391–1395.

[7] Arthritis Foundation (2020). ARTHRITIS BY THE NUMBERS. Technical report.

[8] Baldoli, I., Maselli, M., Cecchi, F., and Laschi, C. (2017). Development and characterization of a multilayer matrix textile sensor for interface pressure measurements. *Smart Materials and Structures*, 26(10):104011.

[9] Batra, S. and Kanvinde, R. (2007). Osteoarthritis of the thumb trapeziometacarpal joint. page 10.

[10] Betts, J. G., Desaix, P., Johnson, E. W., Johnson, J. E., Korol, O., Kruse, D., Poe, B., College, O., Wise, J., Womble, M. D., and Young, K. A. (2013). *Anatomy & Physiology*. OpenStax College, Rice University. Google-Books-ID: dvVgngEACAAJ.

[11] Brown, M., Bainbridge, C., Wong, J., and Phillips, A. (2020). Wide Awake Hand Surgery Handbook. page 8.

[12] Camprubi, J. P., Castells, I. S. T., Escudero, G. J., Garcia, U. D., and Ridao, G. M. (2009). Torsion and/or Tension And/or Pressure Textile Sensor.

[13] Carvalho, H., Yao, Y., and Gonçalves, L. M. (2017). Flexible force sensors for e-textiles. *IOP Conference Series: Materials Science and Engineering*, 254:072007.

[14] Casanova Canals, X., Ferreres Claramunt, A., Del Valle Jou, M., Pérez Abad, M., Noriego Muñoz, D., and Rodríguez Baeza, A. (2019). Study of intraarticular pressures in the elbow joints. *Journal of Biomechanics*, 97:109378.

[15] Cheema, T., Salas, C., Morrell, N., Lansing, L., Reda Taha, M. M., and Mercer, D. (2012). Opening Wedge Trapezial Osteotomy as Possible Treatment for Early Trapeziometacarpal Osteoarthritis: A Biomechanical Investigation of Radial Subluxation, Contact Area, and Contact Pressure. *The Journal of Hand Surgery*, 37(4):699–705.

[16] Choi, Y. W., Kang, D., Pikhitsa, P. V., Lee, T., Kim, S. M., Lee, G., Tahk, D., and Choi, M. (2017). Ultra-sensitive Pressure sensor based on guided straight mechanical cracks. *Scientific Reports*, 7(1):40116.

[17] Christen, P., Ito, K., Knippels, I., Müller, R., van Lenthe, G. H., and van Rietbergen, B. (2013). Subject-specific bone loading estimation in the human distal radius. *Journal of Biomechanics*, 46(4):759–766.

[18] Cork, R. (2007). XSENSOR technology: a pressure imaging overview. *Sensor Review*, 27(1):24–28.

[19] da Saúde, M. (2009). Decreto-Lei n.º 145/2009 de 17 de Junho de 2009 do Ministério da Saúde.

[20] D'Agostino, P. (2017). *How does the Trapeziometacarpal joint really function ? Anatomy and Biomechanics of the thumb*. PhD thesis.

[21] Dela Rosa, T. L., Vance, M. C., and Stern, P. J. (2004). Radiographic Optimization of the Eaton Classification. *Journal of Hand Surgery*, 29(2):173–177.

[22] D'Lima, D. D., Steklov, N., Fregly, B. J., Banks, S. A., and Colwell, C. W. (2008). In vivo contact stresses during activities of daily living after knee arthroplasty: CONTACT STRESSES AFTER KNEE ARTHROPLASTY. *Journal of Orthopaedic Research*, 26(12):1549–1555.

[23] Domalain, M. F., Seitz, W. H., Evans, P. J., and Li, Z.-M. (2011). Biomechanical effect of increasing or decreasing degrees of freedom for surgery of trapeziometacarpal joint arthritis: A simulation study. *Journal of Orthopaedic Research*, 29(11):1675–1681.

[24] Dornacher, D., Lippacher, S., Nelitz, M., Reichel, H., Ignatius, A., Dürselen, L., and Seitz, A. M. (2018). Impact of five different medial patellofemoral ligament-reconstruction strategies and three different graft pre-tensioning states on the mean patellofemoral contact pressure: a biomechanical study on human cadaver knees. *Journal of Experimental Orthopaedics*, 5(1):25.

[25] Dourthe, B., Nickmanesh, R., Wilson, D. R., D'Agostino, P., Patwa, A. N., Grinstaff, M. W., Snyder, B. D., and Vereecke, E. (2019). Assessment of healthy trapeziometacarpal cartilage properties using indentation testing and contrast-enhanced computed tomography. *Clinical Biomechanics*, 61:181–189.

[26] Eaton, R. G. and Glickel, S. Z. (1987). Trapeziometacarpal osteoarthritis. Staging as a rationale for treatment. *Hand Clinics*, 3(4):455–471.

[27] Eaton, R. G., Lane, L. B., Littler, J. W., and Keyser, J. J. (1984). Ligament reconstruction for the painful thumb carpometacarpal joint: A long-term assessment. *The Journal of Hand Surgery*, 9(5):692–699.

[28] Electronics, I. (2020). FSR® Integration Guide.

[29] Erhart, J., Unger, E., Schefzig, P., Krumboeck, A., Hagmann, M., Vecsei, V., and Mayr, W. (2016). In vitro experimental investigation of the forces and torque acting on the scaphoid during light grasp: BIOMECHANICS OF THE SCAPHOID BONE. *Journal of Orthopaedic Research*, 34(10):1734–1742.

[30] Erhart, S., Lutz, M., Arora, R., and Schmoelz, W. (2012). Measurement of intraarticular wrist joint biomechanics with a force controlled system. *Medical Engineering & Physics*, 34(7):900–905.

[31] Eschweiler, J., Stromps, J.-P., Fischer, M., Schick, F., Rath, B., Pallua, N., and Radermacher, K. (2016). A biomechanical model of the wrist joint for patient-specific model guided surgical therapy: Part 2. *Proceedings of the Institution of Mechanical Engineers, Part H: Journal of Engineering in Medicine*, 230(4):326–334.

[32] Fatema, A., Poondla, S., Mishra, R. B., and Hussain, A. M. (2021). A Low-Cost Pressure Sensor Matrix for Activity Monitoring in Stroke Patients Using Artificial Intelligence. *IEEE Sensors Journal*, 21(7):9546–9552.

[33] Filardi, V. (2019). Tibio talar contact stress: An experimental and numerical study. page 15.

[34] Freeman, D. E. and Auer, J. A. (2012). Chapter 9 - Instrument Preparation, Sterilization, and Antiseptics. In Auer, J. A. and Stick, J. A., editors, *Equine Surgery (Fourth Edition)*, pages 98–111. W.B. Saunders, Saint Louis.

[35] Fu, J., Nguyen, H., Kim, D. W., Shallal, C., Cho, S. M., Osborn, L., and Thakor, N. (2018). Dynamically Mapping Socket Loading Conditions During Real Time Operation of an Upper Limb Prosthesis. In *2018 40th Annual International Conference of the IEEE Engineering in Medicine and Biology Society (EMBC)*, pages 3930–3933, Honolulu, HI. IEEE.

[36] Garcia-Elias, M. and Orsolini, C. (2011). Relationship between thumb laxity and trapezium kinematics. *Chirurgie de la Main*, 30(3):224–227.

[37] Gerlach, C., Krumm, D., Illing, M., Lange, J., Kanoun, O., Odenwald, S., and Hubler, A. (2015). Printed MWCNT-PDMS-Composite Pressure Sensor System for Plantar Pressure Monitoring in Ulcer Prevention. *IEEE Sensors Journal*, 15(7):3647–3656.

[38] Gong, S., Schwalb, W., Wang, Y., Chen, Y., Tang, Y., Si, J., Shirinzadeh, B., and Cheng, W. (2014). A wearable and highly sensitive pressure sensor with ultrathin gold nanowires. *Nature Communications*, 5(1):3132.

[39] Guerrieri, R., Manaresi, N., Monnier, J., and Tartagni, M. (2004). Textile-like capacitive pressure sensor and method of mapping the pressure exerted at points of a surface of a flexible and pliable object, particularly of a sail.

[40] Halilaj, E., Moore, D. C., Patel, T. K., Laidlaw, D. H., Ladd, A. L., Weiss, A.-P. C., and Crisco, J. J. (2015). Older asymptomatic women exhibit patterns of thumb carpometacarpal joint space narrowing that precede changes associated with early osteoarthritis. *Journal of Biomechanics*, 48(13):3634–3640.

[41] Hara, T., Horii, E., An, K.-N., Cooney, W. P., Linscheid, R. L., and Chao, E. Y. (1992). Force distribution across wrist joint: Application of pressure-sensitive conductive rubber. *The Journal of Hand Surgery*, 17(2):339–347.

[42] Hasenkamp, W., Thevenaz, N., Villard, J., Bertsch, A., Arami, A., Aminian, K., Terrier, A., and Renaud, P. (2013). Design and test of a MEMS strain-sensing device for monitoring artificial knee implants. *Biomedical Microdevices*, 15(5):831–839.

[43] Hemmingsen, C. K., Thillemann, T. M., Elmengaard, B., Raedt, S., Nielsen, E. T., Mosegaard, S. B., Stentz-Olesen, K., and Stilling, M. (2020). Elbow Biomechanics, Radiocapitellar Joint Pressure, and Interosseous Membrane Strain Before and After Radial Head Arthroplasty. *Journal of Orthopaedic Research*, 38(3):510–522.

[44] Hoang, P. T., Phung, H., Nguyen, C. T., Dat Nguyen, T., and Choi, H. R. (2017). A highly flexible, stretchable and ultra-thin piezoresistive tactile sensor array using PAM/PEDOT:PSS hydrogel. In *2017 14th International Conference on Ubiquitous Robots and Ambient Intelligence (URAI)*, pages 950–955, Jeju. IEEE.

[45] Horie, J., Kuryu, S., Onose, Y., Satou, S., Shimada, S., and Watanabe, A. (2003). Capacitance-type pressure sensor.

[46] Huang, Y., Fan, X., Chen, S., and Zhao, N. (2019). Emerging technologies of flexible pressure sensors: Materials, modeling, devices, and manufacturing. *Advanced Functional Materials*, 29.

[47] Hughes, E. and Knowles, G. (2006). High-sensitivity pressure conduction sensor for localized pressures and stresses.

[48] Imaeda, T., An, K. N., and Cooney, W. P. (1992). Functional anatomy and biomechanics of the thumb. *Hand Clinics*, 8(1):9–15.

[49] Inc., T. S. (2009). FSR sensor | Operational Amplifier | Electronic Oscillator.

[50] Izaki, M., Nagano, H., Nakaya, T., Okamoto, O., Renbutsu, K., Suzuki, S., Ueno, J., Usui, Y., Yabuuchi, K., Yamaguchi, I., and Kamimura, H. (2002). Pressure-distribution sensor for controlling multi-jointed nursing robot.

[51] Jensen, K. and Graf, B. K. (1993). The effects of knee effusion on quadriceps strength and knee intraarticular pressure. *Arthroscopy: The Journal of Arthroscopic & Related Surgery*, 9(1):52–56.

[52] Kalichman, L. and Hernández-Molina, G. (2010). Hand Osteoarthritis: An Epidemiological Perspective. *Seminars in Arthritis and Rheumatism*, 39(6):465–476.

[53] Kapandji, A. (2007). *The Physiology of the Joints*, volume One. Elsevier/Churchill Livingstone, sixth edition edition.

[54] Katarincic, J. (2001). Thumb kinematics and their relevance to function. *Hand clinics*, 17:169–74.

[55] Ken Kawahata, M.-k. J. (2005). Surface Pressure Distribution Sensor.

[56] Kipphan, H. (2001). *Handbook of print media: technologies and production methods*. Springer Science & Business Media.

[57] Komistek, R. D., Mahfouz, M. R., and Wasielewski, R. C. (2008). Smart joint implant sensors.

[58] Kovler, M., Lundon, K., McKee, N., and Agur, A. (2004). The human first carpometacarpal joint: Osteoarthritic degeneration and 3-dimensional modeling. *Journal of hand therapy : official journal of the American Society of Hand Therapists*, 17:393–400.

[59] Ladd, A. L., Weiss, A.-P. C., Crisco, J. J., Hagert, E., Wolf, J. M., Glickel, S. Z., and Yao, J. (2014). The Thumb Carpometacarpal Joint: Anatomy, Hormones, and Biomechanics. page 30.

[60] Lalonde, D. (2015). Wide awake local anaesthesia no tourniquet technique (WALANT). *BMC Proceedings*, 9(S3):A81, 1753–6561–9–S3–A81.

[61] Lee, B.-Y., Kim, J., Kim, H., Kim, C., and Lee, S.-D. (2016). Low-cost flexible pressure sensor based on dielectric elastomer film with micro-pores. *Sensors and Actuators A: Physical*, 240:103–109.

[62] Lerouge, S. (2010). 13 - Sterilisation and cleaning of metallic biomaterials. In Niinomi, M., editor, *Metals for Biomedical Devices*, Woodhead Publishing Series in Biomaterials, pages 303–326. Woodhead Publishing.

[63] Leumann, A., Fortuna, R., Leonard, T., Valderrabano, V., and Herzog, W. (2013). Dynamic in-vivo force transfer in the lapine knee loaded by quadriceps muscle contraction. *Clinical Biomechanics*, 28(2):199–204.

[64] Leumann, A., Fortuna, R., Leonard, T., Valderrabano, V., and Herzog, W. (2015). Tibiofemoral loss of contact area but no changes in peak pressures after meniscectomy in a Lapine in vivo quadriceps force transfer model. *Knee Surgery, Sports Traumatology, Arthroscopy*, 23(1):65–73.

[65] Li, H., Maniar, P., and Wei, Y. (2009). Transparent Pressure Sensor and Method for Using.

[66] Li, S., Li, R., Chen, T., and Xiao, X. (2020). Highly Sensitive and Flexible Capacitive Pressure Sensor Enhanced by Weaving of Pyramidal Concavities Staggered in Honeycomb Matrix. *IEEE Sensors Journal*, 20(23):14436–14443.

[67] Liang, B., Chen, W., He, Z., Yang, R., Lin, Z., Du, H., Shang, Y., Cao, A., Tang, Z., and Gui, X. (2017). Highly Sensitive, Flexible MEMS Based Pressure Sensor with Photoresist Insulation Layer. *Small*, 13(44):1702422.

[68] Lim, S. J., Bae, J. H., Han, J. H., Jang, S. J., Oh, H. J., Lee, W., Kim, S. H., and Ko, J. H. (2020). Foldable and washable fully textile-based pressure sensor. *Smart Materials and Structures*, 29(5):055010.

[69] Lin, C.-L., Yeh, M.-L., Su, F.-C., Wang, Y.-C., Chiang, C.-H., Hong, C.-K., and Su, W.-R. (2019). Different suture anchor fixation techniques affect contact properties in humeral greater tuberosity fracture: a biomechanical study. *BMC Musculoskeletal Disorders*, 20(1):26.

[70] Logan, C. A., Aman, Z. S., Kemler, B. R., Storaci, H. W., Dornan, G. J., and LaPrade, R. F. (2019). Influence of Medial Meniscus Bucket-Handle Repair in Setting of Anterior Cruciate Ligament Reconstruction on Tibiofemoral Contact Mechanics: A Biomechanical Study. *Arthroscopy: The Journal of Arthroscopic & Related Surgery*, 35(8):2412–2420.

[71] Luo, Y., Wu, D., Zhao, Y., Chen, Q., Xie, Y., Wang, M., Lin, L., Wang, L., and Sun, D. (2019). Direct write of a flexible high-sensitivity pressure sensor with fast response for electronic skins. *Organic Electronics*, 67:10–18.

[72] Manapongpun, P., Mattayasinchai, P., and Bunnjaweht, D. (2020). Development of a Piezoresistive Sitting Pressure Distribution Sensor: Experiments on Standard Shape Objects. In *2020 8th International Electrical Engineering Congress (iEECON)*, pages 1–4, Chiang Mai, Thailand. IEEE.

[73] Marenzi, E., Lombardi, R., Bertolotti, G. M., Cristiani, A., and Cabras, B. (2012). Design and development of a novel capacitive sensor matrix for measuring pressure distribution. In *2012 IEEE Sensors Applications Symposium Proceedings*, pages 1–6, Brescia, Italy. IEEE.

[74] Martin, J. R., Paclet, F., Latash, M. L., and Zatsiorsky, V. M. (2013). Changes in the flexor digitorum profundus tendon geometry in the carpal tunnel due to force production and posture of metacarpophalangeal joint of the index finger: An MRI study. *Clinical Biomechanics*, 28(2):157–163.

[75] McGorry, R. W., Fallentin, N., Andersen, J. H., Keir, P. J., Hansen, T. B., Pransky, G., and Lin, J. (2014). Effect of grip type, wrist motion, and resistance level on pressures within the carpal tunnel of normal wrists. *Journal of Orthopaedic Research*, 32(4):524–530.

[76] Media, M. D. C. (2009). Force Sensors for Design. (4):9.

[77] Melville, D. M., Taljanovic, M. S., Scalcione, L. R., Eble, J. M., Gimber, L. H., DeSilva, G. L., and Sheppard, J. E. (2015). Imaging and management of thumb carpometacarpal joint osteoarthritis. *Skeletal Radiology*, 44(2):165–177.

[78] Morris, A. S. (2001). *Measurement and instrumentation principles*. Butterworth-Heinemann, Oxford [England] ; Boston. OCLC: ocm46812553.

[79] Nela, L., Tang, J., Cao, Q., Tulevski, G., and Han, S.-J. (2018). Large-Area High-Performance Flexible Pressure Sensor with Carbon Nanotube Active Matrix for Electronic Skin. *Nano Letters*, 18(3):2054–2059.

[80] Nicholas, J. W., Corvese, R. J., Woolley, C., and Armstrong, T. J. (2012). Quantification of hand grasp force using a pressure mapping system. *Work*, 41:605–612.

[81] on Legal Affairs and the Internal Market, C. (2003). Guide with recommendations to the Commission on a European disability rating scale 2003/2130(INI)).

[82] Pain, M. T. G., Tsui, F., and Cove, S. (2008). *In vivo* determination of the effect of shoulder pads on tackling forces in rugby. *Journal of Sports Sciences*, 26(8):855–862.

[83] Parida, K., Bhavanasi, V., Kumar, V., Bendi, R., and Lee, P. S. (2017). Self-powered pressure sensor for ultra-wide range pressure detection. *Nano Research*, 10(10):3557–3570.

[84] Patel, T. J., Beredjiklian, P. K., and Matzon, J. L. (2013). Trapeziometacarpal joint arthritis. *Current Reviews in Musculoskeletal Medicine*, 6(1):1–8.

[85] Penedo, J. M. V. d. S., Gonçalves, G. F. C., Ormonde, L. P. d. C., Barros, M. J. D. d. M. M., Carvalho, M. G. B., Gomes, P. P. S. d. A., Vasconcelos e Sá, R. A. M. d., and Ribeiro, V. I. C. (2015). Avaliação da Situação Nacional dos Blocos Operatórios. Technical report, Ministério da Saúde do Governo de Portugal.

[86] Qin, J., Barbour, K. E., Murphy, L. B., Nelson, A. E., Schwartz, T. A., Helmick, C. G., Allen, K. D., Renner, J. B., Baker, N. A., and Jordan, J. M. (2017). Lifetime Risk of Symptomatic Hand Osteoarthritis: The Johnston County Osteoarthritis Project. *Arthritis & Rheumatology*, 69(6):1204–1212.

[87] Quandt, B. M., Hufenus, R., Weisse, B., Braun, F., Wolf, M., Scheel-Sailer, A., Bona, G.-L., Rossi, R. M., and Boesel, L. F. (2017). Optimization of novel melt-extruded polymer optical fibers designed for pressure sensor applications. *European Polymer Journal*, 88:44–55.

[88] Rajala, S., Mattila, R., Kaartinen, I., and Lekkala, J. (2017). Designing, Manufacturing and Testing of a Piezoelectric Polymer Film In-Sole Sensor for Plantar Pressure Distribution Measurements. *IEEE Sensors Journal*, 17(20):6798–6805.

[89] Rikli, D. A., Honigmann, P., Babst, R., Cristalli, A., Morlock, M. M., and Mittlmeier, T. (2007). Intra-Articular Pressure Measurement in the Radioulnocarpal Joint Using a Novel Sensor: In Vitro and In Vivo Results. *The Journal of Hand Surgery*, 32(1):67–75.

[90] Rocha, J., Carvalho, H., Duarte, F., Carvalho, M. A. F., and Moreira, V. (2008). System providing discomfort monitoring for people in wheelchairs. In *2008 IEEE International Symposium on Industrial Electronics*, pages 961–966, Cambridge, UK. IEEE.

[91] Rouvière, H. .-. A. (1962). *Anatomie humaine : descriptive et topographique*. Masson. Paris.

[92] Sakamoto, Y., Sasaki, S., Kimura, Y., Yamamoto, Y., Tsuda, E., and Ishibashi, Y. (2020). Patellofemoral Contact Pressure for Medial Patellofemoral Ligament Reconstruction Using Suture Tape Varies With the Knee Flexion Angle: A Biomechanical Evaluation. *Arthroscopy: The Journal of Arthroscopic & Related Surgery*, 36(5):1390–1395.

[93] Sartiano, D. and Sales, S. (2017). Low Cost Plastic Optical Fiber Pressure Sensor Embedded in Mattress for Vital Signal Monitoring. *Sensors*, 17(12):2900.

[94] Schnaser, E., Lee, Y.-y., Boettner, F., and Gonzalez Della Valle, A. (2015). The Position of the Patella and Extensor Mechanism Affects Intraoperative Compartmental Loads During Total Knee Arthroplasty. *The Journal of Arthroplasty*, 30(8):1348–1353.e3.

[95] Schneider, M. T. Y. (2018). Early morphologic changes in trapeziometacarpal joint bones with osteoarthritis. *Osteoarthritis and Cartilage*, page 7.

[96] Seeley, R. R., Tate, P., and Stephens, T. D. (2008). *Anatomy & physiology*. McGraw-Hill, Dubuque, IA, 8th ed edition.

[97] Shirinov, A. and Schomburg, W. (2008). Pressure sensor from a PVDF film. *Sensors and Actuators A: Physical*, 142(1):48–55.

[98] Simmons, A. (2012). 11 - Future trends for the sterilisation of biomaterials and medical devices. In Lerouge, S. and Simmons, A., editors, *Sterilisation of Biomaterials and Medical Devices*, Woodhead Publishing Series in Biomaterials, pages 310–320. Woodhead Publishing.

[99] Standring, S., editor (2016). *Gray's anatomy: The Anatomical basis of clinical practice*. Elsevier Limited, New York, forty-first edition edition.

[100] Suprapto, S., Setiawan, A., Zakaria, H., Adiprawita, W., and Supartono, B. (2017). Low-Cost Pressure Sensor Matrix Using Velostat. In *2017 5th International Conference on Instrumentation, Communications, Information Technology, and Biomedical Engineering (ICICI-BME)*, pages 137–140, Bandung. IEEE.

[101] Swanson, A. B., Göran-Hagert, C., and de Groot Swanson, G. (1987). Evaluation of impairment in the upper extremity. *The Journal of Hand Surgery*, 12(5 Pt 2):896–926.

[102] Tanabe, F., Yoshimoto, S., Noda, Y., Araki, T., Uemura, T., Takeuchi, Y., Imai, M., and Sekitani, T. (2017). Flexible sensor sheet for real-time pressure monitoring in artificial knee joint during total knee arthroplasty. In *2017 39th Annual International Conference of the IEEE Engineering in Medicine and Biology Society (EMBC)*, pages 1591–1594, Seogwipo. IEEE.

[103] Taylor, G. L. (2003). Pressure measurement sensor with piezoresistive thread lattice.

[104] Taş, S. and Çetin, A. (2019). An investigation of the relationship between plantar pressure distribution and the morphologic and mechanic properties of the intrinsic foot muscles and plantar fascia. *Gait & Posture*, 72:217–221.

[105] Teo, A. J., Mishra, A., Park, I., Kim, Y.-J., Park, W.-T., and Yoon, Y.-J. (2016). Polymeric Biomaterials for Medical Implants and Devices. *ACS Biomaterials Science & Engineering*, 2(4):454–472.

[106] Tuan, C.-C., Lu, C.-H., Wu, Y.-C., Yeh, W.-L., Chen, M.-C., Lee, T.-F., Chen, Y.-J., and Kao, H.-K. (2019). Development of a System for Real-Time Monitoring of Pressure, Temperature, and Humidity in Casts. *Sensors*, 19(10):2417.

[107] Varga, P., Schefzig, P., Unger, E., Mayr, W., Zysset, P. K., and Erhart, J. (2013). Finite element based estimation of contact areas and pressures of the human scaphoid in various functional positions of the hand. *Journal of Biomechanics*, 46(5):984–990.

[108] Vergara, M., Sancho-Bru, J., Gracia-Ibáñez, V., and Pérez-González, A. (2014). An introductory study of common grasps used by adults during performance of activities of daily living. *Journal of Hand Therapy*, 27(3):225–234.

[109] Volf, J. and Novák, V. (2016). Pressure Distribution Measurement in Knee Arthoplasty. *Procedia Engineering*, 168:892–895.

[110] Wakabayashi, S., Arie, T., Akita, S., and Takei, K. (2020). Very Thin, Macroscale, Flexible, Tactile Pressure Sensor Sheet. *ACS Omega*, 5(28):17721–17725.

[111] Webster, J. (2009). *Medical Instrumentation Application and Design, 4th Edition*. John Wiley Sons, Incorporated.

[112] Webster, J. G., Jr., J. W. C., Neuman, M. R., Olson, W. H., Peura, R. A., Jr., F. P. P., Seidband, M. P., and Wheeler, L. A. (2010). *Medical instrumentation: application and design*. Wiley, Hoboken, NJ, fourth edition edition.

[113] Wilke, H., Neef, P., Caimi, M., Hoogland, T., and Claes, L. E. (1999). New In Vivo Measurements of Pressures in the Intervertebral Disc in Daily Life:. *Spine*, 24(8):755–762.

[114] Wu, J., Li, H., Lai, X., Chen, Z., and Zeng, X. (2020). Conductive and superhydrophobic F-rGO@CNTs/chitosan aerogel for piezoresistive pressure sensor. *Chemical Engineering Journal*, 386:123998.

[115] Yang, W., Li, N.-W., Zhao, S., Yuan, Z., Wang, J., Du, X., Wang, B., Cao, R., Li, X., Xu, W., Wang, Z. L., and Li, C. (2018). A Breathable and Screen-Printed Pressure Sensor Based on Nanofiber Membranes for Electronic Skins. *Advanced Materials Technologies*, 3(2):1700241.

[116] Yu, G., Hu, J., Tan, J., Gao, Y., Lu, Y., and Xuan, F. (2018). A wearable pressure sensor based on ultra-violet/ozone microstructured carbon nanotube/polydimethylsiloxane arrays for electronic skins. *Nanotechnology*, 29(11):115502.

[117] Yuanzheng Luo, Qi Xiao, and Buyin Li (2017). A Stretchable Pressure-Sensitive Array Based on Polymer Matrix. *Sensors*, 17(7):1571.

[118] Zhang, H. and Tao, X.-M. (2012). A single-layer stitched electrotextile as flexible pressure mapping sensor. *The Journal of The Textile Institute*, 103(11):1151–1159.